FUEL PLATE FAILURE EXPERIMENTS AND ANALYSES IN IRRADIATED U-10Mo ALLOY

A Thesis
Presented in Partial Fulfillment of the Requirement for the
Degree of Master of Science
with a
Major in Nuclear Engineering
in the

College of Graduate Studies

University of Idaho

by

Francine Joyce Rice

Major Professor**:** Indrajit Charit, Ph.D.

Committee Members: Richard Christensen, Ph.D.; Daniel Wachs, Ph.D.

Department Chair: Richard Christensen, Ph.D.

May 2017

Authorization to Submit Thesis

This thesis of Francine Joyce Rice, submitted for the degree of Master of Science with a major in Nuclear Engineering and titled "Fuel Plate Failure Experiments and Analyses in Irradiated U-10Mo Alloy," has been reviewed in final form. Permission, as indicated by the signatures and dates below, is now granted to submit final copies to the College of Graduate Studies for approval.

Major Professor:	_____	Date:	_____
	Indrajit Charit, Ph.D.		
Committee Members:	_____	Date:	_____
	Richard Christensen, Ph.D.		
	_____	Date:	_____
	Daniel Wachs, Ph.D.		
Department Administrator:	_____	Date:	_____
	Richard Christensen, Ph.D.		

Abstract

The Materials Management and Minimization (M3) Program intends to qualify a new high-density low-enriched-uranium (LEU) U–Mo monolithic fuel to enable conversion of six US high-performance research reactors (USHPRRs). This thesis presents the preliminary results and discussions related to post-irradiation blister anneal studies and fission product release scoping studies performed on U–Mo monolithic fuel plates.

Blister anneal testing on irradiated fuel plates is a temperature-resolved failure-threshold measurement technique historically used to assess fuel plate stability under off-normal operating conditions. The effects of fuel composition, geometry, fission density, and irradiation conditions are presented herein as parameters that were investigated for their impact on blister-threshold temperatures. The fission-product-transport scoping study successfully characterized the release, transport and temperature-resolved deposition behavior of iodine and cesium. Two failure temperatures were evaluated: 600 and 1250°C. Testing was performed in the main hot cell at the Materials and Fuels Complex located at Idaho National Laboratory.

Acknowledgements

I would like to gratefully acknowledge the National Nuclear Security Administration for the funding this work performed under the direction of the Fuel Development Technical Leads for the Materials Management and Minimization Program. Dr. Daniel Wachs is responsible for setting me on the path to earn a Master Degree in Nuclear Engineering in the course of performing the work with subsequent results reported herein. Dr. Mitchell Meyer was instrumental in helping to gather and organize the historical data and literature (much of which was obscure and difficult to find) needed to put the data into the correct context (our benchmarks), of the currently qualified fuel systems. Dr. Meyer's in process reviews were exhaustive and constructive. These two men have been my professional and technical standards for working hard and being persistent even when it is not fun. Finally, I would like to acknowledge the unfailing patience of my advisor, Dr. Indrajit Charit in understanding that working fulltime and maintaining a healthy personal life means that sometimes finishing takes longer than anticipated. His feedback and encouragement did much to help keeping me moving forward, even when the pace was slow.

Dedications

This work is dedicated to my Lord and Savior, Jesus Christ, who sustained me during this very long journey. To my husband, Randolph Rice, who unfailingly supported me in every way possible. To my mother, Sally Ann Irving, who nagged me relentlessly and I love her dearly for that. To all the other people, my co-workers/friends who made this project possible and encouraged me along the way.

Table of Contents

List of Figures

List of Tables

Chapter 1: Preliminary Blister Threshold Testing Results For U–Mo Monolithic Fuel Plates

1.1 Introduction

The Office of Materials Management and Minimization (M3) within the U.S. DOE/National Nuclear Security Administration (NNSA) is working to convert research reactors globally from highly enriched uranium (HEU) fuel to low-enriched uranium (LEU) fuel. Of the 200 candidate research reactors, over 80 have been converted using LEU fuel developed in the 1980s. Additional reactor conversions using this fuel are currently underway. However, there is a small set of high-performance research reactors that require a new high-density LEU fuel for conversion which include six U.S. high-performance research reactors (USHPRRs), one of which is a critical facility. Combined, the high-performance reactors in the U.S., Russia, and Europe are responsible for 650–750 kg of HEU use annually.[1]

The USHPRR Conversion Program is developing replacement LEU fuels and associated fuel-fabrication capabilities for the remaining USHPRRs that cannot convert with existing LEU fuels. These remaining USHPRRs include nuclear research reactors at:

- The Massachusetts Institute of Technology (Massachusetts Institute of Technology Reactor [MITR])
- The University of Missouri (University of Missouri Research Reactor [MURR])
- The National Institute of Standards and Technology (National Bureau of Standards Reactor [NBSR])
- Oak Ridge National Laboratory (High Flux Isotope Reactor [HFIR])

- Idaho National Laboratory (Advanced Test Reactor [ATR], including the ATR-Critical Facility [ATRC]).

This chapter focuses on blister threshold temperatures of the high-density U–10Mo monolithic fuel system (described in Section 1.4) being developed as a fuel for conversion of high-performance research reactors. Blister thresholds of plate fuels are a part of the design safety basis whereby fuel-failure thresholds are established as a function of plate fission density. As fission gas inventories increase and begin to coalesce during the service life of a fuel element, there is a predictable decrease in blister-threshold temperatures. The blister-threshold temperature of a fuel plate is considered to be the first failure temperature related threshold of a plate. The ATR, for example, has established a 2-sigma design bases margin during normal operations to avoid reaching the lowest threshold. Should a temperature-transient event occur such that the design bases temperature is exceeded, fuel plates may be examined for evidence of blistering prior to returning to service.

Evaluation of fuel system to determine this first temperature failure threshold is necessary to determine the reactor operation envelop relative to the fuel plate fission densities so that design-bases margins can be established.

1.2 The Blister Threshold Test

Blister Threshold testing is a destructive characterization method used in a variety of materials to detect defects, non-uniform and excessive porosity, and coalescence of gas bubbles. The test has been applied as a tool for measuring adhesion strength in thin coatings.[2,3] Blisters themselves can be indicative of an excess of defect and impurity sites for hydrogen-gas coalescence[4] in cast materials. In cast aluminum,[5] blister formation during the heating and rolling segments of fabrication are indicative of defects (shrink cavities) and

hydrogen gas introduced during the casting process. Casting- and rolling-process adjustments were identified in the study that incorporated Blister Thresholding as a destructive characterization to evaluate the efficacy of the different methods applied to reduce the gas and defect inventories. Blister size, shape, and location can be characterized to determine initiation sites and failure mechanisms. A study performed at the Idaho National Laboratory (INL) used Blister Threshold testing determine whether incidents of debonding can go undetected by the ultrasonic testing (UT) that is used to evaluate cladding-to-cladding and cladding-to-fuel bonding in the laminated U–10Mo fuel plate system.[6]

Non-destructive blister anneal testing is still performed on each dispersion fuel plate during fabrication for virtually all research test reactors worldwide prior to acceptance for irradiation. The test is used to reveal the presence, size and locations of defects and as an indication of gas entrapment during fabrication and/or bond integrity. The temperature thresholds for blister formation and their size and location on a test specimens have proven useful for trend development relative to a number of post-irradiation fuel performance parameters.

Nuclear Regulatory Guide (NUREG)-1313[7] developed for U_3Si_2 dispersion fuel designs concludes that, "The resistance of a fuel plate to blistering (caused by gas bubble agglomeration) when it is heated to elevated temperatures has been used as a measure of fuel plate stability for many years in the development of dispersion fuels."

Hence, the blister-threshold temperatures and morphologies unique to the U–10Mo monolithic fuel system are evaluated for a range of fission densities using test plates that were irradiated during the research and development phase of the M3 program. Several fuel

plate failure characteristics unique to the monolithic fuel system are discussed in addition to the blister-threshold temperatures.

1.3 Blister Threshold Testing of Dispersion Plate Fuels

The Blister Threshold test has been applied to determine the failure thresholds for several qualified dispersion plate-type fuel systems[8,9] (UAl_x, U_3Si_2 and U_3O_8), and those results are presented in herein. These data provided information that enabled the reactors using these qualified fuels to set thresholds for fuel burnup, operating power, and temperature.

Blister Threshold testing has also proven useful in correlation of observed changes in blister threshold temperature with changes in fuel composition or irradiation conditions. For example, it was noted in Blister Threshold tests of the U–Al_x dispersion fuel system that low-temperature and fission-rate regions in a fuel plate had reduced blister threshold temperatures due to coalescence of fission gases before plastic behavior could close pores.[10] The reduction of the blister threshold temperature[11] in the silicide and uranium oxide fuel systems has also been observed following the addition of B_4C as a burnable poison.

Three types of dispersed fuel phases are currently used in material test reactors (MTRs) in the United States. These fuels all use nominally the same aluminum matrix and 6061 aluminum alloy cladding material. The three fuel-particle types are uranium aluminide intermetallic (UAl_x),[10] uranium oxide (U_3O_8)[12], and uranium silicide (U_3Si_2) [NUREG-1313]. An overview of dispersion fuel that contains blister threshold temperature data for aluminide, silicide, and oxide fuel has been compiled by Snelgrove.[13]

It is important to recognize that reporting of fission density for “fuel foil” in the case of monolithic fuel plates and “fuel meat” in the case of dispersion fuel plates emphasizes a

difference in the way results may be reported for dispersion fuel. Dispersion fuel meat is comprised of the fuel particles and the matrix material which, in effect, results in a lower volumetric fission density compared to the fission density exhibited by the fuel particles only. Fuel loading (i.e., grams U/cm^3) can be used to determine the volumetric ratio of the fuel in the fuel meat, allowing the fission density within the fuel particles to be calculated. For the purposes of this report, fission density for dispersion fuel plates is reported as fuel-meat fission density.

1.3.1 Uranium-aluminide Dispersion Fuel (UAl_X)

UAl_x dispersion fuel is currently used in MURR, MITR, and ATR. Several blister-threshold testing campaigns have been conducted during the development of this fuel. Blister threshold data for aluminide fuel are plotted in Figure 1. The majority of development and testing of aluminide fuels was conducted with boron included as a burnable absorber. Plates which contain burnable absorber are denoted in Figure 1 as closed points; plates that did not contain boron as a burnable absorber are denoted as open data points. Data from Tables 1–6 are plotted in Figure 1.

The most recent blister threshold measurements were completed in conjunction with the Extended Life Aluminide Fuel (ELAF) testing campaign in the 1980s.[8] The objective of the ELAF program was to increase fuel in-core lifetime to reduce fuel costs. The ELAF program irradiated UAl_2 fuel with 40, 45, and 50 vol% fuel-meat loading to fuel-meat fission densities of up to 3 x 10^{21} f/cm^3, along with 50 vol% UAl_x reference plates (UAl_x in this reference denotes the mass composition of UAl_2 and UAl_3). These fuel plates contained 1.4–1.5 wt.% B_4C as a burnable absorber. During irradiation, ^{10}B generates helium. Because of the additional helium-gas inventory and high fission density, blister testing of the ELAF

plates thus likely represents the most severe testing conditions for aluminide-fuel blister-threshold temperature.

Thirty fuel plates were fabricated and irradiation tested in the ATR I-9 and I-12 positions. Twelve plates were blister tested, as listed in Table 1. Blister-threshold temperature was not a strong function of fission density within the range of conditions tested. The average blister temperature for UAl_3 plates was 490°C, while that for UAl_2 plates was 503°C. The UAl_2 plates exhibited a range of blister threshold temperatures from 440° to greater than 560°C.

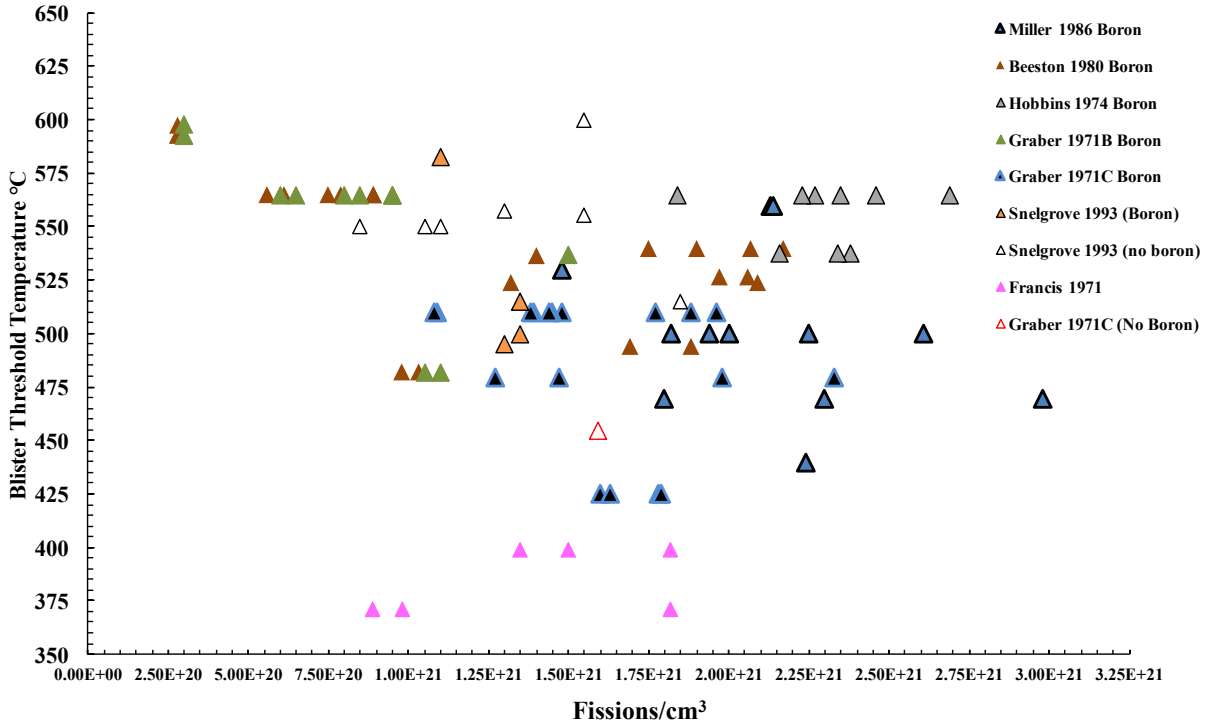

Figure 1. Blister threshold temperature data for UAl_x dispersion fuel. Plot includes data from fuel plates with (filled points) and without boron (open points).

Table 1. ELAF blister test data from [8]. Fuel plate compositions are provided in Appendix C, Table C-1.

Plate Type	Plate No.	Average Fuel Meat Fission Density (Calculated)[a] 10^{21} f/cm^3	Blister Temperature, °C
50 vol.% UAl_3	005	1.80	470
50 vol.% UAl_3	006	2.30	470
50 vol.% UAl_3	007	1.48	530
50 vol.% UAl_2	013	2.98	470
50 vol.% UAl_2	019	2.13	560[b]
50 vol.% UAl_2	020	2.24	440
45 vol.% UAl_2	022	1.82	500
45 vol.% UAl_2	027	1.94	500
45 vol.% UAl_2	028	2.61	500
40 vol.% UAl_2	030	2.25	500
40 vol.% UAl_2	032	2.14	560[b]
40 vol.% UAl_2	033	2.00	500

a. Note that calculated and measured burnup values differ and are not reconciled in the report from which this data was obtained.

b. Plate did not blister at 560°C.

Much of the blister threshold data on UAlX fuels that preceded the ELAF program was summarized in Reference 10 and is presented in Table 2. Note that these fuel plates also contain B4C as a burnable poison.

Hobbins reported testing of aluminide fuel plates in a sodium bonded experiment capsule to compare the blister threshold temperature occurring in reactor to that measured in post-irradiation testing.[14,15] Although sample temperatures sufficient to test in-pile blistering were not achieved, post-irradiation out-of-pile blister-threshold-temperature data were collected. These data are also provided in Table 2, as reported by Reference 10. It should be noted that the fission densities reported by Reference 10 differ from those reported earlier by Hobbins. The later fission densities reported by Beeston were used in Table 2 and Figure 1. Whitacre published similar data in 1990.

Table 2. Blister threshold temperature data from [10]. Data on fuel compositions is reported in Appendix C, Tables C 2, C 4, and C 6.

Element	Sample No.	Element Type	Fuel Meat Fission Density (1021 f/cm3)	Blister Temperature (°C)
XA3G	2-21	0.976 g U/cm3, 0.0142 g B/cm3	0.98	482
	7-0	1.488 g U/cm3, 0.0011 g B/cm3	0.61	565
	7-7	1.488 g U/cm3, 0.0011 g B/cm3	0.79	565
	7-14	1.488 g U/cm3, 0.0011 g B/cm3	0.89	565
	7-21	1.488 g U/cm3, 0.0011 g B/cm3	0.89	565
	7-28	1.488 g U/cm3, 0.0011 g B/cm3	0.89	565
	7-35	1.488 g U/cm3, 0.0011 g B/cm3	0.75	565
	7-42	1.488 g U/cm3, 0.0011 g B/cm3	0.56	565
	15-25	1.488 g U/cm3, 0.0011 g B/cm3	1.40	537
	16-21	1.232 g U/cm3, 0.0075 g B/cm3	1.03	482
XA8G	7-T	7F element, ATR core II	~0.28	598
UAlx-7F	11-T	1.488 g U/cm3, 0.0011 g B/cm3	~0.28	593
	11-B	1.488 g U/cm3, 0.0011 g B/cm3	~0.28	593
XA130K	0-7	-	0.56	—
	0-6	-	1.11	—
	0-5	-	1.69	494
	0-4	-	1.88	494
	0-3	-	1.97	527
	0-2	-	2.06	527
	0-1	-	2.12	—
XA135K	5-2	-	0.82	—
	5-3	-	1.32	524
	5-4	-	1.75	540
	5-5	-	1.9	540
	5-6	-	2.07	540
	5-7	-	2.17	540
	5-1	-	2.09	524

Table 3. Blister threshold temperature data originally documented in Reference 15 and reported in Reference 10. Note that fission densities reported by Reference 10 are used here. Fuel plate compositions are provided in Appendix C, Table C-3.

Sample No.	Element Type	Fuel Meat Fission Density (10^{21}f/cm^3)	Blister Temperature (°C)
169-4	ATR 7F High	2.46	565
169-5	ATR 7F High	2.69	565[a]
169-11	ATR 7F High	2.16	538
169-12	ATR 7F Medium	2.27	565
169-19	ATR 7F Medium	1.84	565
169-36	ATR 7F Low	2.35	565[a]
169-37	ATR 7F Medium	2.38	538
169-38	ATR 7F Medium	2.34	538
169-39	ATR 7F Medium	2.23	565

a. Did not blister at 565°C.

Table 4 provides additional blister threshold temperature data reported in Reference 16.

Table 4. Additional blister threshold temperature data.[16] Fuel plate compositions are provided in Appendix C, Table C-6.

Plate No.	Plate Type	Average Fuel Meat Fission Density (10^{21} f/cm^3)	Blister Temperature, °C
157-30	51.6 wt.% UAlx, 0.197 wt.% B4C (7F element)	1.98	480
157-31	51.6 wt.% UAlx, 0.197 wt.% B4C (7F element)	1.77	510
157-35	51.6 wt.% UAlx, 0.197 wt.% B4C (7F element)	1.77	510
157-38	51.6 wt.% UAlx, 0.197 wt.% B4C (7F element)	1.48	510
158-54	61.4 wt.% UAlx, 0.037 wt.% B4C (7F 'high loading' fuel element)[a]		
158-65	61.4 wt.% UAlx, 0.037 wt.% B4C (7F 'high loading' fuel element) [a]	1.39	510
158-67	61.4 wt.% UAlx, 0.037 wt.% B4C (7F 'high loading' fuel element) [a]	1.96	510
159-14	ATR 7F high 0.030" fuel meat	1.45	510
159-24	ATR 7F high 0.030" fuel meat	1.38	510
160-37	ATR 7F low loading	1.47	480
160-34	ATR 7F low loading	1.27	480
162-1	ATR 7F Low, Low Void	1.44	510

Plate No.	Plate Type	Average Fuel Meat Fission Density (10^{21} f/cm^3)	Blister Temperature, °C
162-4	ATR 7F Low, Low Void	1.09	510
163-4	ATR Regular, Low Void	1.88	510
163-16	ATR Regular, Low Void	1.08	510

a. ANCR-1016 [16] lists 158 series plates as 7F high loading. [M. J. Graber, "ATR Extended Burnup INC-16-1 Results," INEL internal letter report (1971)[17]] lists plate 158 as a 7F plate.

Data for aluminide fuel mini-plates irradiated in the Oak Ridge Reactor (ORR) that do not contain boron are outlined in Table 5 and plotted in Figure 1. Snelgrove provides additional data, summarized in Reference 18 as ranges of blister-threshold temperature for ranges of fission density. These data are not plotted in Figure 1.

Francis reported a substantial decrease in blister threshold temperature at high fuel particle fission densities attributed to microcracking in the fuel meat initiated by fuel particles.[19] It was postulated that higher fuel-particle fission densities were the result of lower fuel-particle loading for an equivalent fuel-meat burnup and, also, observed that lower operating temperatures resulted in lower-density fuel-core volume fractions. Thirteen of 56 plates exhibited reduced blister-threshold temperatures.

Table 5. Blister threshold temperature data from UAlx mini-plates. Plates RA-132 and RA-143 are UAl_2 plates.

Plate No.	Source	Uranium Density (g-U/cm^3)	Average Fuel Meat Fission Density (10^{21} f/cm^3)	Blister Temperature °C
177[a]	Hrovat	2.14	1.19	550
407	Hrovat	2.2	1.71	550
RA-124	Perez	2.52	1.03	550
RA-128	Perez	2.32	0.95	550
RA-132	Gomez	3.09	1.37	475
RA-143	Gomez	3.01	1.33	500
RA-116	Gomez	2.28	1.15	>550

a. It is assumed that this is plate is listed as both 177 and 117 in Reference 20.

Table 6 provides information on the blister threshold temperature for these plates. Fuel plates irradiated to similar fuel-particle fission densities in subsequent tests at higher temperatures did not exhibit this phenomenon. It is likely that irradiation at low temperatures builds gas inventory (helium and fission product gas) early in life with little reaction between the fuel particles and the aluminum matrix or closure of fabrication porosity.[21] During post-irradiation heating, a fuel/matrix reaction occurs, and the accumulated gases are released, resulting in blisters.

Table 6. Aluminide fuel plates with reduced blister threshold temperatures. Fuel plate compositions are provided in Appendix B.4.

Plate No.	Expected Blister Temperature (C)	Measured Blister Temperature (C)	Fuel Meat Fission Density (10^{21} f/cm^3)	Fuel Particle Fission Density 10^{21} f/cm^3)
154-47	477	260	1.36	3.78
154-63	477	288	1.56	4.11
154-54	477	288	1.55	3.69
154-51	477	316	1.57	---
154-53	477	316	1.39	---
154-58	477	316	1.36	4.00
160-44	477	343	1.36	2.72
154-45	482	371	0.89	---
154-59	479	371	0.98	---
157-41	477	371	1.82	---
154-60	477	399	1.35	---
154-55	477	399	1.50	---
157-42	477	399	1.82	3.31

1.3.2 U_3O_8 Dispersion Fuel

U_3O_8 dispersion fuel is currently used in both NBSR and HFIR. Early development of U_3O_8 dispersion fuel was conducted in the U.S. by Oak Ridge National Laboratory (ORNL) for the High Flux Isotope Reactor (HFIR)[12] and by Idaho National Engineering Laboratory (INEL) for the ATR.[22] Blister-threshold-temperature data for oxide fuel are plotted in

Figure 2. Note that Figure 2 contains data for U_3O_8 fuel that contains boron as a burnable absorber (filled points) and fuel that does not contain burnable absorber (open points).

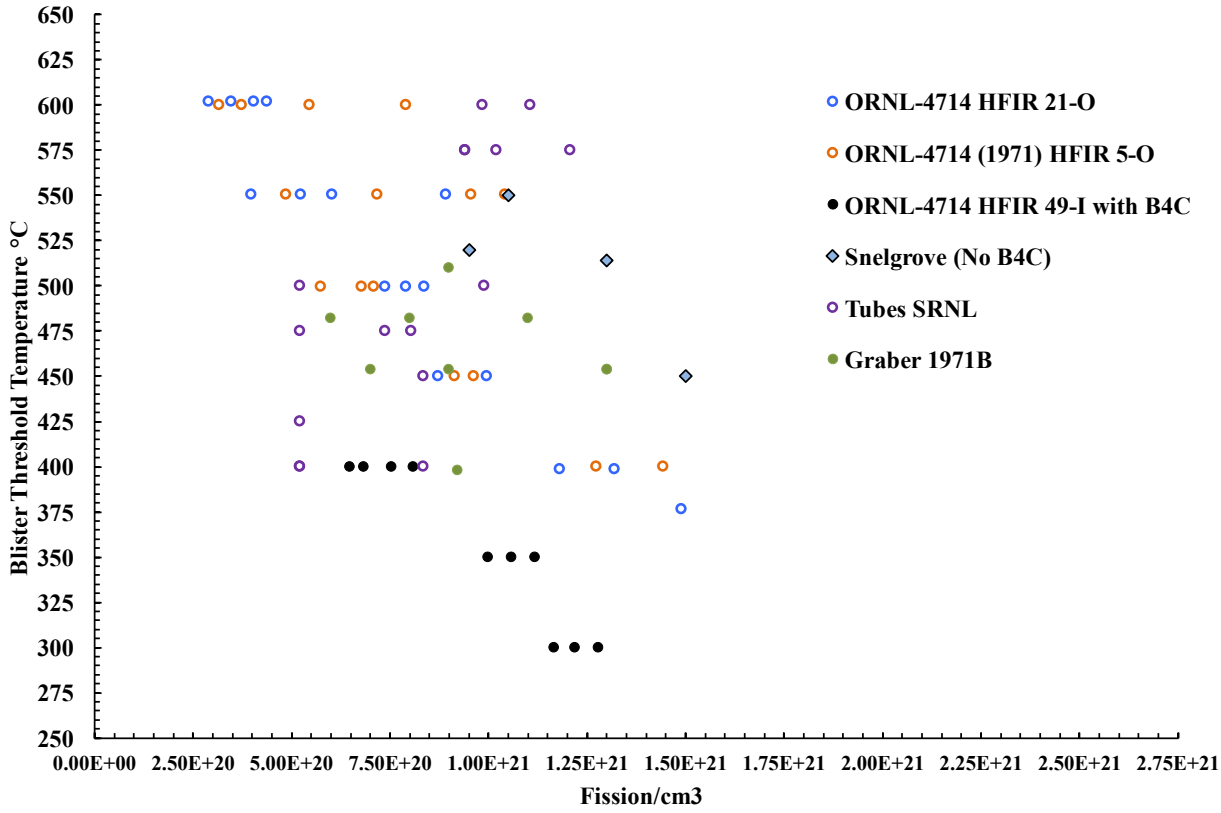

Figure 2. Blister threshold temperature data for U_3O_8 dispersion fuel. Plot includes data from fuel plates with (filled points) and without (open points) boron.

Table 7 lists data from Reference 12 for both HFIR inner (I) and outer (O) fuel elements. No data on fuel composition are provided in the report, and it is assumed that the fuel composition tested in 1971 is the same as the current HFIR fuel composition. The boron-containing inner fuel elements, listed in Table 8, exhibited lower blister-threshold temperatures relative to the outer fuel elements. A temperature effect similar to that observed by Reference 19 for aluminide fuel was also observed, whereby fuel plates irradiated at lower temperatures exhibited lower blister-threshold temperatures. Whitacre postulated the cause of this phenomenon for aluminide fuel as discussed above.[21]

Table 7. Blister threshold temperature data for HFIR outer fuel elements.

Fuel Meat Fission Density (10^{21} f/cm^3)	Measured Blister Temperature(C)
Fuel Element 21-O (outer fuel element, no boron)	
0.44	602
0.41	602
0.35	602
0.29	602
0.89	550
0.40	550
0.52	550
0.60	550
0.74	500
0.79	500
0.84	500
0.87	450
1.00	450
1.18	399
1.32	399
1.49	377
Fuel Element 5-O (outer fuel element, no boron)	
0.79	600
0.55	600
0.37	600
0.32	600
0.49	550
0.72	550
0.96	550
1.04	550
0.58	500
0.68	500
0.71	500
0.91	450
0.96	450
1.27	400
1.44	400

Table 8. Blister threshold temperature data for HFIR inner fuel element 49-I.

Fuel Meat Fission Density (10^{21} f/cm^3)	Measured Blister Temperature(C)
Fuel Element 49-I (inner fuel element, contains boron)	
0.81	400
0.65	400
0.68	400
0.75	400
1.00	350
1.06	350
1.12	350
1.17	300
1.22	300
1.28	300

U_3O_8 blister threshold data from Reference 22 is listed in Table 9. Plates listed in Table 9 were of ATR design and includes boron as a burnable poison.

Table 9. U_3O_8 blister threshold temperature data for fuel element A172C. Fuel plate compositions are provided in Appendix C, Table C-2.

Plate No.	Average Fuel Meat Fission Density (10^{21} f/cm^3)	Blister Temperature °C
2	0.9	510
2	1.1	482
2	1.3	454
2	1.3	454
18	0.7	454
18	0.6	482
18	0.8	482
18	0.9	454
18	0.92	398

Table 10 provides blister threshold temperature data for mini-plates without boron irradiated in the ORR from References 20, 23, 24, 25, also plotted in Figure 2. An overview of blister threshold temperature data for oxide fuel has been compiled by Snelgrove[18], and data for tube-type fuel from that reference are plotted in Figure 2.

Table 10. Blister threshold temperature data from mini-plates.

Plate No.	Source	Uranium Density (g-U/cm^3)	Average Fuel Meat Fission Density (10^{21} f/cm^3)	Blister Temperature °C
308	Hrovat	2.3	1.27	490
407	Hrovat	2.4	1.9	470
506	Hrovat	3.07	1.32	510
614	Hrovat	3.12	1.76	490
RA-222	Perez	3.12	1.25	478
RA-218	Perez	2.91	1.16	525
RA-234	Gomez	3.55	1.56	450
RA-223	Gomez	3.12	1.37	500
NA	Thamm	2.34	1.91	400

1.3.3 U_3Si_2 Dispersion Fuel

U_3Si_2 was developed as a high-density fuel for conversion of research reactors that require uranium density in the fuel meat of up to 4.8 g-U/cm^3.[7] Many low-power research reactors have successfully been converted to the use of LEU with this fuel type. The blister-threshold behavior of U_3Si_2 is similar to that of UAl_x, both being intermetallic compounds. Blister-threshold temperature data for U_3Si_2 are plotted in Figure 3. The blister threshold temperature of U_3Si_2 is relatively insensitive to fuel meat fission density at the qualified fuel density limit of 4.8 gU/cm^3. Most of the available U_3Si_2 blister-threshold data was acquired from testing of fuel plates from the qualification irradiation of six fuel test assemblies[7] in the Oak Ridge Reactor (ORR).[26] These data are listed in Table 11. Blister testing results from miniature fuel test plates were reported by Krug,[27] Marajofsky,[28] and Sakai[29] are listed in Table 12. Blister threshold data are summarized by Snelgrove in References 30 and 31.

No typical blister-threshold data exist for U_3Si_2 that contains boron as a burnable poison, although some longer-term annealing studies have been conducted.[13] These data are not included in Figure 3.

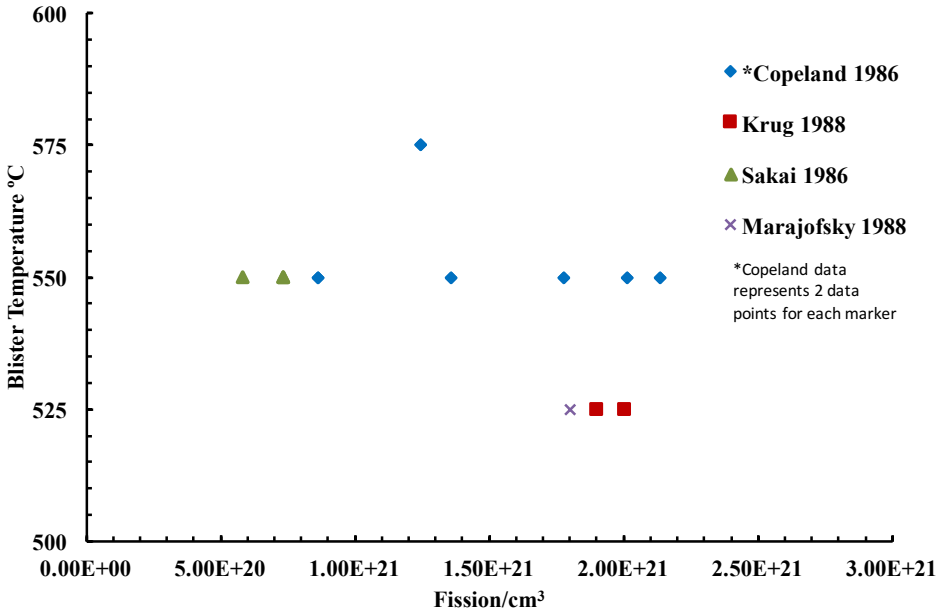

Figure 3. Blister-threshold-temperature data for U_3Si_2 dispersion fuel.

Table 11. U_3Si_2 blister-threshold-temperature data from ORR element testing. Note that the fuel-meat fission densities are estimated based on fuel-element burnup data and fuel density from Reference 9.

Fuel Plate No.	Uranium Density (g U/cm^3)	Average Fuel Meat Fission Density (10^{21} f/cm^3)	Blister Temperature °C
S-3-211-13	4.6	1.24	575
S-3-210-23	4.6	1.24	575
S-3-213-15	4.6	1.77	550
S-3-212-19	4.6	1.77	550
OSIIW-065	5.2	1.35	550
OSIIW-054	5.2	1.35	550
OSIIW-044	5.2	2.14	550
OSIIW-026	5.2	2.14	550
ORR-092	4.9	0.86	550
ORR-100	4.9	0.86	550
ORR-144	4.9	0.86	550
ORR-114	4.9	2.01	550
ORR-123	4.9	2.01	550

Table 12. U_3Si_2 blister threshold temperature data from References 27, 28, and 29.

Fuel Plate No.	Uranium Density (g U/cm^3)	Average Fuel Meat Fission Density (10^{21} f/cm^3)	Blister Temperature °C	Reference
2	4.75	1.9	525	Krug
3	5.04	2.0	525	Krug
NA	4.8	1.8	525	Marajofsky
A1-001	4.8	0.73	550	Sakai
A1-009	4.8	0.73	550	Sakai
B1-020	5.3	0.58	550	Sakai

NA: Not Available

1.4 Monolithic Fuel

1.4.1 Monolithic Fuel Design

The selected design for the conversion fuel system is referred to as "base monolithic fuel" or simply "base fuel", and comprises a uranium–10 wt.% molybdenum alloy (U–10Mo) in the form of a monolithic foil, with thin zirconium (Zr) interlayers, clad in 6061 aluminum (Al), as shown schematically in Figure 4.[32]

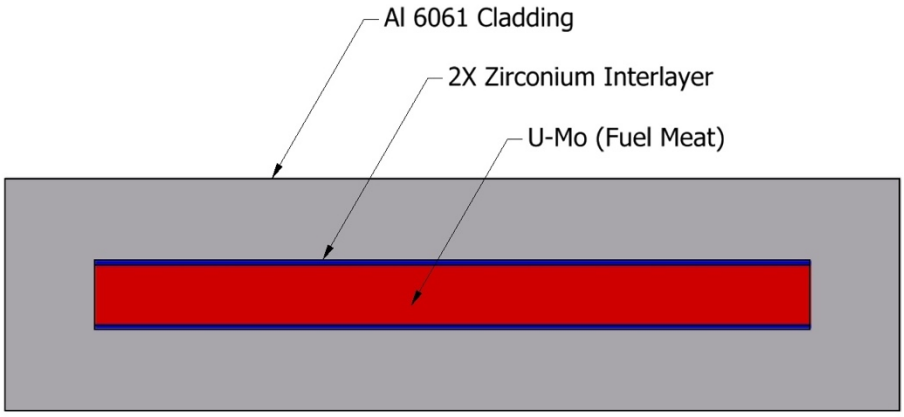

Figure 4. Schematic diagram of the base monolithic fuel.

The fuel foil is formed from a U–10Mo alloy, cast into a coupon, canned in stainless steel using a picture-frame assembly then-hot rolled to desired thickness. The zirconium interlayer is bonded to the U–10Mo alloy via co-rolling during the in-can rolling process. A

detailed description of this process is found in the RERTR–12 Fabrication Summary Report.[33] After rolling and decanning, the foil is sized to meet the nominal geometry shown in the hashed area of Figure 5 for the case of a typical RERTR mini-plate, representing the geometry from which most monolithic blister-anneal-threshold data in this report were obtained. Aluminum cladding is bonded to the fuel foil using hot-isostatic-pressing (HIP) or the friction-bonding (FB) process. The HIP process was selected for fuel qualification, and the FB process is no longer being developed. Some monolithic blister-anneal-threshold data were also obtained from AFIP–4 test plates. The AFIP–4 fuel plates are larger; a drawing is provided in Figure 6. Figure 7 shows an example of the metallographic cross-section of a monolithic fuel plate. Fuel thickness for mini-plates are nominally 0.010, 0.020 and 0.025 in. (0.254, 0.508 and 0.635 mm), and the thickness was 0.013 in. (0.330 mm) for the AFIP–4 plates.

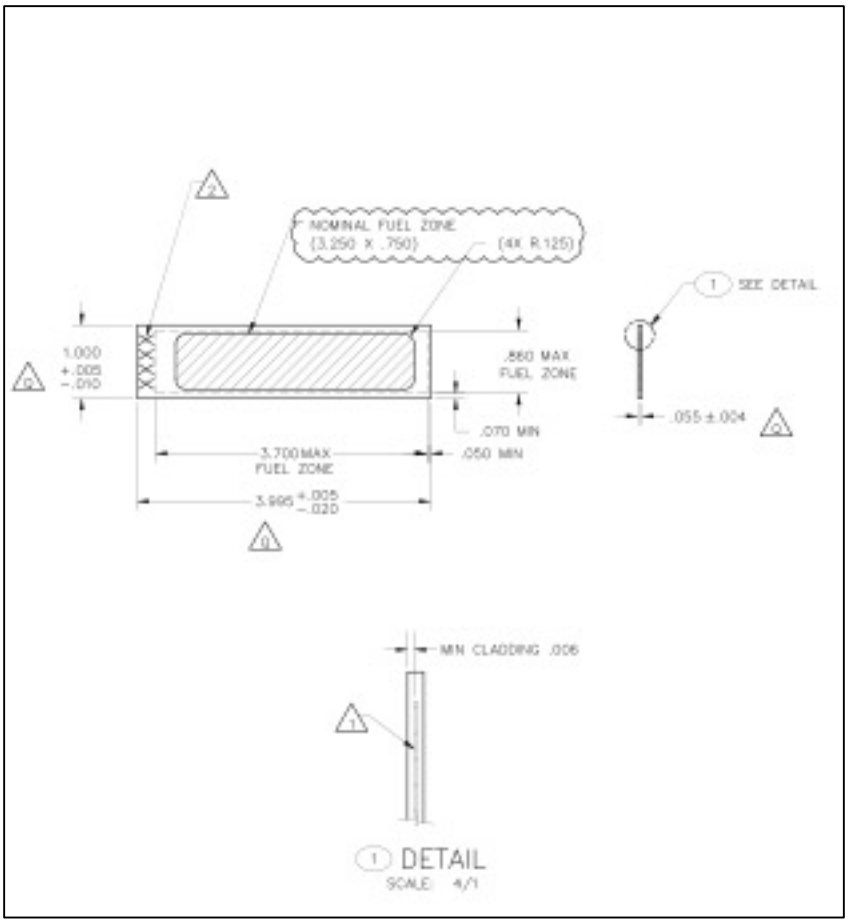

Figure 5. RERTR mini-plate geometry. Dimensions are in inches.

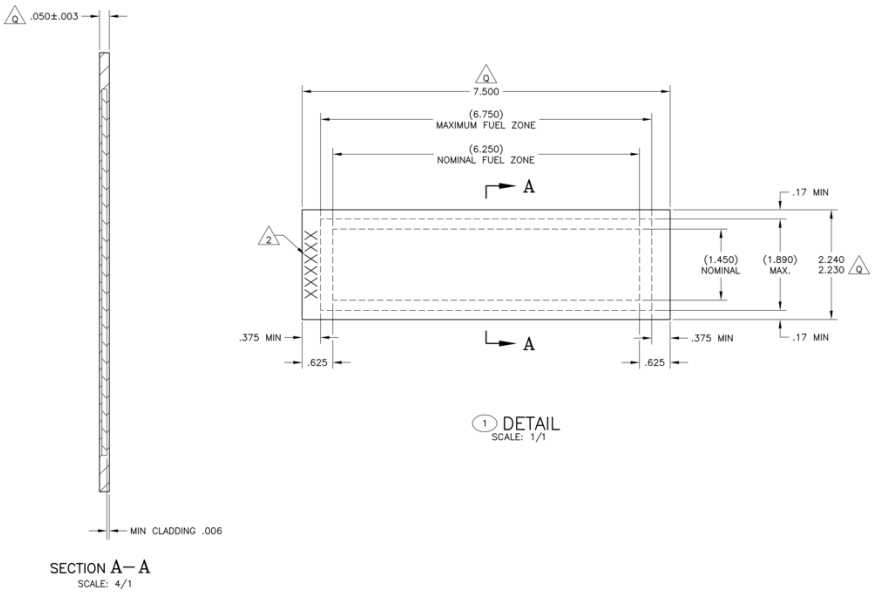

Figure 6. AFIP–4 plate geometry. Dimensions are in inches.

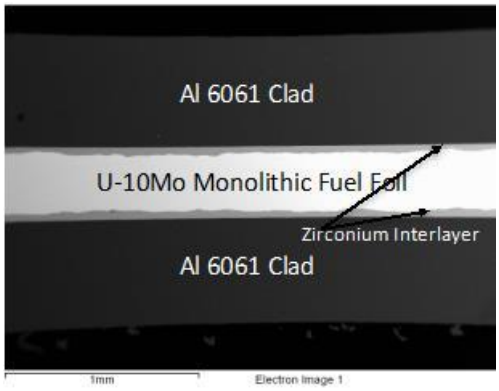

Figure 7. Example of typical cross-section of an unirradiated monolithic fuel plate.

1.5 Blister Threshold System And Test Method

1.5.1 System Description

A top-loading tube-furnace configuration was used for performing Blister Threshold tests on the RERTR and AFIP–4 experimental plates discussed in this report. A sample holder was designed to mate with the furnace that included two independent thermocouples to directly measure the temperature of the fuel plates and to minimize temperature gradients across the test plate. All thermocouples used in the furnace for measurements during blister testing are purchased calibrated from the vendor and verified at the INL Standards and Calibration Laboratory. Figure 8 and Figure 9 illustrate the configuration of the furnace. The entire furnace cavity was characterized for temperature uniformity using the grid resolution show in Figure 9. The specimen test region as indicated by P5 and P6 exhibited a temperature uncertainty of within ±13°C which is the sum of possible error/uncertainty of the instrument strings for the control and independent thermocouple probe readouts.

The independent temperature-monitoring capability was added in 2012 following the discovery of a system vulnerability that resulted in the reset of both temperature readouts to factory settings, likely as a result of a facility power surge. Details for the findings and corrective actions can be found in TEV-1745, “Bakeout Furnace Investigation.” [34] The details

for the corrective actions, which included a formal system evaluation and qualification, can be found in PLN-4434, “Bakeout Furnace Qualification For Testing Of GTRI Fuel Plates,” and TEV-1854, “Bakeout Furnace Qualification for Testing of GTRI Fuel Plates,”[35] respectively. The undetected reset resulted in the reporting of incorrect blister-threshold data. These data were subsequently corrected based on error identification, system-error evaluation, and performance of an additional Blister Threshold campaign[36] using similar plates to qualify the corrected data. The corrected data are identified in Table 13.

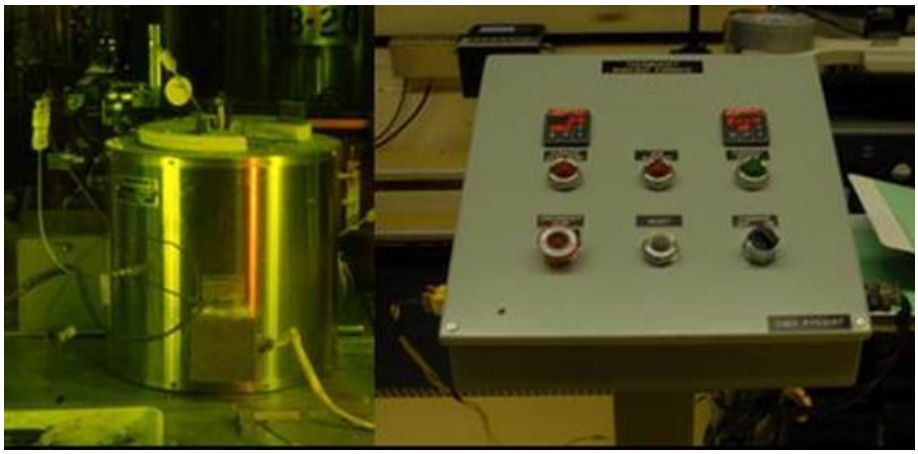

Figure 8. Bakeout furnace system. Left to right, furnace with lid in place and control console.

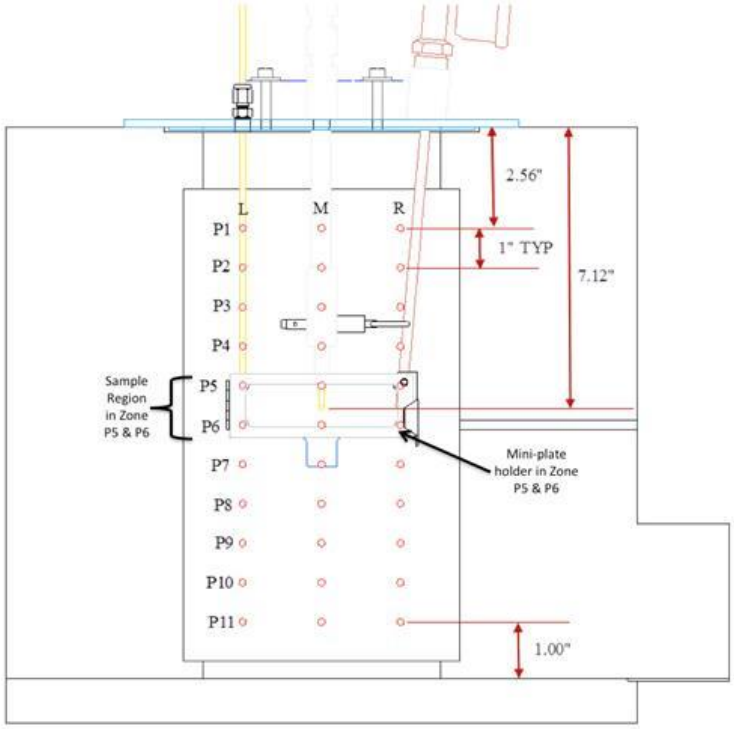

Figure 9. Inner furnace configuration with temperature profile grid.

1.5.2 Test Method

Blister threshold temperature data are obtained by heating irradiated fuel plates at successively higher temperatures between 350 and 550ºC. A plate is held at temperature for a period of time (20 minutes), the furnace is turned off, and then the plate is removed from the furnace and visually examined for blisters. If no blister is observed, the plate is returned to the still warm (~70–130°C) furnace for the next anneal cycle at the next higher temperature setting (increasing in 25°C increments). This process is repeated until a blister is observed. The test is then concluded, and the temperature at which the blister was first observed is recorded as the blister-threshold temperature. The plates are heated per the maximum ramp rate of the furnace (~8°C/min) and cool during inspection for blisters in the ambient cell atmosphere (argon) when withdrawn for inspection, in a way similar to the procedure used in

most of the previous blister testing. The cell in which testing is conducted has an argon atmosphere, which is typically at ~30°C.

The visual examination for identification of blisters is accomplished using a telescopic camera lens, binoculars, and additional local in-cell lighting. Verification of the presence or absence of blisters is provided by at least two observers. Photographs are taken of the plate being tested between each blister-anneal cycle to provide a record of blisters and other changes in the appearance of the plate.

The inherent temperature uncertainty of the system and test protocol is ±13°C (comprising accuracy of the thermocouple and controller/readout, furnace temperature uniformity and test-environment noise) and ±24°C (introduced by the temperature-increment increase), respectively.

1.6 Blister Threshold Test Results

A total of 28 mini-plates plates were tested using the standard blister testing protocol and four AFIP–4 plates were used to study the effect of thermal cycling on blister-threshold temperature. Blister-threshold temperature data for all 32 plates tested are provided in Table 13. The data reported for the RERTR–12 are based on preliminary neutronic analyses. An H or P in the plate identification (ID) number indicates a plate fabricated using HIP (26 plates). An F or B in the plate ID indicates a plate fabricated by FB (6 plates).

Blister threshold temperature data are plotted as a function of plate-average fission density in Figure 10. Thirty-two (32) plates were tested. Data were fit to the trend model of equation 1:

$$T_b = 1.05\times10^6\times f^{-0.158} \quad (1)$$

where T_b is the measured blister threshold temperature, and f is the plate average fission density in fissions/cm^3. Trend development was accomplished using linear regression[37] methods. The trend model represents expected blister-threshold temperatures as a function of fission density. The 95% confidence interval is generated relative to the trend model, and the scatter in the actual data and is approximately ±50°C. The trend and confidence intervals are plotted with the measured blister-threshold data in Figure 10. A summary of irradiation test conditions is included in Appendix B.

The blister-threshold temperature of monolithic fuel and the scatter in the data are consistent with the blister-threshold temperature of previously qualified fuel systems within the range of fission densities previously tested, as shown in Figure 11. However, the monolithic fuel data extend to much higher fission-density and burnup levels. Moreover, some HEU monolithic plates achieved fission densities beyond those achievable with LEU. The estimated fission density[38] for 100% LEU burnup is 7.78 x 10^{21} fissions/cm^3.

Table 13. Monolithic fuel blister-anneal-test data.

Experiment	Plate ID	Description	Average Fission Density (fissions/cm^3)	Blister-threshold Temperature (°C)
RERTR–9B	L1P10T	U–10Mo Monolithic; 0.010 inch fuel foil; HIP; 58% Enriched; Co-Rolled Zr	5.70 x 10^{21}	400
RERTR–10A	L1P30Z	U–10 Mo; 0.010 inch fuel foil; HIP; 67% Enriched; Co-Rolled Zr	2.88 x 10^{21}	400
	L2P15Z[c]	U–10 Mo; 0.020 inch fuel foil; HIP; 33% Enriched; Co-rolled Zr; Constrained Plate	1.34 x 10^{21}	475
RERTR–10B	L2F47Z[c]	U–10 Mo; 0.020 inch fuel foil; FB; 33% Enriched; Co-rolled Zr	1.75 x 10^{21}	500
	L2F46Z[a,c]	U–10 Mo; 0.020 inch fuel foil; FB; 33% Enriched; Co-rolled Zr	2.25 x 10^{21}	456
RERTR–12 X1	L1P772[a]	U–10Mo; 0.010 inch fuel foil; HIP; 70% Enriched; Co-rolled Zr; Foil Anneal 1 hr@650C	4.95 x 10^{21}	424
	L1P460[a,c]	U–10Mo; 0.010 inch fuel foil; HIP; 40% Enriched; Co-rolled Zr	1.96 x 10^{21}	521

Experiment	Plate ID	Description	Average Fission Density (fissions/cm^3)	Blister-threshold Temperature (°C)
	L1P592[a]	U–10Mo; 0.010 inch fuel foil; HIP; 50% Enriched; Co-rolled Zr	2.35 x 10^{21}	456
	L1P774[a]	U–10Mo; 0.010 inch fuel foil; HIP; 70% Enriched; Co-rolled Zr; Foil Anneal 1 hr@650C	4.78 x 10^{21}	424
RERTR–12 X2	L1P595[a]	U–10Mo; 0.010 inch fuel foil; HIP; 50% Enriched; Co-rolled Zr	2.95 x 10^{21}	424
	L1P758[a]	U–10Mo; 0.010 inch fuel foil; HIP; 70% Enriched; Co-rolled Zr	4.33 x 10^{21}	391
	L1P463[a,c]	U–10Mo; 0.010 inch fuel foil; HIP; 40% Enriched; Co-rolled Zr	2.45 x 10^{21}	456
	L1P756[a]	U–10Mo; 0.010 inch fuel foil; HIP; 70% Enriched; Co-rolled Zr	5.88 x 10^{21}	391
RERTR–12 X3	L1P596[a]	U–10Mo; 0.010 inch fuel foil; HIP; 50% Enriched; Co-rolled Zr	3.83 x 10^{21}	398
	L1P464[a]	U–10Mo; 0.010 inch fuel foil; HIP; 40% Enriched; Co-rolled Zr	3.19 x 10^{21}	398
	L1P590[a]	U–10Mo; 0.010 inch fuel foil; HIP; 50% Enriched; Co-rolled Zr	4.02 x 10^{21}	398
	L1P465[a]	U–10Mo; 0.010 inch fuel foil; HIP; 40% Enriched; Co-rolled Zr; Foil Anneal 1 hr@650C	3.28 x 10^{21}	398
RERTR–12 Z	L1P787[a]	U–10Mo; 0.010 inch fuel foil; HIP; 70% Enriched; Co-rolled Zr	6.38 x 10^{21}	365
	L1P7A1[a]	U–10Mo; 0.010 inch fuel foil; HIP; 70% Enriched; Co-rolled Zr	4.28 x 10^{21}	365
RERTR–12 Y1	L5P1B5	U–10Mo; 0.025 inch fuel foil; HIP; 10% Enriched; Co-rolled Zr	3.64 x 10^{20}	>550[b]
RERTR–12 Y3	L5P3B2	U–10Mo; 0.025 inch fuel foil; HIP; 30% Enriched; Co-rolled Zr	2.42 x 10^{21}	475
	L5P2C8	U–10Mo; 0.025 inch fuel foil; HIP; 20% Enriched; Co-rolled Zr	1.11 x 10^{21}	>550[b]
	L5P1B8	U–10Mo; 0.025 inch fuel foil; HIP; 10% Enriched; Co-rolled Zr	6.91 x 10^{20}	>550[b]
RERTR–12 Z	L2P498	U–10Mo; 0.020 inch fuel foil; HIP; 40% Enriched; Co-rolled Zr	2.02 x 10^{21}	475
AFIP–4	L1H34Z[a]	U–10Mo; 0.013 inch fuel foil; HIP; 20% Enriched; Co-rolled Zr	2.51 x 10^{21}	456
	L1H36Z[a]	U–10Mo; 0.013 inch fuel foil; HIP; 20% Enriched; Co-rolled Zr	4.45 x 10^{21}	391
	L1B33Z[a]	U–10Mo; 0.013 inch fuel foil; FB; 20% Enriched; Co-rolled Zr	4.06 x 10^{21}	391
	L1B51Z[a]	U–10Mo; 0.013 inch fuel foil; FB; 20% Enriched; Co-rolled Zr	4.56 x 10^{21}	391
Thermal Cycle Test Plates				
AFIP–4 Thermal Cycle	L1B32Z[a]	U–10Mo; 0.013 inch fuel foil; FB; 20% Enriched; Co-rolled Zr	4.09 x 10^{21}	359

Experiment	Plate ID	Description	Average Fission Density (fissions/cm^3)	Blister-threshold Temperature (°C)
	L1B52Z	U–10Mo; 0.013 inch fuel foil; FB; 20% Enriched; Co-rolled Zr	4.20 x 10^{21}	N/A
	L1H35Z[a]	U–10Mo; 0.013 inch fuel foil; HIP; 20% Enriched; Co-rolled Zr	3.80 x 10^{21}	391
	L1H38Z[a]	U–10Mo; 0.013 inch fuel foil; HIP; 20% Enriched; Co-rolled Zr	3.90 x 10^{21}	391

a. Blister-threshold temperatures for all the Blister Threshold tested X1, X2 and X3 capsule plates from RERTR-12 and AFIP-4 plates do not demonstrate the 25 degree temperature increment due to a system reset that went undetected following the Blister Threshold tests performed on the previous the RERTR experiment plates. The furnace console Watlow controller reset to a Type J readout/control instead of a Type K readout. The thermocouple probe for the furnace control is a Type K and therefore the anneal temperatures were controlled based on Type J signal voltage instead of the Type K signal voltage. These values were later corrected based on millivolt and cold junction correction values for Type K thermocouples, the resultant test temperatures are not incremented the same as for the Type K controller setting.

b. Plates did not exhibit any blister indications during visual exam following the maximum Blister Threshold test temperature of 550°C.

c. Plates that exhibited Type-1 blisters. See Blister Morphology section.

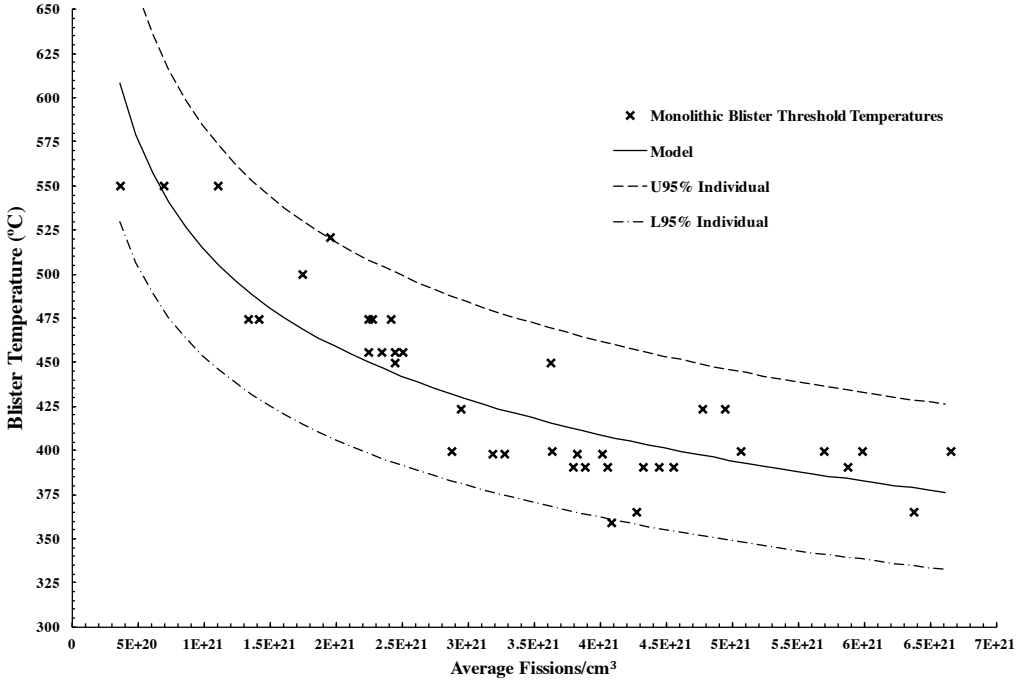

Figure 10. Monolithic fuel blister-threshold temperatures as a function of plate average fission density. 95% confidence intervals are shown. This plot includes plates that were part of thermal cycle testing and blistered; plate L1B52Z did not fail during this testing and is not shown. Three additional plates (indicated) did not fail after testing to 550°C.

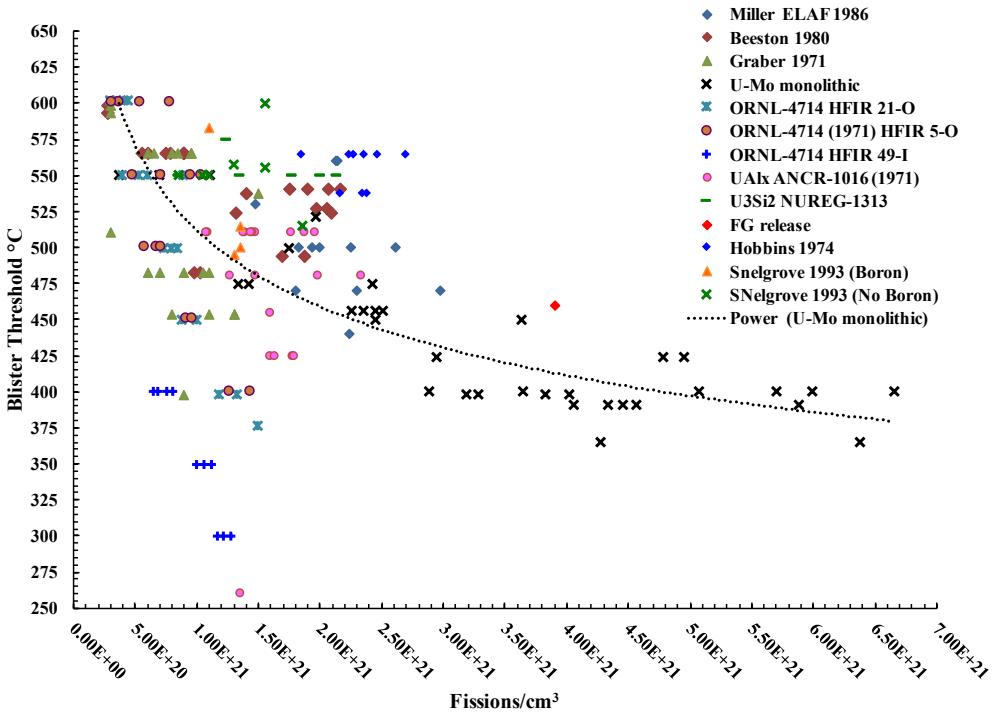

Figure 11. Monolithic and dispersion blister-threshold temperatures as a function of plate average fission density. Equation 1 for U–Mo monolithic fuel is plotted as a trend line.

1.6.1 Blister Location

A total of 71 blisters were identified over or adjacent to the fueled region of the plate on the 32 fuel plates tested. Because of the increased moderator-to-fuel ratio at the edges of the fuel plates, fission rates and fission densities are higher in the edge and corner regions of the fuel zone. The influence of edge/corner-peaking effect is illustrated in Figure 12 for plate L1P756 from the RERTR–12 campaign, with a contour plot of the plate local fission densities as a function of location on the plate. Figure 13 of the top two node rows for L1P756 provides additional clarity regarding the fission-density peaking effect. All blisters formed are associated with the higher fission density edge and/or corner regions of the plates. In addition to being locations where fission density is high, the fuel foil edges and corners are also high-stress regions because of in-plane creep of the fuel meat resulting in a thick

"bulged" region slightly in from the fuel-foil edge. [39, 40] An example of the bulged-edge region of a fuel plate is shown in Figure 14.

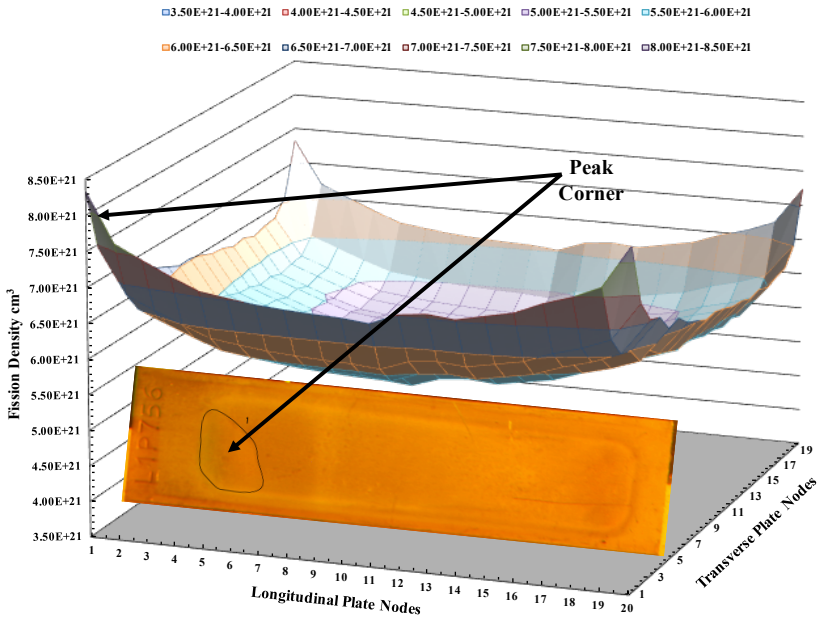

Figure 12. Photograph of blister on plate L1P756 along with the fission-density profile. Blister occurred in the highest fission-density region of the fuel plate.

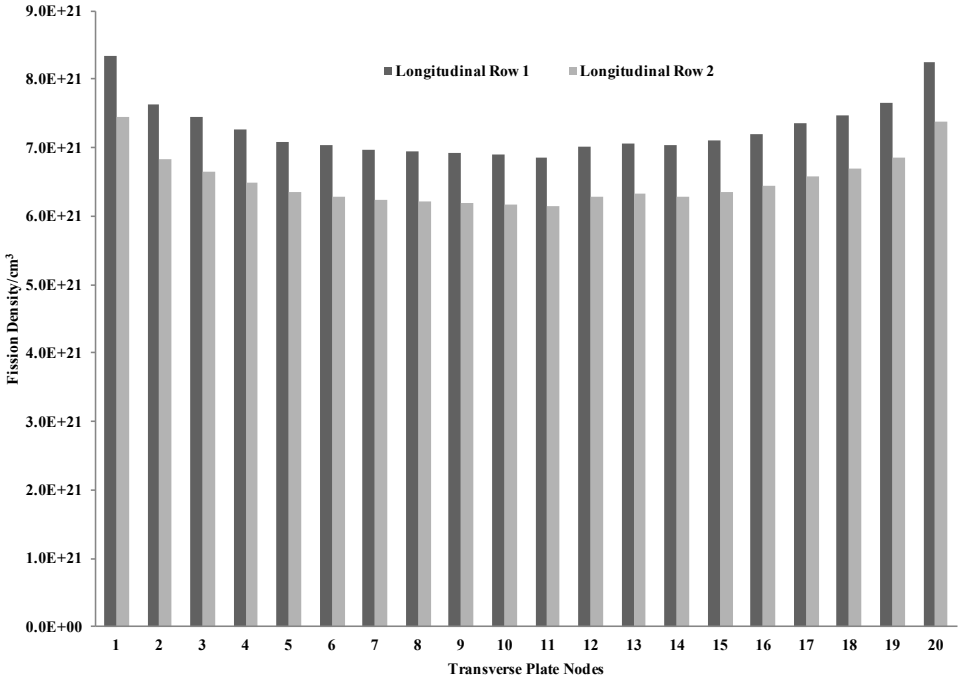

Figure 13. Nodal gradient for the two top longitudinal node rows for plate L1P756.

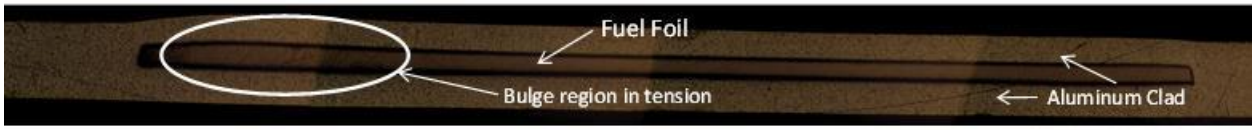

Figure 14. Plate L1P784 montage illustrating bulge in the region near the edges of the fuel foil resulting from fuel relocation caused by fuel creep. The fuel region is 0.75 in. (19 mm) across and the plate average fission density is 5.70 x 10^{21} fissions/cm^3.

1.6.2 Blister Morphology

Two blister types have been identified in the monolithic fuel system. Examples of the surface morphology of both blister types are shown in Figure 15. Type 1(T1) blisters are found in some plates with fission densities less than 4.0E+21 fissions/cm^3. They are characterized by minimal encroachment of the blister into the fuel foil, with the primary growth moving into the cladding-to-cladding bond and propagation toward the edge of the fuel plate, in some cases resulting in a breach (Figure 17). Type 2 (T2) blisters are different from Type 1 blisters in that they do not involve the cladding-to-cladding interface. These blisters form only in the fuel region and extend into or over the fuel foil. The fuel cracking pattern is illustrated in Figure 17, showing the cross-sections of both types of blisters on plate L1P460. Examples of larger Type 2 blisters are shown in Figure 18. Type 1 blisters only occurred at low fission density and exhibited high blister-threshold temperatures. Figure 16 plots the occurrence of Type 1 and Type 2 blisters as a function of fission density. While Type 1 blisters represented ~20% of the blisters evaluated only ~13% of the plates blister threshold tested exhibited this type. Moreover, 60% of the Type 1 blisters were found on plate L1P460.

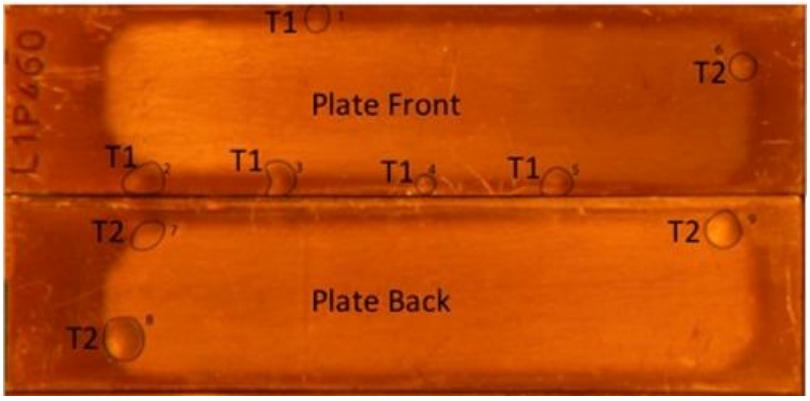

Figure 15. Plate L1P460, with average fission density of 1.96 x 10^{21}, features both T1 and T2 blister types.

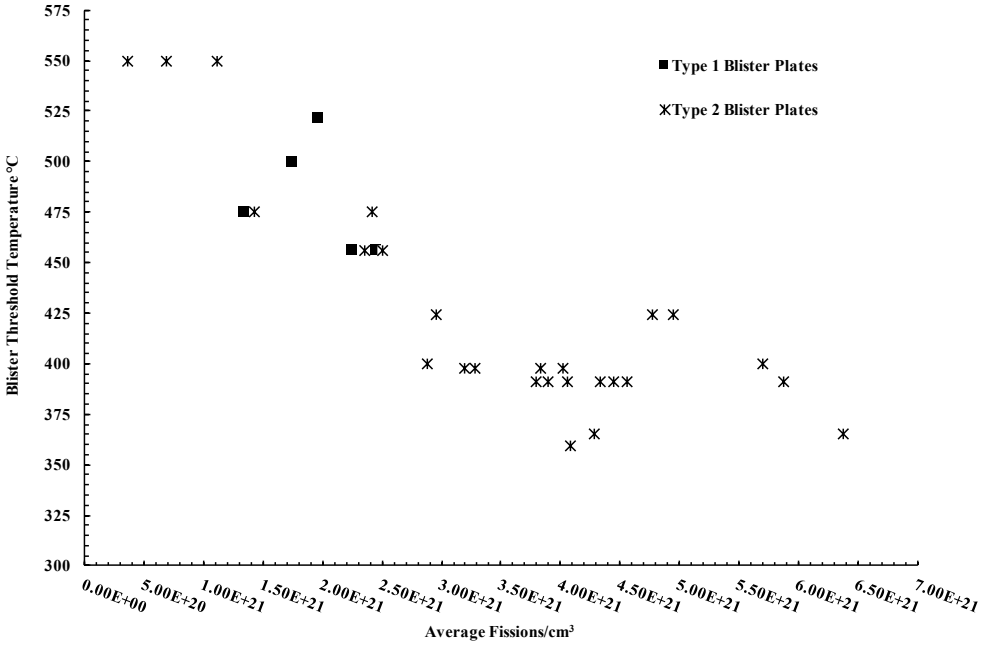

Figure 16. Type 1 and Type 2 blister-threshold temperatures.

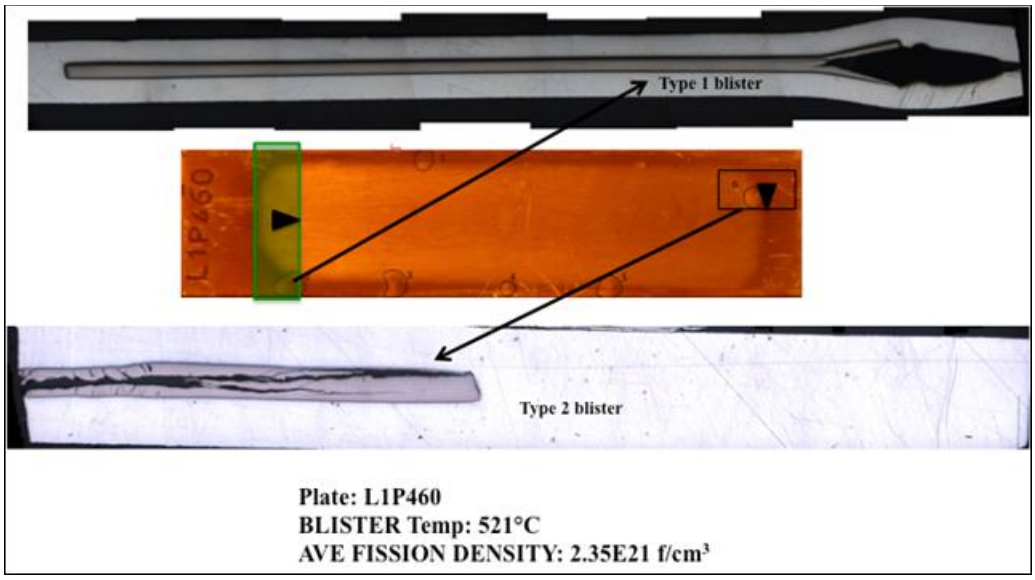

Figure 17. Plate L1P460 (blister threshold: 521°C; fissions/cm^3: 1.90 x 10^{21}) micrographs featuring both Type 1 (top) and Type 2 (bottom) blister propagation behavior.

Figure 18. Larger T2 blister types shown for plates L1P774 with an average fission density of 4.78 x 10^{21} fissions/cm^3.

1.6.3 Blister Termination

The region of the fuel plate where the blisters terminate has been characterized in blistered fuel plates L1P772 and L1P774 using neutron radiography. Figure 19 shows both a photograph of a blistered fuel plate and a radiograph of the fuel foil in the same orientation. The radiographic images of the fuel foils show that fuel cracking has occurred at the edge of Type 2 blisters, and it is hypothesized that termination of blisters is associated with this cracking.

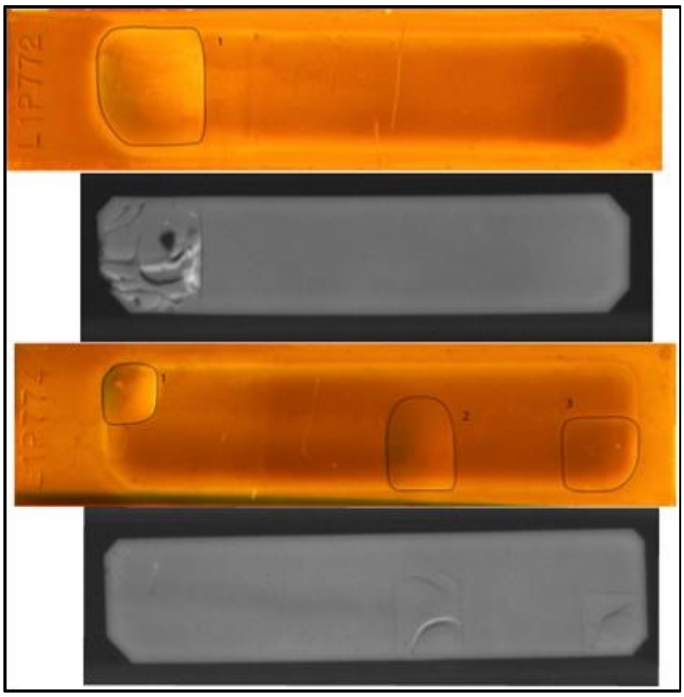

Figure 19. Neutron radiography of plates L1P772 (top) and L1P774 (bottom) both with blister thresholds of 424°C and fissions/cm^3 of 4.95 x 10^{21} and 4.78 x 10^{21} respectively, showing breaks in the fuel foil at the blister-termination locations.

1.6.4 Effects of Fabrication Process

Figure 20 compares the blister threshold temperature of fuel plates fabricated by FB and HIP bonding. Blister-threshold temperature from only five blistered plates are included in the friction bonding data set; the remaining 26 plates were fabricated using HIP. The sixth friction-bonded plate (L1B52Z) did not fail as part of thermal cycle testing. The limited data set for the FB plates do result in a wider 95% confidence interval, with the lower-fission-density plates overlapping the HIP plates more uniformly while the higher-fission-density plates appear to trend to lower blister-threshold temperatures. Nonetheless, blister-threshold temperatures and data scatter are similar with the fitted trend models, and their overlapping 95% confidence intervals indicate there is not a statistically significant difference in blister-threshold temperature for plates fabricated by the two different methods. Figure 21 shows that the data points for the FB plates lay within the 95% confidence interval for the

distribution. Therefore, for the purposes of this report, data on FB plates have been included as part of the blister-threshold temperature data set, even though the cladding bonding process is different than the down selected fuel fabrication process to be qualified for use in reactor conversion.

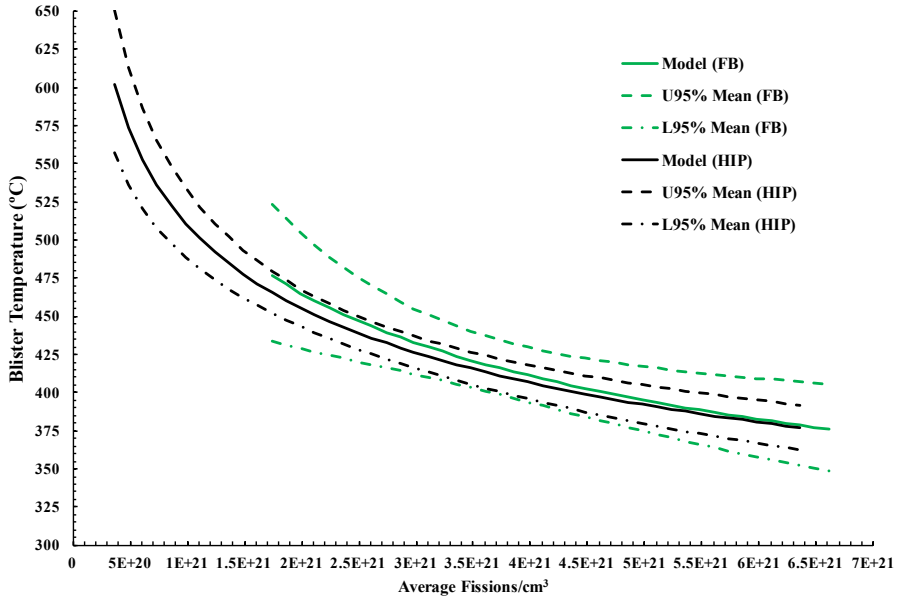

Figure 20. Best fit models for HIP and FB different bonding methods between the fuel meat and clad material. Note that no high-burnup data were available for the FB method, which accounts for greater agreement at low-burnup values, as opposed to high.

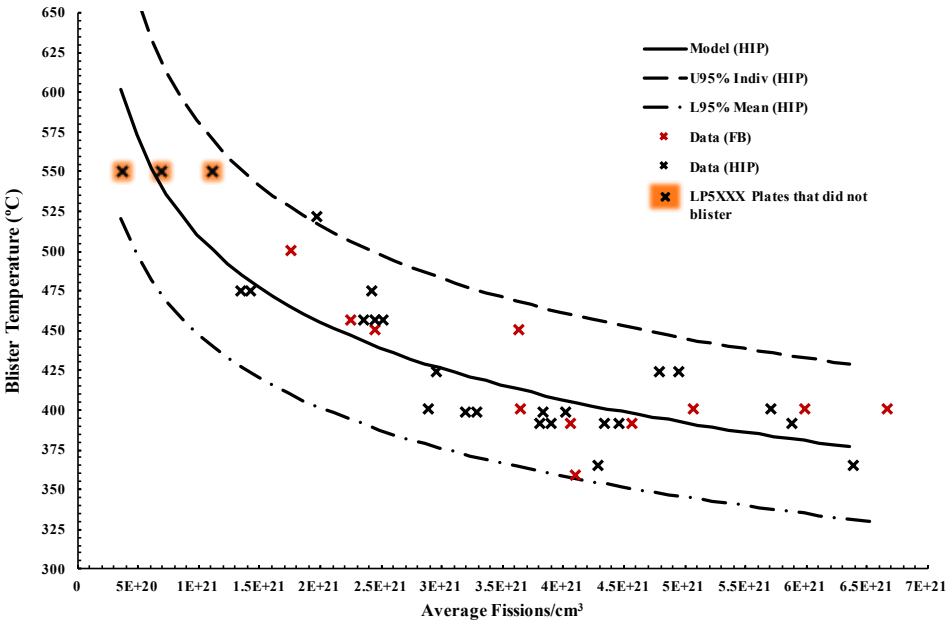

Figure 21. Blister threshold results for HIP and FB with HIP Model and 95% confidence uncertainty bounds.

1.6.5 Foil Thickness

Figure 22 plots blister-threshold data differentiated by fuel foil thickness. The blister-threshold data plotted in Figure 22 do not indicate that a change in blister-threshold temperature results from a change in fuel foil thickness. However, the uncertainty of the trend (a plot illustrating the uncertainties is found in Appendix A) for each set is significant due, in part, to the small individual data sets for fuel plates with thicker fuel foils, these being fuel foil thicknesses (nominal) of 0.013 (AFIP–4 plates), 0.020 (L2PXXX plates) and 0.025 (L5PXXX plates) in. (0.33, 0.51 and 0.64 mm). Fuel plates with thicker fuel foils and, thus, thinner cladding, have not been tested at fission densities >5.0 x 10^{21} fissions/cm^3.

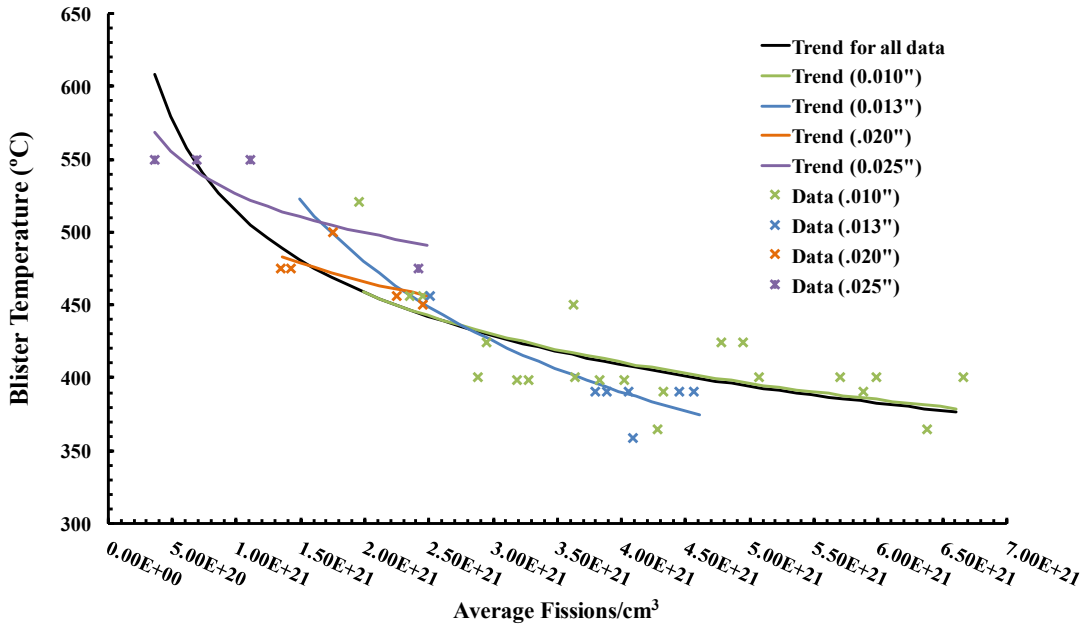

Figure 22. Trend plot for blister-threshold temperatures relative to fuel meat thickness.

1.7 Scale-up Observations

AFIP–4 experiment plates are the first scale-up plate geometry from the monolithic fuel system to be Blister Threshold tested. The statistical analysis with the 95% confidence intervals placed about the trend for the means of both the mini-plate data and the AFIP–4 plate data (see Figure 23) show an overlap of the two intervals. An overlap in confidence intervals is an indication that the difference in trend behavior between two model fits is not statistically significant at lower fission densities. However, while this is apparent in the lower fission densities of the larger plates that have been Blister Threshold tested to date, it can be seen that at fission densities greater than, for example, 3.80 x 10^{21} fissions/cm^3, where much of the monolithic data exist, the model and confidence intervals do not overlap, suggesting there could be a size effect. Moreover, the confidence interval around the one data point at the lower fission density is clearly wider than around the other six data points. Future Blister

Threshold testing on larger plates are expected to reduce the uncertainties in the trend model for larger fuel plates and will better elucidate scale-up effects.

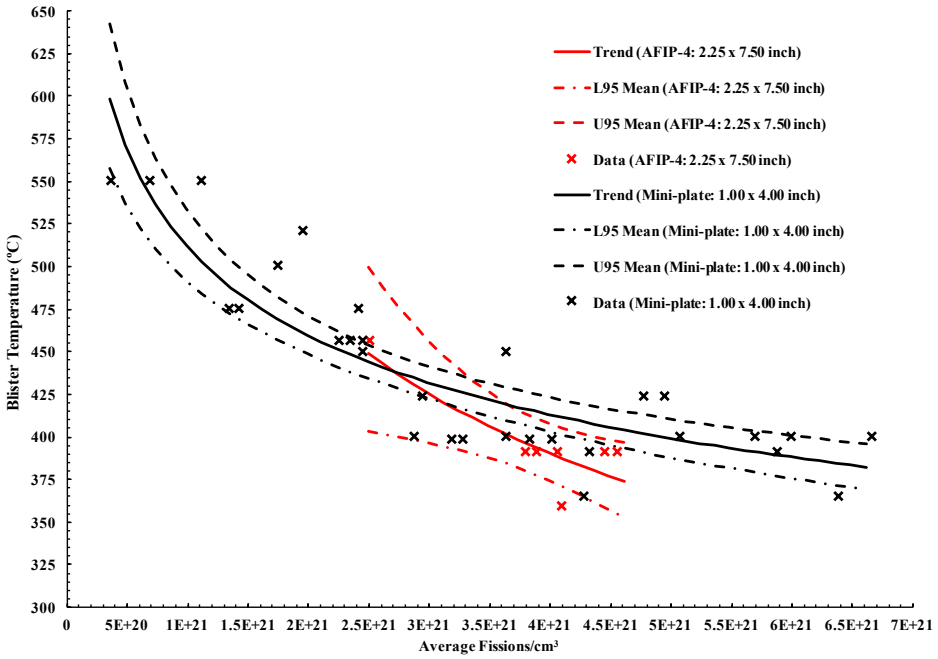

Figure 23. Mini-plate and AFIP-4 blister threshold prediction models with 95% confidence intervals showing evaluation of statistical significance between trend behaviors.

1.8 Irradiation Variables

1.8.1 Fission Heating Rate

Because LEU fuel plates tested over the same range of fission densities (maximum average value 6.38 x 10^{21} fissions/cm^3 and maximum peak value 9.20 x 10^{21} fissions/cm^3) would have a lower fission heating rate compared to HEU plates, there is interest in knowing whether fission-heat rate plays a role in blister threshold temperature. Blister-threshold temperature is plotted against fission heat rate in Figure 24. The type of fabrication process and fuel-foil thickness is also identified on the plot. The data demonstrate significant scatter, with a weak correlation between blister-threshold temperature and fission-heat rate. No effect of fission-heat rate on blister-threshold temperature was noted for the different clad-

application methods or for thick versus thin fuel foils. A co-variant analysis suggests that blister-threshold temperature is a function of both fission density and fission-heat rate.

A model for blister temperature was generated using an analysis of variance based on the factors fission density, heat rate, and their interaction (i.e., the product of heat rate and fission density), and the results are represented in Figure 25. The resulting model was statistically significant, with an R-squared value of 0.86. The fission-density term was identified as the most significant contributor to variability in blister temperature, followed by the interaction between heat rate and fission density. The fission-heat-rate term itself was not statistically significant.

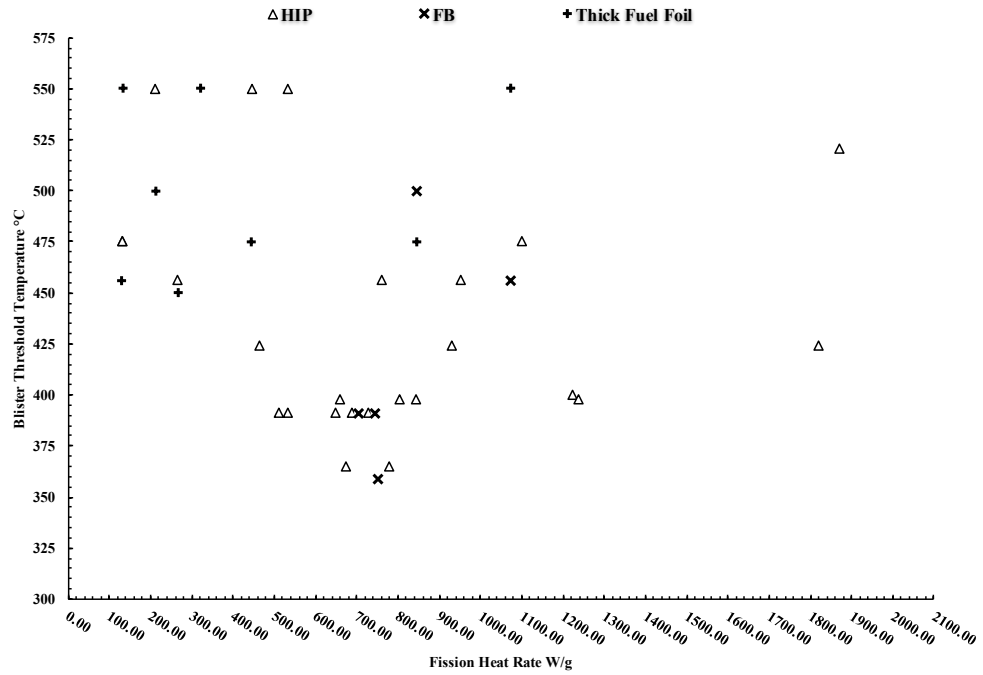

Figure 24. Plot of fabrication variables relative to fission heat rate during irradiation.

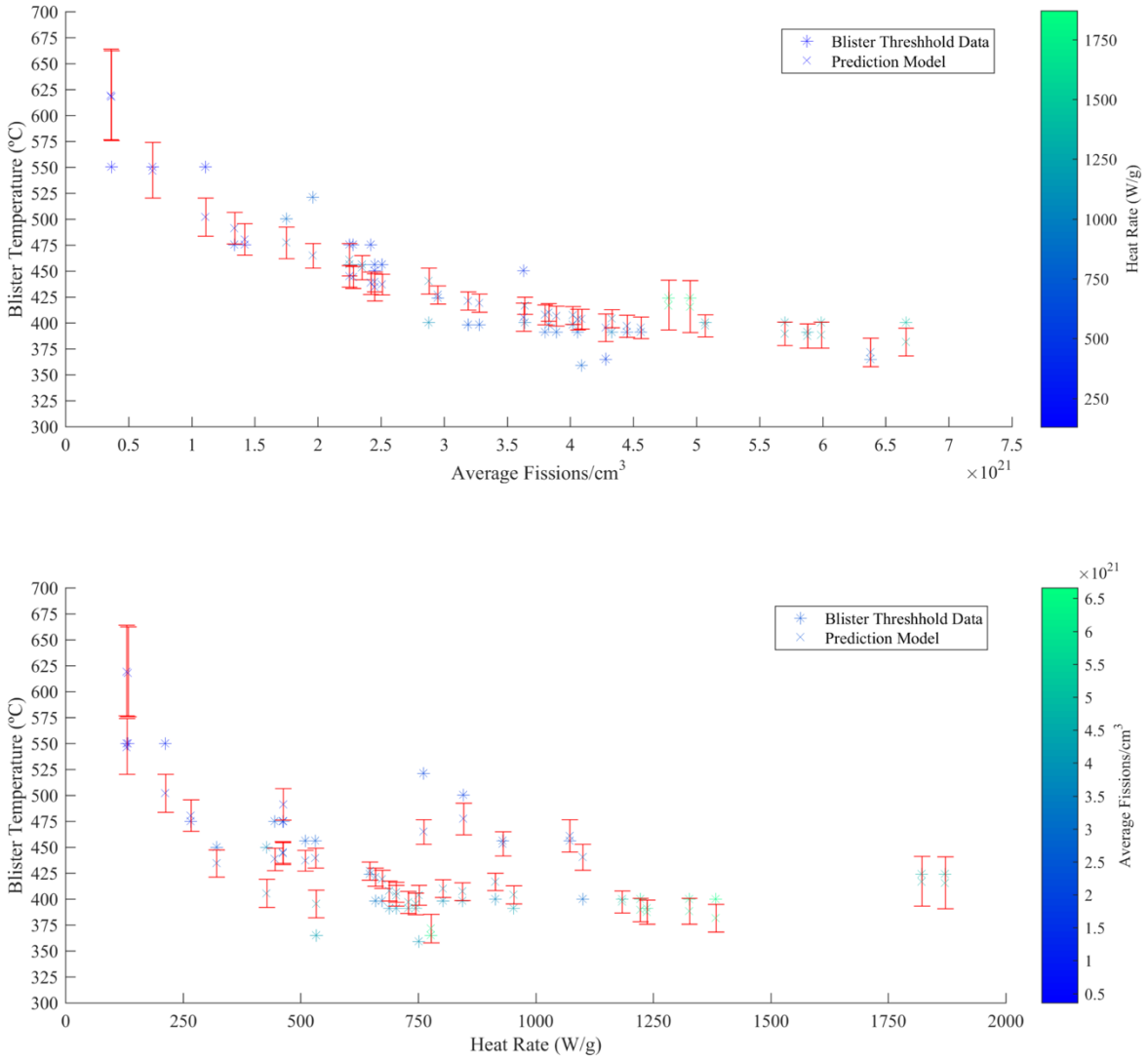

Figure 25. Co-variant analysis of fission heat rate and fission density.

1.9 The Effect of Thermal Cycling on Blister Threshold Temperature

Plates were tested in pairs to determine whether there is a significant effect of thermal cycling during blister-threshold testing on the measured blister-threshold temperature. Paired AFIP–4 plates of similar fission density and the same method of clad bonding were used in this testing. One plate in each pair was subjected to thermal cycling at a given temperature. The second, nominally identical plate was annealed at constant temperature for the same total time-at-temperature. After a predetermined number of thermal cycles-(or time)-at-

temperature, the furnace temperature was increased, and the testing repeated on each plate until a blister formed. In this way, a direct comparison of the effect of thermal cycling on blister-threshold temperature can be made.

To clarify the testing protocol, the furnace schedule used for testing is provided in Table 14. The blister-threshold temperature of each plate is listed in Table 15. Figure 26 plots the thermal profile of plates that were thermally cycled alongside those that were subjected to an integrated (steady-state) anneal. The formation of the first blister is indicated on the plots. Figure 27 shows that when plates are subjected to thermal cycling, no notable decrease in blister-threshold temperature was observed. This limited data set suggests that time at temperature is the primary influence on the formation of blisters during the Blister Threshold test.

It is also noteworthy that three mini-plates (L5PXXX plates with 0.025 inch [0.63 mm] fuel foil thickness [see Table 13, note b]) did not blister at the maximum anneal temperature (550°C) following the nine thermal cycles that result from the standard blister-testing protocol. This implies that the monolithic fuel system is robust with regard to thermal cycling.

Table 14. Thermal cycle and steady state blister testing schedules.

Temperature, °C	326	359	391
# Cycles	13	12	11
Integrated annealing cycle time (min)	260	240	220

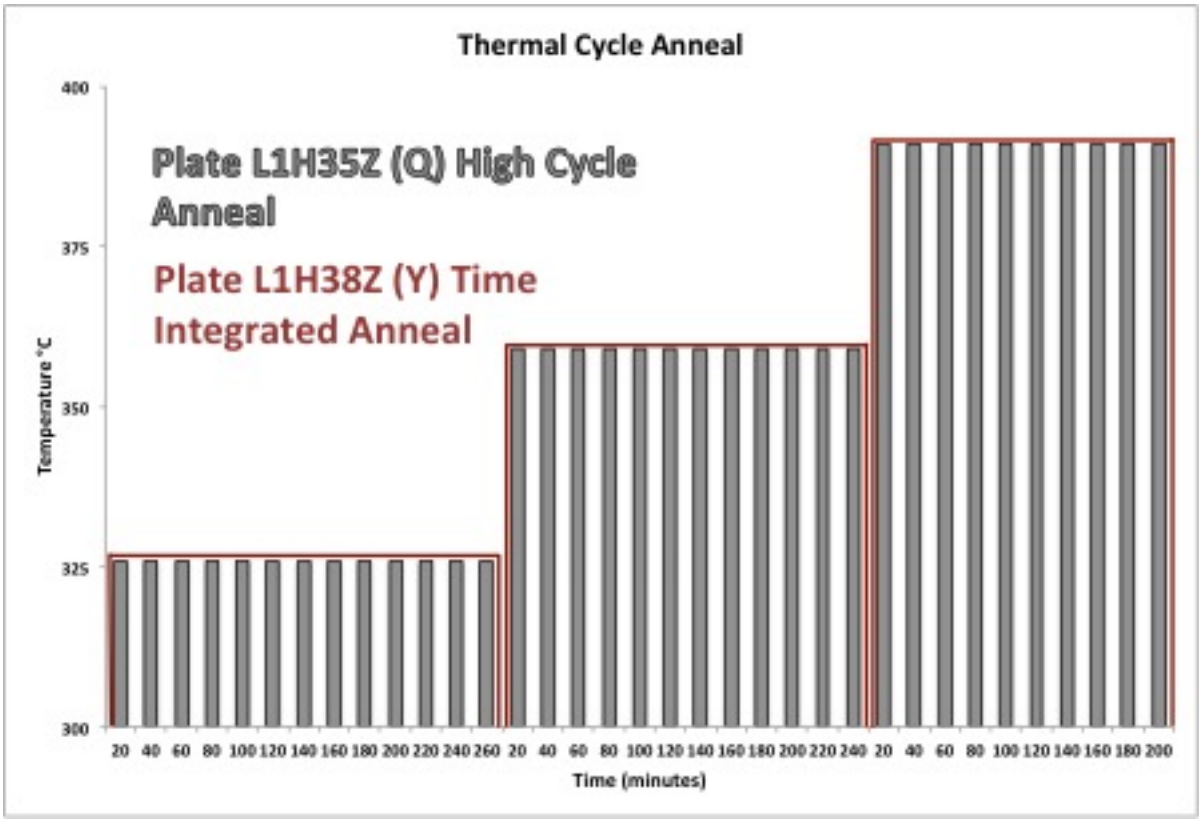

Figure 26. Thermal cycle anneal history of plate pair L1H35Z and L1H38Z. Both plates were fabricated using hot isostatic pressing.

Table 15. Thermal cycle test results.

Sample		Average Fission Density	Anneal Type	Number Cycles at 326°C	Number Cycles at 359°C	Number Cycles at 391°C	Final Blister Temp °C	Total Thermal Cycles
Plate Set 1	L1B32Z (Q)	4.09×10^{21}	Cycle	13	12	None	359	25
	L1B52Z (Y)	4.20×10^{21}	Integrated	1 for 260 min	1 for 100 min	None	N/A	2
Plate Set 2	L1H35Z (Q)	3.80×10^{21}	Cycle	13	12	10	391	35
	L1H38Z (Y)	3.90×10^{21}	Integrated	1 for 260 min	1 for 240 min	1 for 200 min	391	3

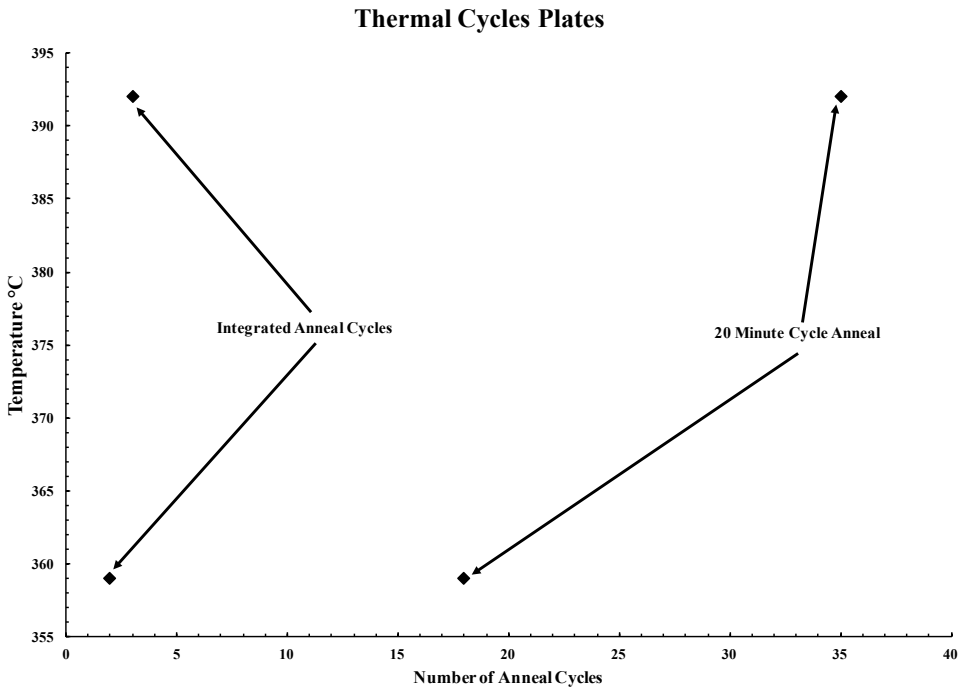

Figure 27. Plot of blister-threshold temperature for plates that were subject to thermal cycling (right side of plot) vs. annealing at constant temperature for the same time at temperature (left side of plot).

1.10 Effect of Additional Testing on Confidence Interval

Figure 29 shows the monolithic fuel blister-threshold-temperatures as a function of plate-average fission density, along with the power law trend curve (Equation 1) and the 95% mean and individual confidence bounds. The scatter in the data and the number of data points used in the regression are contributing factors to the width of both the mean and individual confidence intervals. For the power law fit based on 32 data points, the width of the mean confidence interval is approximately 10°C, corresponding to a standard error of approximately 5°C.

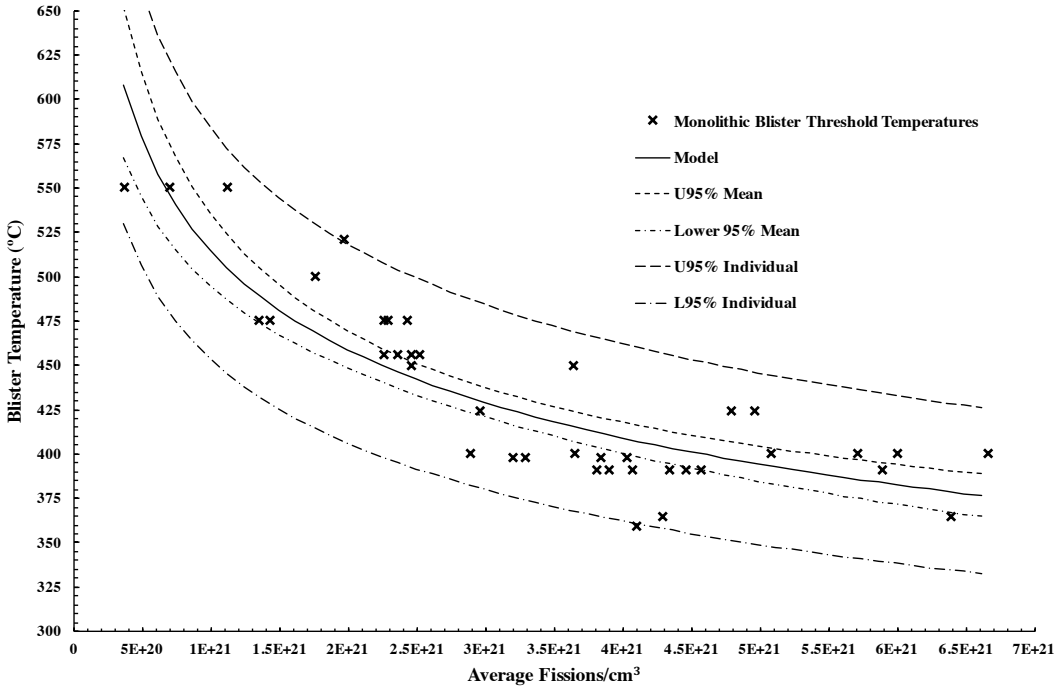

Figure 28. Illustration of the mean and individual confidence intervals relative to the regression model.

Additional blister-threshold testing is planned during future irradiation testing, with a focus on plates fabricated using commercially viable fabrication processes. Assuming that future blister-threshold-temperature data have the same distribution about the trend line as the current data set, testing of additional specimens would reduce the width of the mean confidence interval approximately 2°C as shown in Figure 29. Reduction of the individual (distribution) confidence bounds will follow a similar trend. The number of blister tests to be performed will be based on reactor data requirements.

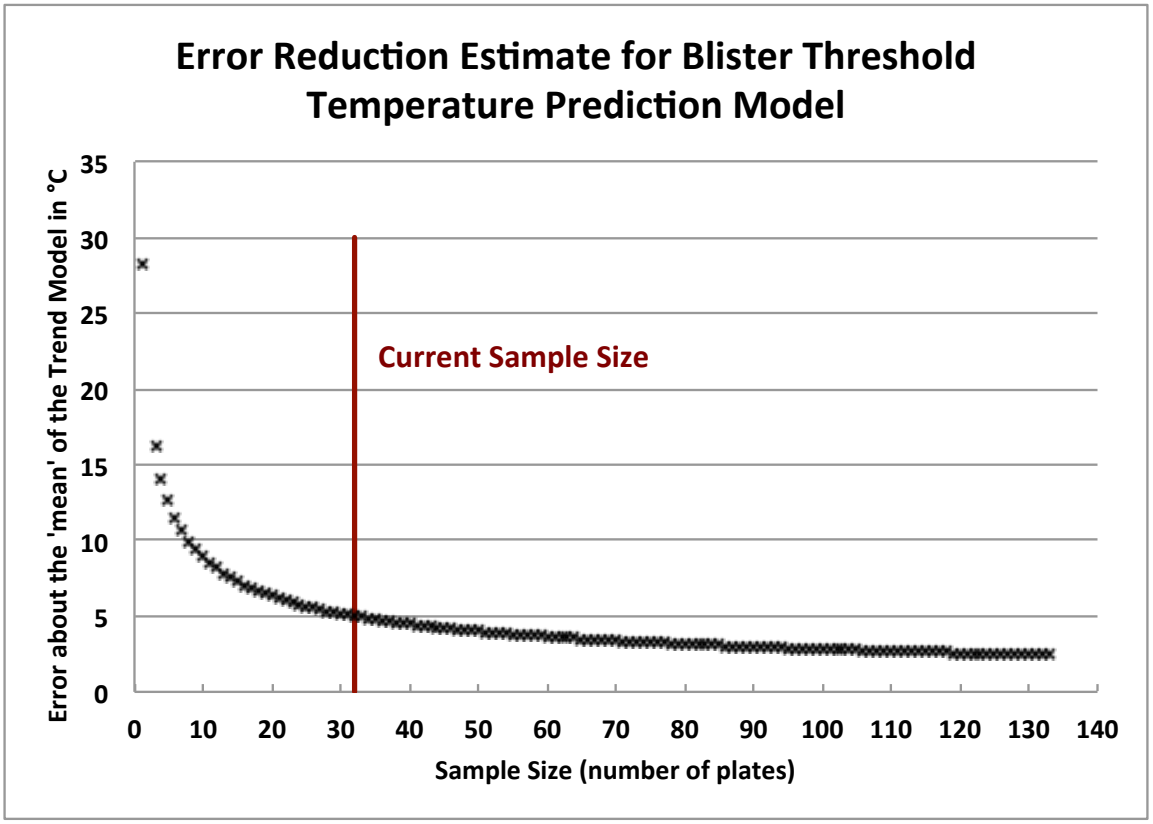

Figure 29. Error reduction estimate for blister threshold prediction model using the effect of sample size on the confidence interval.

•

Chapter 2: Fission-product Release Scoping Study Results For U–Mo Monolithic Fuel Plates

2.1 Introduction

The qualification and licensing of new fuel systems requires evaluation of the failure and fission-product-release mechanisms during off-normal reactor events. Massachusetts Institute of Technology Reactor (MITR) and the Advanced Test Reactor (ATR) will require data on fuel failure thresholds and fission-product release to license a new low-enriched uranium (LEU) fuel system being qualified for the replacement of current highly enriched uranium (HEU) fuels. Although not necessarily required for licensing, Missouri University Research Reactor (MURR), National Bureau of Standards Reactor (NBSR) and High Flux Isotope Reactor (HFIR) will benefit from these data. The pertinent data are essentially applicable for all the Nuclear Regulatory Commission (NRC)-regulated reactors that are candidates for conversion.

Results from this study include the transport and deposition behavior of the source term elements presented in Section 2.5 and listed in Table 22. Similar to the previous studies[41,42] that have been performed on aluminide (UAl_X) dispersion fuels, oxide fuels (U_3O_8, UO_2) and uranium alloys (U, U-Al) to establish the safety basis of different dispersion-fuel types during off-normal events, fuel failure experiments were conducted on U–10Mo high-density monolithic fuel plates. U-10Mo is a uranium metal fuel alloyed with 10-weight percent molybdenum. This scoping study was performed to help determine whether the available test methods and subsequent results would provide sufficient data to characterize fission-product transport behaviors for the NRC regulated reactors. Should these data be sufficient, they will contribute to source term development for inclusion in the

respective Safety Analysis Reports (SARs). Should these data be insufficient, they will provide a basis for the development of a more comprehensive test plan.

This chapter does not provide new fuel-plate or fuel-element melt progression data, new time-resolved release rates of fission-products, or new data for fission-product transport in an oxidizing environment. Noble-gas (Xe or Kr) release for U–10Mo is not evaluated or discussed in this report because all high-performance research reactors assume 100% release of these fission-products. However, blister threshold testing performed (results reported in Chapter 1) to determine blister-threshold temperatures of irradiated U–10Mo monolithic fuel plates have suggested fission-gas release from the fuel at temperatures between 425 and 550°C as indicated by the formation of blisters. This correlates well with tests on dispersion fuels during which noble-gas release was observed along with the formation of blisters. While the extent of fission-gas release from U–10Mo monolithic plates during the blister-anneal testing has not been quantified, it is assumed that fission gas is released in sufficient quantities to deform the clad in the cladding-to-fuel interface region. This assumption is further substantiated by a study performed by Burkes[43] et al. showing an onset of fission-gas release in non-encapsulated[a] U–10Mo fuel at 392°C.

2.2 Historical Testing and Analysis

From a historical perspective, measurements of fission-product release points for dispersion plate fuels comprised of UAl_X, U_3O_8, and U_3Si have been quantified at temperatures corresponding to blister threshold, at clad melt, and at fuel reaction with matrix. The U_3Si_2 system was assumed to be comparable[44] to the UAl_X fuel, so

[a]. The specimen was a very small sample taken from the fuel region of a monolithic fuel plate; thus, the fuel edges of the specimen were unclad.

fission-product-release measurements were not performed. The NRC accepted this assumption.[44] Fuel-melt fission-product-release data have been requested by the ATR and MITR for monolithic fuel, but these were not included in NUREG-1313. [44] Other fuels that have undergone accident testing are uranium fuel, uranium-aluminum fuel and uranium-zirconium fuel. The variety in the fuels tested also represents a variety of release behaviors, also influenced by the array of test atmospheres, for the volatile fission products. While this makes it difficult to define a general fission-product-release model that can be applied to any nuclear fuel, it is clear that two common variables influence release rates and quantities in all the fuel types. These are burnup levels and melt temperatures. Higher burnup levels and higher temperatures typically result in higher release rates, and/or higher release quantities. The following sections briefly summarize some past efforts and a form a reference space to frame U-Mo fuel testing efforts and behavior.

2.3 Intermetallics

2.3.1 Aluminide[b] (UAl_X)

Shibata[45] reports that uranium-aluminide plates were held at temperature for 30 minutes in helium to measure fission-product releases. The burnup level for the 40% enriched dispersion plates was ~60% of the original ^{235}U inventory. Onset of the first rapid release of fission gas, which correlated with the formation of a blister, was at 561°C, with the last release at 640°C. Blister anneal tests performed on aluminum clad fuels are typically terminated at 550°C to avoid melting of the aluminum. Approximately 10^{-2}–10^{-3} percent of the total plate inventory of ^{131}I and ^{137}Cs were released with the fission gas as stated in Reference 6. It should be noted that these plates were tested at temperatures lower than some

[b] Dispersion Fuel

other fuel systems discussed later. Iodine- and cesium-release data from sample, E-114, are plotted in Figure 30.

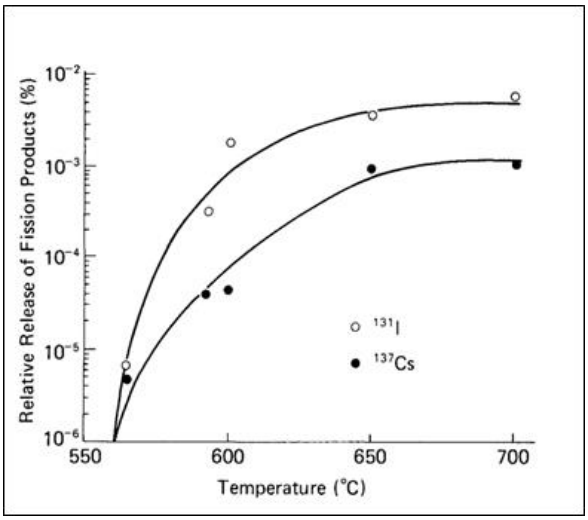

Figure 30. Iodine and cesium release data from sample E114 that was tested up to 700°C in helium in Reference 45.

Saito[46] et al. performed fission-product release measurements in air on both silicide and UAl_X based fuels. Results for the aluminide fuel specimen identified as A-12 from Reference 46 are found in Table 16, recreated from the data shown in Figure 31. Hold time at temperature was 60 minutes. In comparison to the values that Shibata reported above, these were higher-temperature tests than from Reference 45; the test atmosphere was air and the burnup level was ~20% of the 45 percent starting inventory of ^{235}U.

Table 16. Anneal temperatures in air and cumulative ^{131}iodine release data.[46]

Temperature (°C)	Cumulative Percent of Total ^{131}Iodine Inventory Released
600	1.8
700	20
800	28
900	38
1000	51
1100	60

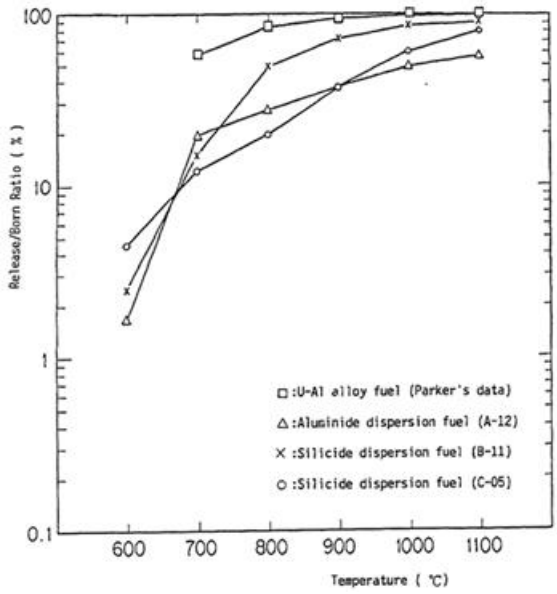

Figure 31. Plotted aluminide ^{131}I release data from Reference 46, from Parker's[c] Reference 47 U–Al alloy data and the Reference 46 silicide-fuel test samples.

2.3.2 Ceramics

2.3.2.1 Oxide[d] (U_3O_8, UO_2)

Data on release after two minutes at temperature in argon, air, and steam from samples with a burnup level of ~52% of the initial ^{235}U inventory, of the fission-products iodine and cesium, for U_3O_8 by Snelgrove et al.[48] are listed in Table 17. Two minutes is a more realistic time interval for representing an off-normal reactor operating event, such as a loss-of-coolant accident, than the longer hold times reviewed and presented in this report. These data for iodine and cesium, shown in Figure 32 and Figure 33 respectively, illustrate that the release behavior of iodine is highest in steam, until 1100°C where the release in all tested environments is essentially equal. The cesium-release quantities remain relatively

[c] The original enrichment for this fuel is not specified in the Parker reference. The fuel burn-up was 20%. The test atmosphere for these data is air. Time at temperature was 60 minutes.

[d] Dispersion fuel.

unaffected by the environment. This is likely due to the abundance of available oxygen in the fuel with which the cesium can chemically bond.

Table 17. Fission-product release data for U_3O_8.

Temperature (°C)	Atmosphere	Release Percent	
		^{129}Iodine	^{137}Cesium
700	Argon	40.0	9.4
850	Argon	38.1	22.2
1000	Argon	65.4	22.2
1100	Argon	91.8	59.7
700	Air	37.4	0
850	Air	55.4	26.1
1000	Air	50.5	22.5
1100	Air	96.2	66.2
700	Steam	63.9	11.2
850	Steam	78.1	23.3
1000	Steam	77.9	31.1
1100	Steam	91.8	n/a

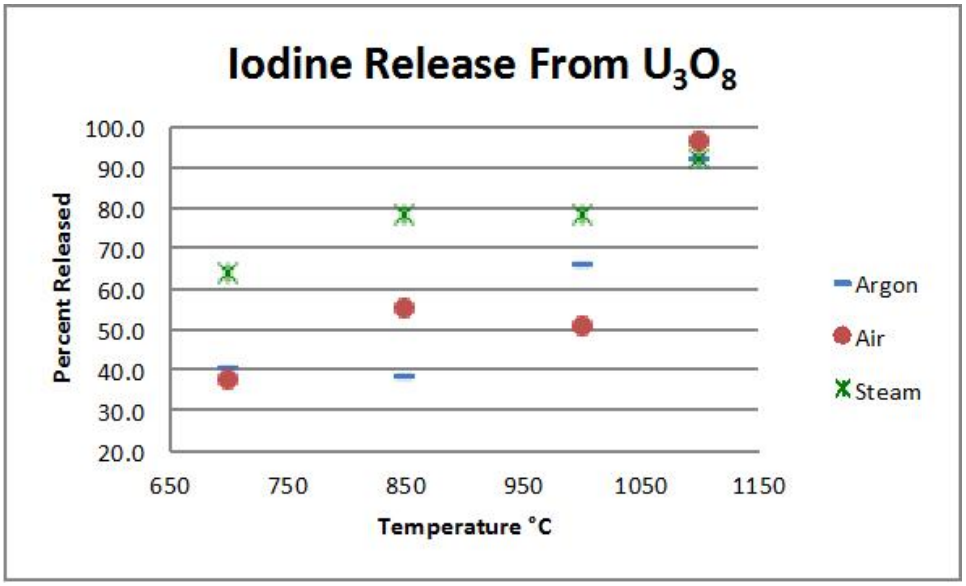

Figure 32. Iodine release from U_3O_8 in argon, air and steam.

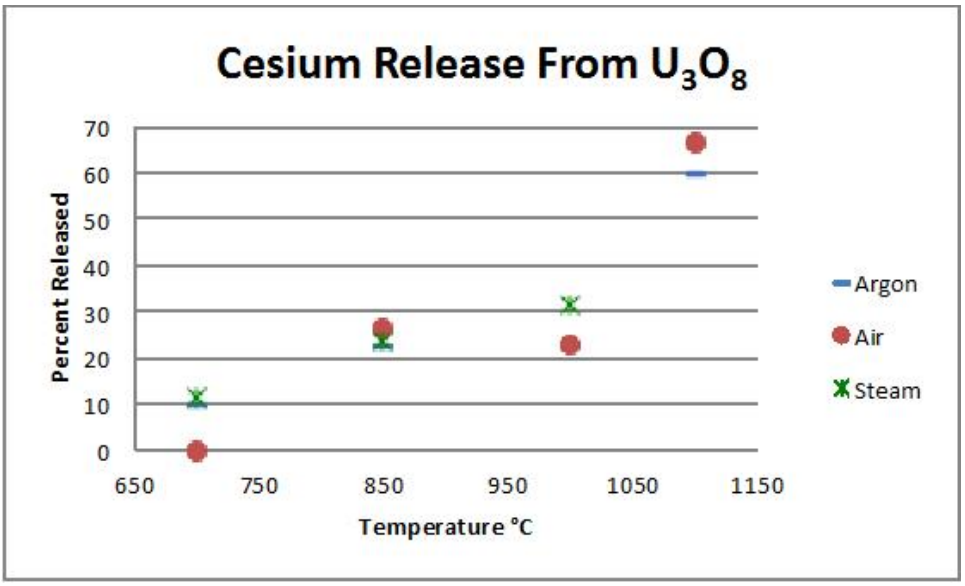

Figure 33. Cesium release from U_3O_8 in argon, air, and steam.

Studies conducted at the Oak Ridge National Laboratory (ORNL)[47] from 1955 through 1965 provide test data on ceramic-fuels fission-product-release behaviors in air and helium. Burnup levels affected fission-product-release behaviors in UO_2. Test temperatures were between 500 and 2260°C. Cesium releases are low and suggest the formation of low volatility Cs_2O. The tabulated results from Reference 47 are re-organized, in part, in Table 18.

Table 18. Fission-product release results from Reference 47 for UO2 fuel test specimens at various burnup levels.

Temperature	Atmosphere (note: all superscripts detailed at end of Table)	Burnup Level (Mwd/T)	Percent of Species Released							
			Iodine	Tellurium	Cesium	Ruthenium	Strontium	Barium	Zirconium	Uranium
500	Air[a]	7000	4.1	<0.5	0.0006	0.1	<0.0007	<0.0004	-	-
600	Air[a]	7000	3.1	<0.1	<0.002	0.7	<0.0004	<0.009	-	-
700	Air[a]	7000	15	<0.08	<0.005	0.1	<0.0005	<0.007	-	-
800	Air[a]	7000	9	<0.3	0.002	9.8	<0.0005	0.03	-	-
850	Air[a]	7000	34	1.4	0.02	35	<0.005	<0.08	-	-
900	Air[a]	7000	29	80	<0.01	78	<0.03	<0.8	-	-
1000	Air[a]	7000	78	37	<0.03	93	<0.04	<0.3	-	-
500	Helium/Air[a,b and c]	4000	3.2	<0.01	<0.0007	<0.01	<0.0004	<0.0008	-	-
600	Helium/Air[a,b and c]	4000	8	8.4	<0.001	1.8	<0.001	<0.004	-	-
700	Helium/Air[a,b and c]	4000	6.5	<0.05	<0.0005	23	<0.0004	<0.002	-	-
800	Helium/Air[a,b and c]	4000	16	<0.06	<0.01	12	<0.0004	<0.001	-	-
900	Helium/Air[a,b and c]	4000	47	6	0.015	53	<0.0008	<0.004	-	-
1000	Helium/Air[a,b and c]	4000	75	32	0.37	92	0.1	0.08	-	0.06
1100	Helium/Air[a,b and c]	4000	84	39	0.2	99	0.006	0.01	-	<0.003
1200	Helium/Air[a,b and c]	4000	95	66	6.4	99.6	0.007	0.7	-	<0.003
500	Helium/Air[a,b and c]	1000	4.7	0.008	<0.002	0.36	<0.004	<0.0008	-	-
600	Helium/Air[a,b and c]	1000	6	0.005	0.003	0.9	<0.0009	<0.0009	-	-
700	Helium/Air[a,b and c]	1000	10	<0.003	0.02	3.8	<0.0008	<0.0007	-	-
800	Helium/Air[a,b and c]	1000	14.1	0.08	<0.007	35.3	<0.001	<0.002	-	-
900	Helium/Air[a,b and c]	1000	26.9	0.41	<0.002	30.3	<0.001	<0.0015	-	-
1000	Helium/Air[a,b and c]	1000	73.3	31.3	0.02	97.9	0.002	0.005	-	<0.0012
1100	Helium/Air[a,b and c]	1000	71.3	58	<0.4	99.9	<0.2	<0.2	-	0.19
1200	Helium/Air[a,b and c]	1000	83.4	75.9	4.5	99.7	0.14	0.14	-	0.142
1515	Helium[d]	Trace	5.8	2.9	1.4	0.9	0.1	-	-	-
1610	Helium[d]	Trace	6.5	12	1.7	1.5	0.1	-	-	-
1710	Helium[d]	Trace	9.6	20	2.7	3.8	0.4	1.3	-	-

Temperature	Atmosphere (note: all superscripts detailed at end of Table)	Burnup Level (Mwd/T)	Percent of Species Released							
			Iodine	Tellurium	Cesium	Ruthenium	Strontium	Barium	Zirconium	Uranium
1800	Helium[d]	Trace	12	21	3.2	6.9	1	-	-	-
1900	Helium[d]	Trace	16	48	8.6	8.5	2.3	-	-	-
1980	Helium[d]	Trace	42	76	15	13	4.2	8.7	1.8	-
2105	Helium[d]	Trace	40	81	24	22	13	21	0.5	0.5
2150	Helium[d]	Trace	74	95	53	49	28	40	12	0.4
2200	Helium[d]	Trace	75	96	70	50	36	59	18	-
2260	Helium[d]	Trace	84	96	65	90	55	75	35	1.3
1400	Helium[d]	1	4	3.9	0.02	0.2	0.001	-	-	-
1610	Helium[d]	1	6.5	12	1.7	1.5	0.1	-	-	-
1780	Helium[d]	1	12	21	3.2	6.9	1	-	-	-
1980	Helium[d]	1	41	75	15	13	4.2	8.7	-	-
1400	Helium[d]	1005	0.9	0.8	2.6	0.001	0.1	0	-	-
1610	Helium[d]	1005	3.7	12	12	0.1	2	17	-	-
1780	Helium[d]	1005	24	67	27	0.4	9	39	-	-
1980	Helium[d]	1005	53	74	84	6	15	57	-	-
1400	Helium[d]	1000	1.6	1.2	0.5	0.001	0.06	1.8	-	-
1610	Helium[d]	1000	5.5	27	20	0.3	0.2	12	-	-
1780	Helium[d]	1000	26	35	22	0.4	3.7	21	-	-
1980	Helium[d]	1000	63	90	70	4.8	10	51	-	-
1400	Helium[d]	4000	23	16	21	0.006	0.08	0.5	-	-
1610	Helium[d]	4000	25	48	43	0.2	0.5	15	-	-
1780	Helium[d]	4000	59	60	40	5.7	5.8	18	-	-
1980	Helium[d]	4000	81	81	98	15	33	60	-	-

a. Samples held at temperature for 90 minutes.

b. Samples held at temperature in helium for ~15 minutes and then held for 90 minutes in air.

c. Only the longest anneal time reported by [7] is presented in this table.

d. Samples held at temperature for 5.5 hours.

Release trends from Reference 47 for iodine, tellurium, cesium, ruthenium, strontium and barium, in air and helium, are shown in Figure 35. The burnup term Mwd/T, refers to the number of megawatt days per metric tonne of fuel. While the temperature range is not the same for air and helium melt tests, the trends with respect to atmosphere are still evident. Iodine (a-1, a-2), tellurium (b-1, b-2) and ruthenium (d-1, d-2) demonstrate higher release quantities in air than in helium while cesium (c-1, c-2) release quantities are lower in air than in helium. Release quantities for strontium (e-1, e-2) and barium (f-1, f-2) seem largely unaffected by the test atmosphere. All fission-product plots in Figure 30 demonstrate increased release quantities for increasing burnup levels.

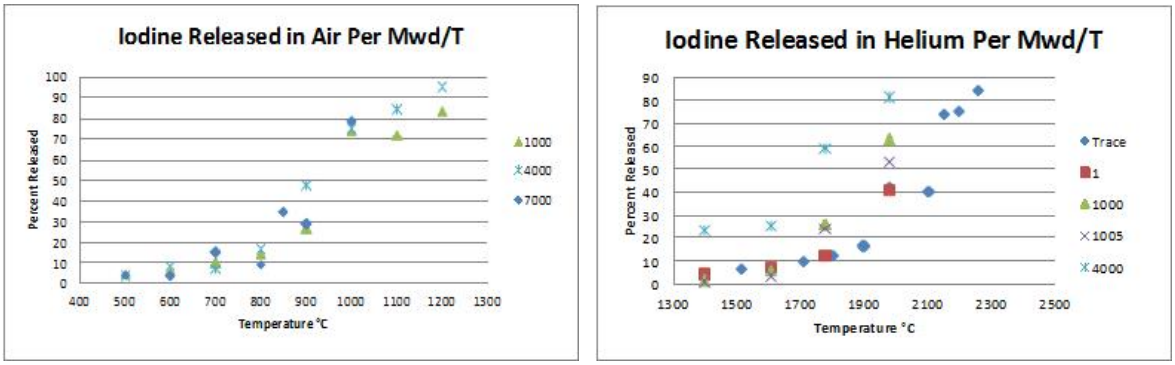

(a-1)

(a-2)

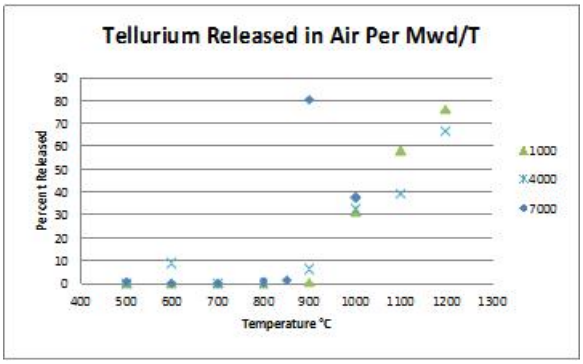

(b-1)

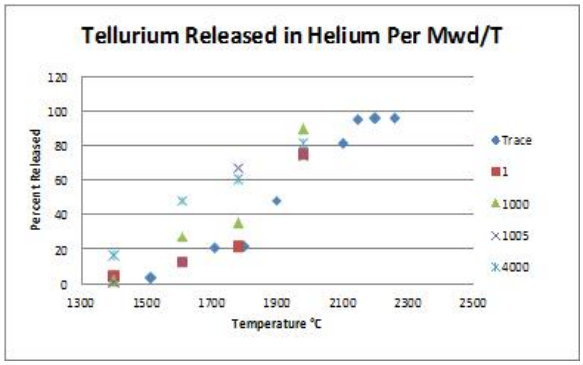

(b-2)

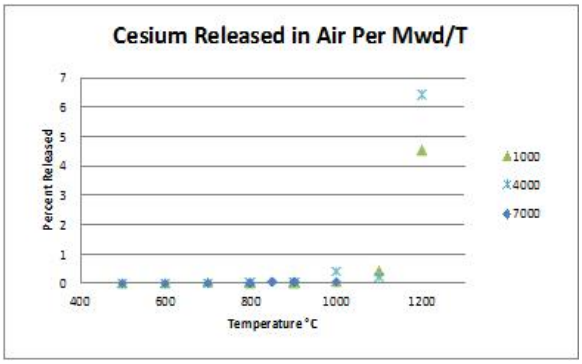

(c-1)

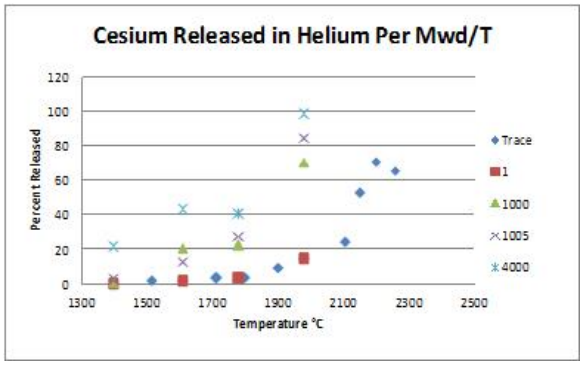

(c-2)

Figure 34. UO_2 fission-product release trends from Reference 47 in air and in helium for iodine (a-1, a-2), tellurium (b-1, b-2), cesium (c-1, c-2), ruthenium (d-1, d-2), strontium (e-1, e-2), and barium (f-1, f-2).

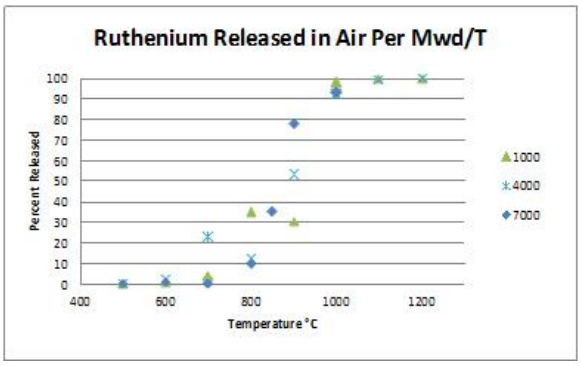

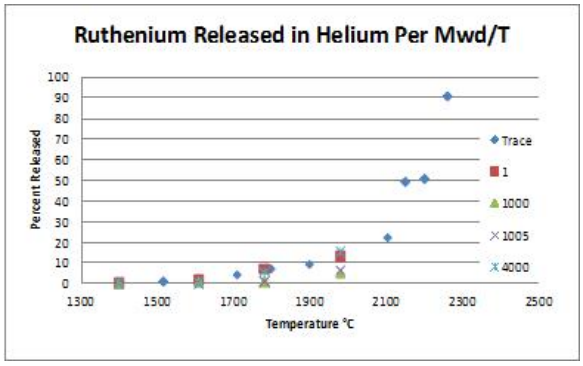

(d-1) (d-2)

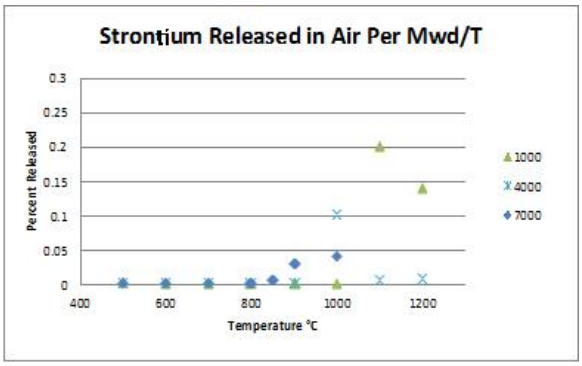

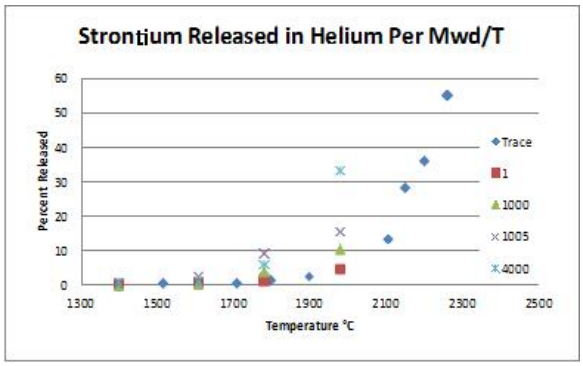

(e-1) (e-2)

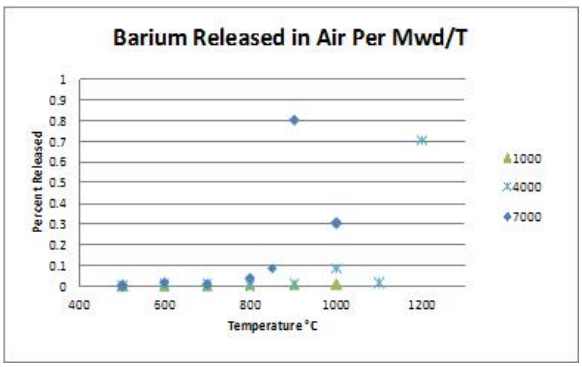

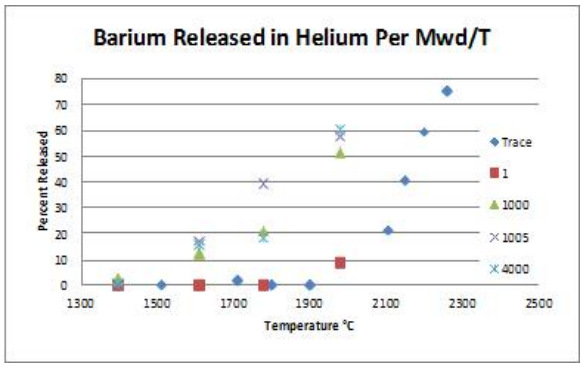

(f-1) (f-2)

Figure 35 (con't). UO_2 fission-product release trends from Reference 47 in air and in helium for iodine (a-1, a-2), tellurium (b-1, b-2), cesium (c-1, c-2), ruthenium (d-1, d-2), strontium (e-1, e-2), and barium (f-1, f-2).

2.3.3 Metallic Fuel

2.3.3.1 Uranium-Aluminum

Release data from Reference 48 for U–Al alloy samples (33.6 wt% U) with a burnup of ^{235}U of ~52% and time at temperature of 2 minutes for the fission-products iodine and

cesium are listed in Table 19. These data, plotted in Figure 36 and Figure 37 for iodine and cesium, respectively, do not appear to exhibit a significant effect of the test atmosphere. The release data for cesium trend higher in all atmospheres and not in agreement with other data from metallic fuel systems presented in this report.

Table 19. Fission-product release data for U-Al alloy.

Temperature (°C)	Atmosphere	Release Percent	
		^{129}Iodine	^{137}Cesium
700	Argon	44.2	16.2
850	Argon	86.7	60.0
1000	Argon	95.4	59.7
1100	Argon	97.8	79.6
700	Air	69.0	18.2
850	Air	88.3	41.1
1000	Air	96.0	73.6
1100	Air	86.8	60.6
700	Steam	24.5	20.2
850	Steam	85.8	57.9
1000	Steam	87.4	50.4
1100	Steam	95.6	72.2

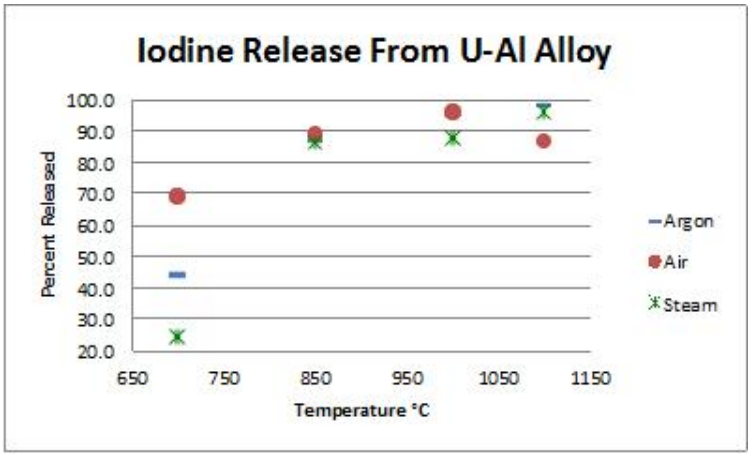

Figure 36. Iodine release from U-Al alloy in argon, air, and steam.

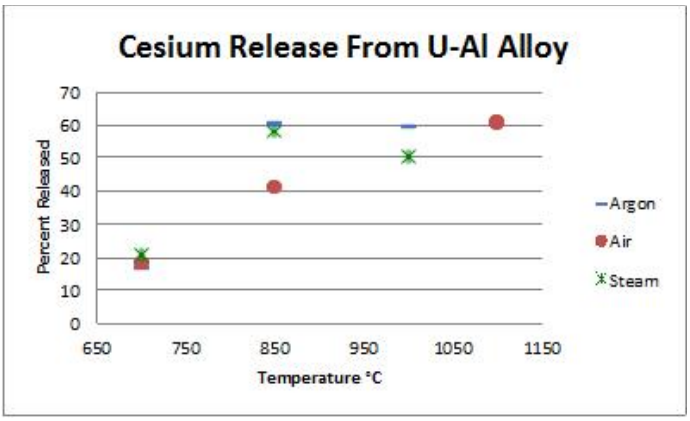

Figure 37. Cesium release from U–Al alloy in argon, air and steam.

Data from Reference 47 are summarized in Table 20 and plotted in Figure 38 for iodine, tellurium, cesium, and ruthenium. It is apparent in this data that *time* at temperature and flow rate have little effect on the release behavior of fission products in the U/Al alloy fuels. However, temperature predictably affects the release behaviors, showing higher release quantities as the temperature increases.

Table 20. Effect of maximum temperature, time at temperature, and atmosphere on fission-product release from U–Al alloy specimens.[b]

Maximum Temp (ºC)	Time at Temp (min)	Atmosphere[a]	Rare Gases	Iodine	Tellurium	Cesium	Ruthenium
800	2	Helium	99.5	29.8	5.3	13.0	0.18
900	2	Helium	100	52.8	4.3	20.8	0.08
1000	2	Helium	100	82.1	2.9	47.7	0.19
1105	2	Helium	100	82.4	2.9	69.5	0.25
700	2	Air	97.9	37.8	0.3	3.1	0.02
800	2	Air	99.4	78.6	0.2	3.8	<0.1
900	2	Air	100	91.9	2.1	6.2	0.1
1000	2	Air	99.8	97.3	<9.7	8.8	0.2
1090	2	Air	100	98.4	44.8	12.4	0.6
1145	2	Air	100	94.2	62.0	18.6	0.4
700	2	Steam-air	98.3	27.0	<0.03	0.6	<0.02
800	2	Steam-air	99.5	76.8	0.3	1.1	0.1
900	2	Steam-air	99.9	90.6	5.7	6.5	0.5
1000	2	Steam-air	100	95.6	22.6	11.0	0.5
1085	2	Steam-air	100	96.8	67.9	30.5	0.8
700	60	Air	97.7	58.0	<0.14	3.5	<0.02
800	60	Air	99.5	84.7	0.7	5.9	0.03
900	60	Air	99.95	95.3	2.9	9.2	0.2
1000	60	Air	99.98	92.8	16.6	23.3	0.1
1090	60	Air	99.98	98.3	78.4	37.8	0.03
840[c]	60	Air	100	94.6	1.5	6.5	0.1
870[c]	60	Air	100	95.8	4.0	6.9	0.7

a. Air gas flow rate was 250 cm^3/min (measured at room temperature). Steam flow rate was 1000 cm^3/min.
b. Burnup level was 23.6 atom percent of ^{235}U. Specimens were 5/16-in.-diameter disks punched from MTR-type fuel plates and re-irradiated to build up the inventory of short-lived fission products.
c. Air-flow rate for these two specimens were 3000 cm^3/min (measured at room temperature).

Atmosphere effects are apparent in the iodine (a) release quantities, with a lower release percent in a non-oxidizing environment. Tellurium (b) release, like that of iodine, is lower in the non-oxidizing environment. By contrast, cesium (c) release increases in the non-oxidizing environment. The test-atmosphere results are consistent with those reported in Reference 46 for UO_2. Ruthenium is below 1% for all temperatures, with no apparent influence of either atmosphere or temperature.

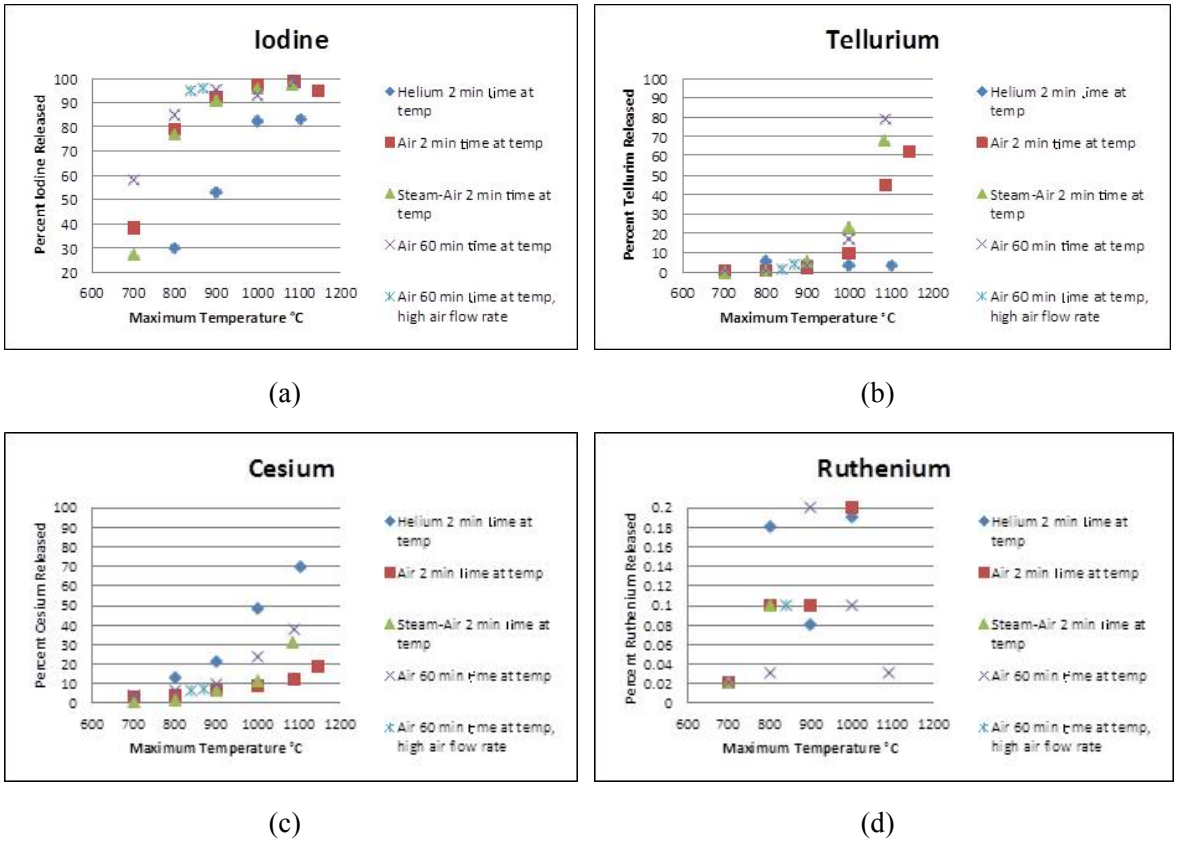

Figure 38. Iodine (a), tellurium (b), cesium (c) and ruthenium (d) temperature-resolved release percent.

The disagreement in release data regarding the U-Al alloy between sources References 48 and 47 for iodine and cesium in the different atmospheres might be attributed to the higher and lower burnup of these fuels, respectively, which can influence the diffusivity of fission products within the fuel, thereby altering the release behaviors of fission products. Data from the UO_2 fuel from Reference 47 show that release quantities are higher from higher-burnup samples for a given temperature.

2.3.3.2 Zirconium-uranium Alloy

Melt tests[47] were performed on zirconium-uranium specimens in both air and steam in the temperature range between 1705 and 1800°C. Results demonstrated that the average iodine and cesium release is nearly double in steam than in air. Perhaps the conclusion

offered for similar behavior in the UO_2 fuel system[47] where most of the Cs_2O would have dissociated at those high temperatures, could be an explanation.

2.3.3.3 Uranium

The chemical behavior of ^{131}I was evaluated[49] for the Sodium Reactor Experiment (SRE) that used slightly enriched, sodium-cooled uranium metal fuel. A leak, which was hypothesized to have released ^{131}I, developed. An analysis (report pending) of fission-product behaviors of iodine and cesium was performed for the metal fuel system. Iodine is assumed to have remained in the fuel in the form of UI_3, a non-volatile species, at the speculated accident temperatures of between 800 and 900°C. At the melt temperature of 1135°C, the thermodynamic models predict that the UI_3 would disassociate to form CsI + U as it diffuses out of the uranium. A thermodynamic equilibrium model reported in Reference 49, using fission-product inventories from the SRE element, is summarized in Table 21. The author states that at the low burnup levels and subsequent low inventories of fission product, the likelihood of UI_3 formation is higher due to an absence of a nearby cesium atom. Iodides that form independent of the equilibrium compositions are influenced by potential barriers, such as diffusion in the uranium matrix, and thus result in the formation of UI_3 until it diffuses out of the matrix. At this point the disassociation is likely when UI_3 encounters the cesium atoms and a U + CsI equilibrium composition occurs.

Table 21. Thermodynamic modeling result for the SRE fission-product equilibrium.

Fission-Product Species	Equilibrium Quantity: Percent of Original Element Comprising Species
U	99.9977
Zr	100
Xe	100
Mo	100
Nd	100
Cs	56.29
Ce	100
Sr	100
Ba	100
La	99.89
Tc	100
URu_3	100 Ru; 0.0032 U
Kr	100
Cs_2Te	39.23 Cs; 100 Te
Nb	100
CsI	3.26 Cs; 100 I
CsBr	1.22 Cs; 100 Br
LaSb	0.11 La; 100 Sb

2.4 Chemical Behavior: DEVAP

The DEVAP study,[50] performed in 1994 by G. Le Marois and M. Megnin of Commissariat a l'Energie Atomique, utilized a deposition tube to characterize fission-product transport and deposition behavior. A specific fuel type was not melted to characterize fission-product behavior; rather, the study introduced the chemical species of interest into the test environment. These species were then removed using steam or hydrogen. The data provided were temperature-related deposition behaviors for a variety of chemical species. The primary deposition temperature of CsI, CsOH and Te was 647˚C.

2.5 Source Term Elements

The source term elements—as organized in NUREG-1465[51] by the NRC—required for a reactor SAR are listed in Table 22, with the highest-dose elements being Kr, Xe, I, Cs, Te and Rb. The NRC-regulated reactor SARs assume 100% release of the krypton and xenon while the other fission-product are captured as fractional releases.

Table 22. Source term elements.

Group Title	Elements in Group
Noble Gases	Xe, Kr
Halogens	I, Br
Alkali Metals	Cs, Rb
Tellurium Group	Te, Sb, Se
Barium, Strontium	Ba, Sr
Noble Metals	Ru, Rh, Pd, Mo, Tc, Co
Lanthanides	La, Zr, Nd, Eu, Nb, Pm, Pr, Sm, Y, Cm, Am
Cerium Group	Ce, Pu, Np

2.6 Experimental Setup and Methods

In this study, the fuel-plate-sample melt experiments were performed using the DEOX furnace[52] shown in Figure 39. A total of four independent temperature zones were controlled, thereby creating a temperature gradient to encourage temperature-driven deposition of the volatile fission products onto the stainless-steel tube. Temperature control and measurements were provided using Type K thermocouples flanking the test apparatus. The test apparatus is shown in Figure 40 and was comprised of a melt crucible at the base, a thermal gradient tube, and a filter system at the top. The crucible region, a cup–shaped outlined inner region, is illustrated in more detail in Figure 41. This removable high-purity alumina crucible was housed in the stainless-steel melt vessel. Welded to the top of the crucible region was a 304-stainless-steel thermal gradient tube that passed through the three heat zones above the crucible region located in the bottom heat zone of the furnace. The exit

point at the top of the furnace was fitted with an activated carbon filter and 45-micron high-efficiency particulate air (HEPA) filter system assembly. Warm argon, along with noble gases, vented through the top of the test assembly through the filter and was released into the cell atmosphere. Temperature-related deposition of volatile fission products was determined using the thermal gradient tube that was indexed and labeled in 1⅜ inch (maximum size that can fit in the transfer container) increments. Labeling correlated with each temperature zone.

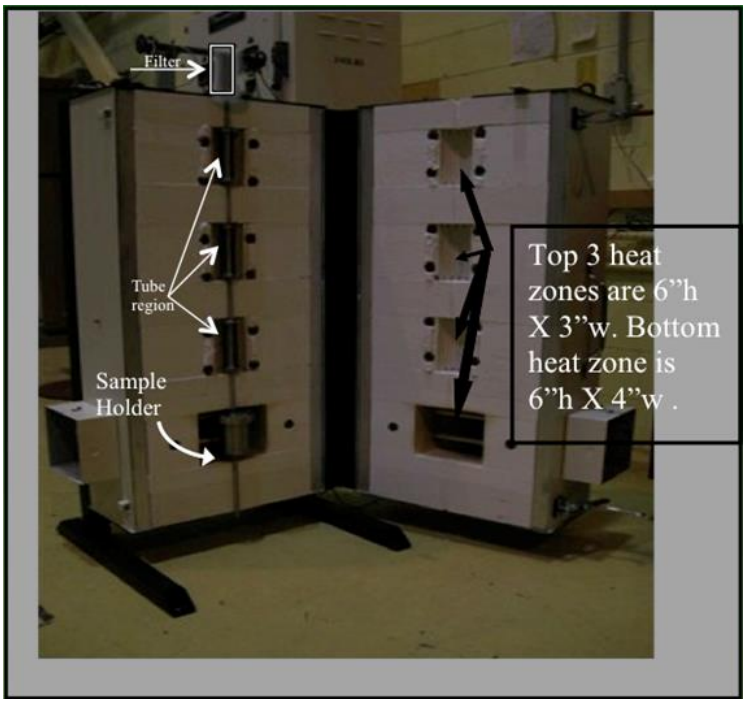

Figure 39. DEOX furnace with sample test apparatus in place.

Figure 40. Test apparatus.

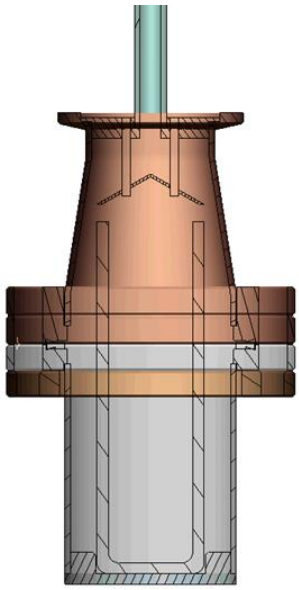

Figure 41. Stainless steel sample holder with alumina crucible inside.

The following are the scoping test parameters employed in the present study:

- A temperature of 1250°C was held for 2 hours to achieve fuel melting.
- A low-temperature test was performed at 600°C to investigate releases at a temperature close to the melting temperature of the cladding. Hold time was 2 hours.
- The test-region atmosphere was static argon, with <100-ppm oxygen content and moisture. There is no gas flow except for that created by natural convection during the experiment.
- Each sample was a 0.500 × 0.375 in. section cut from a mini-plate. Sample sectioning diagrams are provided in Appendix A.

An example of a plate source-term inventory[53] reported in curies (to be consistent with SAR units for core element inventories) and grams is illustrated for L1P490 in Table 23 and represents the total at discharge from the reactor with zero days of decay. Many of the high-dose isotopic inventories, such as ^{131}I, that are required for source-term development

had decayed to undetectable levels since the experiment discharge from the reactor. Long-lived chemical forms were thus used for characterizing fission-product transport behaviors. Thus, this scoping study was successful in characterizing the transport and deposition behaviors of ^{127}I and ^{129}I, ^{133}Cs, ^{135}Cs, and ^{137}Cs in an argon atmosphere.

Table 23. The full-plate source-term-element inventory for U-Mo mini-plate L1P460 at discharge (0 days of decay) from reactor.

Noble Gases	**Curies**	**Grams**	**Noble Metals**	**Curies**	**Grams**	**Lanthanides**	**Curies**	**Grams**
Xe	3.91E+01	4.85E-02	Ru	6.97E+01	1.80E-02	Cm	2.50E-05	9.22E-09
Kr	1.19E-01	4.33E-03	Rh	6.31E+01	2.19E-03	Am	1.68E-06	5.29E-07
Halogens			Pd	5.11E-07	2.13E-03	**Cerium Group**		
I	3.59E+01	1.66E-03	Mo	3.20E+00	2.48E-02	Ce	1.61E+02	3.48E-02
Br	9.49E-06	2.29E-04	Tc	3.08E+00	7.87E-03	Pu	1.39E-02	1.57E-02
Alkali Metals			**Lanthanides**			Np	1.37E+00	7.01E-04
Cs	1.31E+00	2.44E-02	La	1.26E+02	1.21E-02			
Rb	8.90E-03	4.09E-03	Zr	1.10E+02	3.92E-02			
Tellurium Group			Nd	3.42E+01	2.89E-02			
Te	9.32E+00	3.43E-03	Eu	8.39E-01	4.78E-04			
Sb	4.14E-01	1.31E-04	Nb	7.36E+01	1.86E-03			
Se	=	5.82E-04	Pm	4.72E+00	3.59E-03			
Barium, Strontium			Pr	1.50E+02	8.14E-03			
Ba	1.10E+02	1.40E-02	Sm	2.98E-02	3.97E-03			
Sr	9.33E+01	1.42E-02	Y	1.08E+02	6.82E-03			

Three previously blister anneal[e] tested mini-plates were selected for the melt tests. While five segments were tested in 2012, the results presented are limited to the four samples that have been chemically analyzed and are listed in Table 24. This table also lists the target temperatures for each of the four independent temperature zones used to establish the thermal gradient.

A gamma scan was performed on four test assemblies. These were comprised of one empty (dummy) assembly (for a baseline of the test assembly geometry), two with the fuel-melt pieces identified as L1P460-2 and L1P758-4, and one low-temperature melt piece

[e] Irradiated material available for destructive tests was very limited due to the breadth of post irradiated characterization activities performed on each plate. Blister anneal testing may result in relocation of the more volatile fission products (Cs and I) within the fuel region of the plate, which could affect results. This effect would be more evident in higher-fission-density plates.

identified as L1P758-3. Chemical analysis was performed only on the three test assemblies and melt pucks for the 1250°C fuel-melt samples (L1P460-2, L1P756-4, and L1P758-4).

Table 24. Test matrix and test type for the DEOX scoping experiments with targeted zone temperatures.

Plate Sample ID	Average Plate Fission Density (fissions/cm^3)	Test Temperature (°C)	Zone 1 Temp (°C)	Zone 2 Temp (°C)	Zone 3 Temp (°C)	Zone 4 Temp (°C)	Analysis performed
L1P460-2	1.96 x 10^{21}	1250	150	400	900	1250	Gamma scan/ chemistry analysis
L1P758-4	4.33 x 10^{21}	1250	150	400	900	1250	Gamma scan/ chemistry analysis
L1P756-4	5.88 x 10^{21}	1250	150	400	900	1250	Chemistry analysis
L1P758-3	4.33 x 10^{21}	600	400	400	500	600	N/A
L1P756-2	5.88 x 10^{21}	600	150	400	500	600	Gamma scan

The temperature profile of the test apparatus within the furnace is illustrated in Figure 42, with temperature depicted at the top of the figure and the corresponding region within the test assembly at the bottom of the figure. Table 25 provides additional clarity for zone identification and temperatures. The linear equation shown in Figure 42 can be used to interpolate the temperatures between the thermocouple locations. A higher resolution temperature table using the linear equation to fill in the axial temperature profile is found in Table 26.

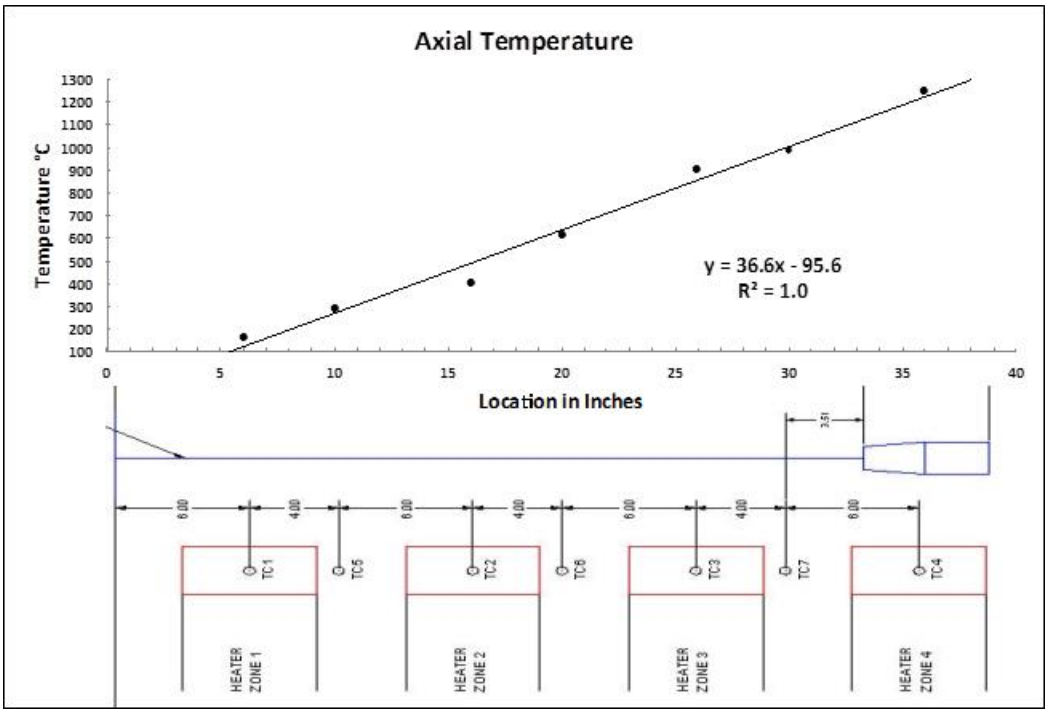

Figure 42. Test-apparatus axial temperature profile.

Table 25. Test apparatus thermocouple and temperature chart.

Test Region	Thermocouple	Temperature Zone	Axial Position (in.)	Temperature (°C)
Crucible	TC4	4	36	1245
Tube	TC7[a]	3.5	30	985
Tube	TC3	3	26	900
Tube	TC6[a]	2.5	20	614
Tube	TC2	2	16	400
Tube	TC5[a]	1.5	10	291
Tube	TC1	1	6	168
a. Between heater zones				

Table 26. Interpolated temperatures for axial position in one-inch intervals using the linear equation from Figure 42. Measured temperature values are in italics. The axial position for 6 inches starts in a location just below the filter at the top of the test apparatus (right side of Figure 10) and end at the middle of the crucible region (left side of Figure 10).

Axial Position (in.)	Temperature Interpolation (°C)	Axial Position (in.)	Temperature Interpolation (°C)	Axial Position (in.)	Temperature Interpolation (°C)
6	124/*168*	17	527	27	893
7	161	18	563	28	930
8	197	19	600	29	966
9	234	20	637/*614*	30	1003/*985*
10	271/*291*	21	673	31	1039
11	307	22	710	32	1076
12	344	23	746	33	1113
13	380	24	783	34	1149
14	417	25	820	35*	1186
15	454	26	856/*900*	36*	1222/*1245*
16	490/*400*				
*Crucible region.					

The stainless-steel tube was segmented into seven temperature regions, identified for simplicity for the chemical analysis batch processing[f] as: 1100, 900, 670, 400, 365, 150 and <150°C and then into sub-segmented (sized for transfer) pieces and batched for chemical analysis. These batched segments comprised several discreet (measured and estimated) temperatures, were relative to gamma scan data, and included a range of deposition behaviors over a particular length of the tube section. These batching details are summarized in Table 27 for specimen L1P460-2 and are consistent for the other samples. Each segment batch was assigned a unique identification that correlated to the temperature region.

[f] Higher resolution (single sample processing rather than batch processing) chemistry analysis was not possible within the scope of this study.

Table 27. Tube section batching details for specimen L1P460-2.

Tube section ID	Cumulative tube length Sections (inches)	Gamma scan cumulative length from top of crucible working up (inches).	Interpolated temperatures (°C) from Table 11 (Temperatures in parenthesis are measured)
DR1-1[@]	1.375	51.9-56	1039-1186
DR1-2[@]	2.75		
DR1-3[@]	4.125		
DR1-4[#]	5.5	46.4-51.9	820-1039
DR1-5[#]	6.875		
DR1-6[#]	8.25		
DR1-7[#]	9.625		
DR1-8[$]	11	42.3-46.4	673-820
DR1-9[$]	12.375		
DR1-10[$]	13.75		
DR1-11[%]	15.125	36.8-42.3	490 (400)-673
DR1-12[%]	16.5		
DR1-13[%]	17.875		
DR1-14[%]	19.25		
DR1-15[^]	20.625	32.6-36.8	344-490 (400)
DR1-16[^]	22		
DR1-17[^]	23.375		
DR1-18[&]	24.75	25.75-32.6	124 (168)-344
DR1-19[&]	26.125		
DR1-20[&]	27.5		
DR1-21[&]	28.875		
DR1-22[&]	30.25		
DR1-23[*]	31.625	21.63-32.6	Temperature not measured but estimated <124
DR1-24[*]	33		
DR1-25[*]	34.375		

[@] 1100°C batch; [#]900°C batch; [$]670°C batch; [%]400°C batch; [^]365°C batch; [&]150°C batch; [*]<150°C batch

All data from the chemical analysis were totaled per element, rather than addressing the transport behavior per isotope because the transport behavior is governed by the element species. Also, the transport and deposition behavior data are presented as ratios relative to the total of those measured within each test assembly for the components analyzed: the filter, the tube, and the melt puck within the crucible. Due to the limited scope of this study, portions

not analyzed using chemistry were the alumina crucible and the stainless-steel crucible region. Not captured or measured were the gaseous species that passed through the filter region.

Uncertainties associated with the present measurements include the following:

1. ± 5–20% for the inductively coupled plasma-mass spectrometry (ICP-MS) data. Details on uncertainty values can be found in Appendix C.
2. Accurate sample fuel mass is unknown due to uncertainties in fuel and cladding thickness and the sample sectioning method. This may create bias in the data when compared to the physics-model estimates.
3. Transport of fission products within the plate due to previously having been subjected to blister anneal testing. The transport phenomenon has been observed in gamma-scan data for the RERTR–12 plates that blistered in-reactor. This may create bias in the data when compared to the physics-model estimates and when calculating ratios of fission products measured.
4. Loss of fuel meat during sample sectioning and during repackaging of the test sample for transfer to the Analytical Laboratory. This may create a bias in the data when compared to the physics-model estimates.
5. Possible deposition and/or adsorption of fission product in the crucible and crucible housing, which were not analyzed.
6. Contamination of components during handling within the hot cell.
7. Release of gaseous-fission-product species to the hot cell.

8. Temperature difference between the inside of the test assembly and the indicated temperature.

9. Uncertainty for gamma scan data is $uncertainty = \frac{1}{\sqrt{\#\ of\ gamma\ counts}}$

In future testing, the uncertainties associated with 2, 3, and 4 could be reduced by testing intact mini-plates. Items 5 and 6 could be addressed, respectively, by performing analysis on the crucible housing and by improving decontamination processes prior to sectioning. Use of a cold trap at the test assembly exit region at the top of the furnace could provide data for gaseous-fission-product species. Finally, for 8, a higher-resolution temperature profile could be attained inside of the apparatus.

2.7 Overview of the Development of the Iodine Recovery Process[54]

2.7.1 Dissolution of Iodide Salts in Bases

Acceptable recovery was obtained using Method II as detailed in TEV-1553[54] "Iodine Chemical Method Development," using a NH_4OH to dissolve iodine. Iodine was applied to stainless steel planchets using a pipette in the form of NH_4I solution (1000 μg/mL certified ICP liquid solution) and allowed to air dry in a lab hood at ambient temperature. Results are summarized in Table 28. This methodology was applied to wash-and-collect iodine from the thermal-gradient-tube sections and to leach the filter medium from the test-assembly tubes and filters for samples L1P460-2, L1P756-4 and L1P758-4.

Table 28. Results using stainless steel planchets.

Analytical Lab ID #	Temp	Elapsed time between leaching and ICP-MS	Iodine Deposited on planchet (μg)	Final Iodine Total/ICP-MS (μg)	Percent recovery Iodine
94900	warm	12 days	50	46.1	92.2
94901				47.6	95.2
94902				46.7	93.4
94903	ambient	11 days		48.3	96.6
94904				48.3	96.6
94905				49.4	98.8

2.8 Visual Examination

The two L1P758 specimens were removed from the test crucibles and photographed to determine the differences in the melt behaviors between the 600 and 1250°C tests. The remaining specimens from the test matrix were not photographed.

2.9 Gamma Scan of Test Assembly

Using the precision gamma scanner (PGS), gamma rays emitted from the test assembly, positioned vertically in front of the collimator, pass through a narrow variable slit and collimator so that photons from only a small and well-defined part of the assembly are counted over a particular time interval. Gamma rays strike a high-purity germanium detector, which emits a pulse of electric charge proportional to the energy of each individual event. The pulses, after shaping and amplification, are counted. The collected data are analyzed to provide information about the isotopic composition of the area analyzed.

A source scan of known isotopes that span the energy range of the isotopes of interest was performed for an operational check prior to measuring the test assemblies. In order to reduce uncertainty while performing assays using the smallest step size, the assembly was oriented to center it as closely as possible in front of the collimator. This was accomplished by incrementally moving the sample horizontally across the slit of the collimator, thereby

determining the relative edge locations (right and left) of the assembly by observing the count rate and spectra collected; by this method, the center line coordinate of the assembly was determined. The settings for the PGS characterization of the assembly were:

- 0.10 in. step size
- 600 second live time
- 6 microsecond shaping time
- 1.5 MeV energy range.

2.10 Results

2.10.1 Visual Examination

The visual exam for melt piece L1P758-4, shown in Figure 43, revealed a small, irregularly shaped melt puck. It appears that the fuel has pooled at the bottom, as shown in the left image, with possible oxide dross partially covering the previously molten fuel in the image on right. These observations were not confirmed using metallography or other characterization methods.

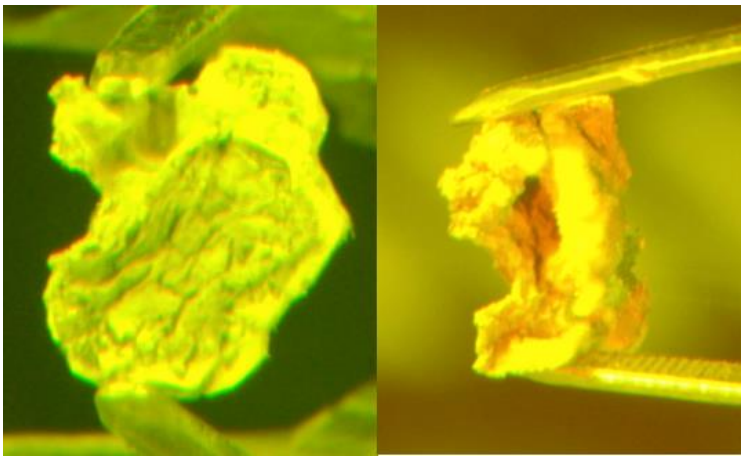

Figure 43. Melt sample L1P758-4, bottom view (left) and side view (right).

2.11 Gamma Scan

The test apparatus for three of the test samples indicated in Table 24 were characterized using the PGS. Cesium-134 and ^{137}Cs are of particular interest due to their relevance to source-term development because of the high dose levels. Iodine, assumed to transport with the Cs, was evaluated using chemical dissolution and is addressed later in this report. A measured and calculated temperature grid is positioned below the ^{137}Cs gamma profile found in Figure 44. Note that the *x*-axis for the gamma-count position relative to the test assembly axial location is different from the axial position indications listed for the test assembly in Table 24 and Table 26 and Figure 42. This is due to the configuration of the gamma-scan equipment. A composite of the gross counts for the dummy and three test assemblies containing fuel are found in Figure 45. The shape of the signal roughly matches the geometry of the test assembly, with the crucible region indicated at the right side of the plot and the filter region at the left. The dummy assembly confirms the geometry profile and provides a baseline for geometric effects and for the likely contamination present on the outside of the assembly. Contamination levels, assumed to be minimal, are expected to vary between the test assemblies.

As expected, the gross gamma-scan plots of L1P460-2 and L1P758-4, two of the 1250°C-temperature tests, show clear evidence of fission-product transport and deposition while the scan of L1P756-2 (low-temperature specimen) does not. The dummy test assembly counts and those for L1P756-2 are similar for the filter and tube regions of the assembly. Because L1P758-4 was dissembled (crucible region removed) immediately following the test in 2012 to inspect the melt puck, the signal for the crucible region is not available.

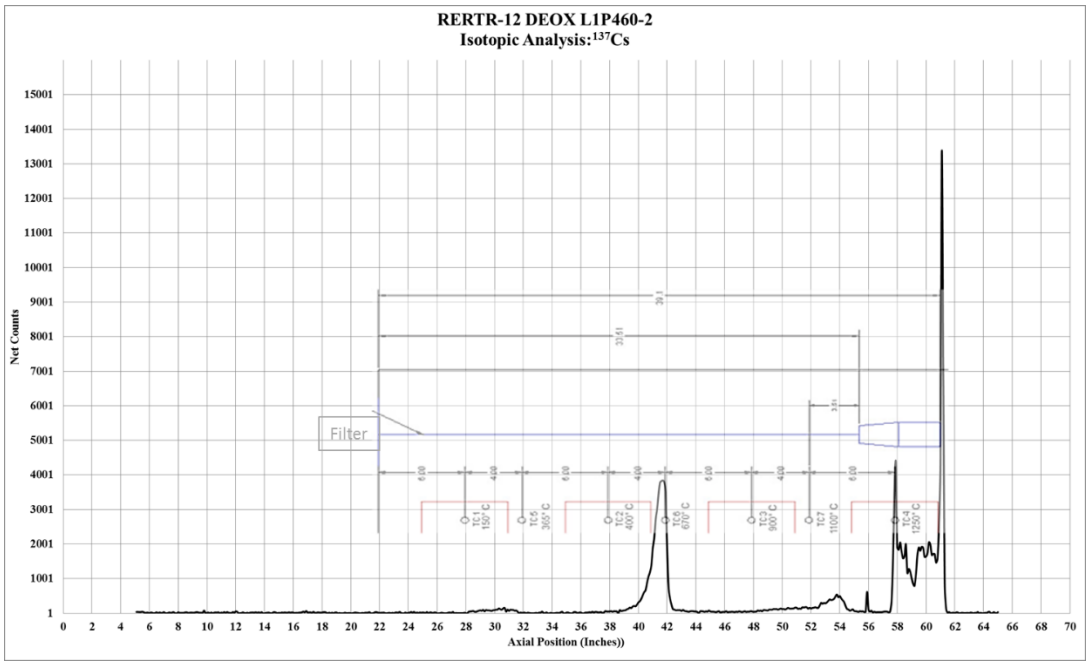

Figure 44. ^{137}Cs gamma-scan results with temperature and test apparatus overlay.

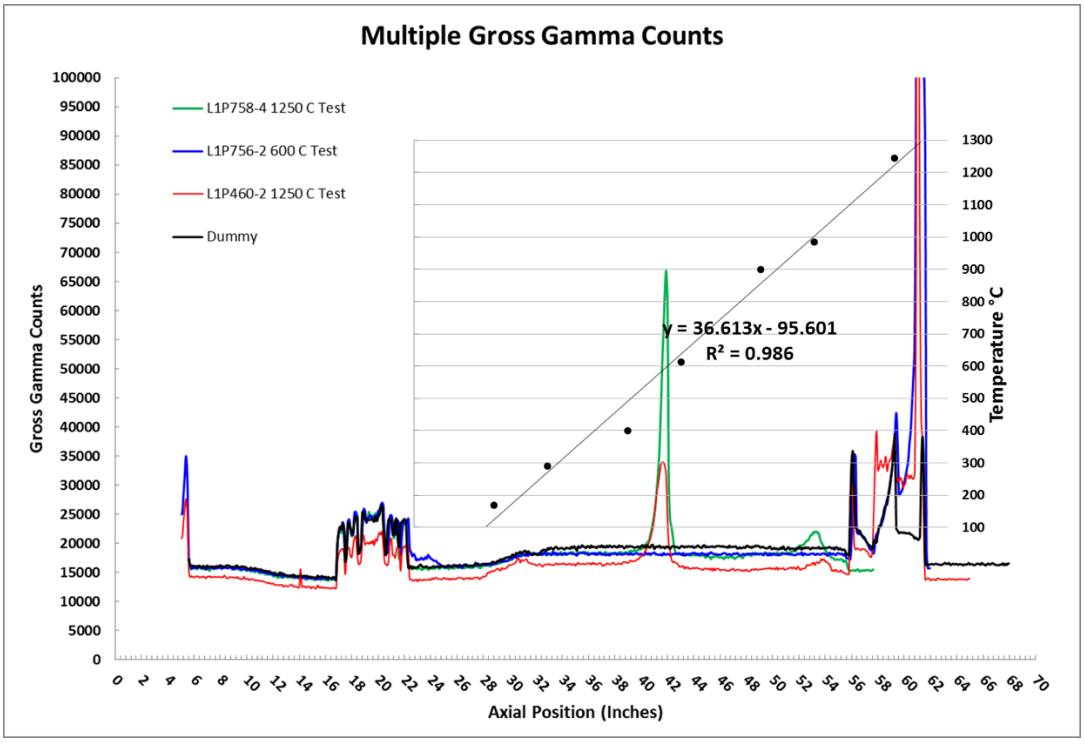

Figure 45. Gross gamma counts for the dummy and the L1P460-2, L1P758-4 and L1P756-2 test assemblies with overlaid test assembly temperature.

Temperature-related deposition behavior provides insight for predicting fission-product transport and deposition for a given hypothetical accident event. The peaks in the

scan profile at different temperatures indicate the gamma-emitting fission-product deposition along the tube. A ratio for ^{137}Cs relative to ^{134}Cs is expected to be approximately 10 to 1. Total counts (not corrected for decay) for ^{137}Cs relative to ^{134}Cs yielded average ratios of 6.26 to 1, 4.82 to 1 and 6.43 for L1P460-2, L1P758-4 and L1P756-2 respectively. The ^{134}Cs data however is barely above background levels in most of the tube regions, so the uncertainty for these regions is higher. For specimen L1P460-2 the ratio was 11.8 to 1 in the crucible region where the ^{134}Cs counts are significantly higher, thus reducing the uncertainty.

Gamma-scan data for the low-temperature test specimen L1P756-2 yielded significant lower fission-product transport and deposition along the tube with a total count of 4.87% for ^{137}Cs relative to total counts in the crucible region. The deposition ratio for ^{137}Cs relative to ^{134}Cs in the crucible region is 8.1 to 1. Deposition profiles for ^{137}Cs and ^{134}Cs for each test PGS crucible assembly are shown in Figure 46, a, b and c, for L1P460-2, L1P758-4, and L1P756-2, respectively.

Gamma scanning of specimen L1P460-2 indicated that approximately 55% of ^{137}Cs remained in the alumina crucible region (bottom region of test assembly containing the fuel melt), with less than 3.74% of this quantity remaining in the fuel. It is likely that adsorption of Cs on the alumina crucible (Al_2O_3) resulted in the Cs holdup in this region given the very low availability of oxygen elsewhere. No other species that are detectable via gamma scan were transported up the tube. Other species for which analysis was performed were ^{144}Ce, ^{106}Rh, ^{125}Sb, ^{144}Pr, and ^{152}Eu, all of which were retained in the crucible region.

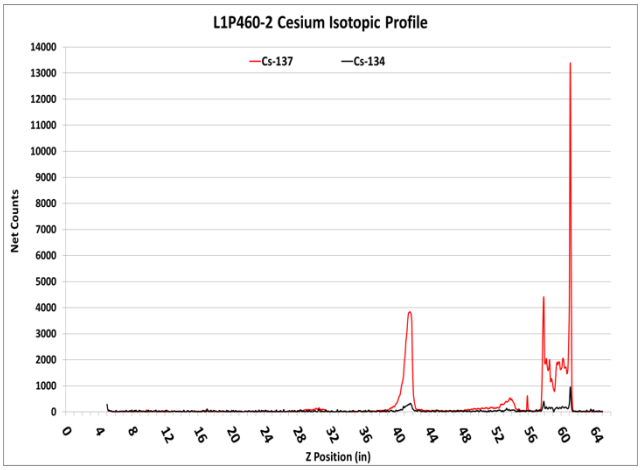

(a)

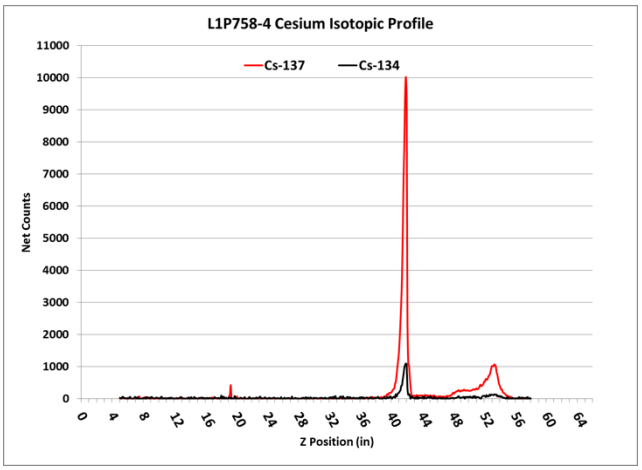

(b)

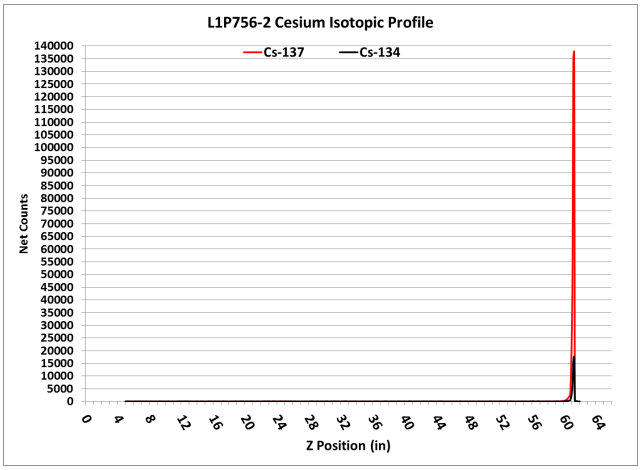

(c)

Figure 46. Cesium isotopic gamma-scan data for L1P460-2 (1250℃), L1P758-4 (1250℃) and L1P756-2 (600°C) plotted in a, b, and c, respectively.

2.12 Chemistry

Following are the results from chemical analysis of the filters, deposition tubes, and melt pucks. The crucible was not analyzed. Chemistry raw-data results and the respective uncertainties for each species, which range from 5–20%, can be found in Appendix C. Because of the uncertainties associated with sampling, detailed earlier, results are presented relative to totals measured in the tube and relative to totals of both the tubes and melt pucks. Where possible and applicable, gamma-scan data are used to scale the results. Chemistry data and the fission product inventories calculated using ORIGEN-MCNP (data found in Appendix D) for the heavy metals U and Pu are compared in Table 29 for specimen L1P460-2. This provides a baseline for estimating retention of ^{137}Cs, retained quantities measured using the PGS, and to some degree, iodine which was not measured using PGS due to the decay of ^{131}I. Plate L1P460-2 is also the lowest-fission-density plate and the most likely to have retained all the fuel in the specimen during the sectioning activity.

Table 29. ORIGEN-MCNP gamma scan and chemistry data comparison for specimen L1P460-2.

Specimen	Element/Isotope	ORIGEN-MCNP	Chemistry Result Totals	Difference relative to ORIGEN-MCNP %
L1P460-2	U total (g)	4.40×10^{-1}	3.68×10^{-1}	-16
	Pu Total (g)	1.17×10^{-3}	1.09×10^{-3}	-7
	^{137}Cs Total (g)	7.48×10^{-4}	3.78×10^{-4}	-49
	^{127}I+^{129}I (g)	1.13×10^{-4}	3.79×10^{-6}	-97[#]

#This value may not be representative of the true difference since the dissolution method of the melt puck would have volatilized off any remaining iodine.

2.12.1 Filter Chemistry Analysis

Chemical analysis was performed on the filter medium that comprises both a 0.45 micron particulate filter and activated charcoal and was located at the top of the test

apparatus. The charcoal medium was crushed, and leaching methods were applied using the chemistry methods reported in TEV-1553[54] for Method II and detailed in Section 2.7.1. Results of the analysis yielded measured quantities that were less than 1% of the iodine transported up the tube. The detection limit for ICP-MS for iodine is 10 μg[g] so, if iodine present were below this threshold, it would be undetectable. Based on the detection limits of the ICP-MS, deposit fractions as low as 5% of estimated[h] total sample inventory would still be detectable. Any cesium and iodine still in gaseous form would not have been captured in the filter.

2.12.2 Melt-puck Chemistry Analysis

All measurements in this section are presented as relative to the totals obtained by summing the measured inventories from the tube, the tube etch, and the melt puck. No iodine recovery was possible using aqua regia with HF to dissolve the melt pucks. While this dissolution did not result in a temperature hot enough to volatilize the Cs, the reaction was warm enough to volatilize any remaining iodine. Should iodine-retention data for the melt puck be required to measure any retained inventories, other recovery methods would need to be developed.

The melt-puck retention percent for the elements measured for all the specimens were found to be consistently lower for L1P460-2 than for those measured for the L1P756-4 and L1P758-4 specimens. The reason for this is uncertain.

---

[g] The uncertainty is ±5–10 percent. Smaller specimen sizes result in higher uncertainties.

[h]. Estimates can be determined using sample volume and fission-product inventories calculated using MCNP-ORIGEN.

2.12.2.1 Halogens and Alkali Metals: Iodine, Cesium and Rubidium

Iodine was not measured in the puck due to the dissolution methods volatilizing any remaining inventories. Cesium remaining in the pucks, measured using chemical analysis, and then scaled using gamma-scan and ORIGEN-MCNP data, was 3.7%. Retention of rubidium in the melt puck was 3, 2, and 6% for L1P460-2, L1P756-4, and L1P758-4, respectively.

2.12.2.2 Tellurium Group: Tellurium

The tellurium percent left in the melt pucks relative to the totals measured for L1P460-2, L1P756-4, and L1P758-4 are 92, 99, and 99 percent, respectively. Table 30 summarized the relative percentages in the melt pucks.

Table 30. Percent tellurium remaining in melt puck.

Specimen	Percent Tellurium Remaining in Melt Puck
L1P460-2	91.88%
L1P756-4	99.27%
L1P758-4	98.98%

2.12.2.3 Barium and Strontium Group: Barium and Strontium

Barium and strontium retained in the melt pucks, relative to the totals measured for L1P460-2, L1P756-4, and L1P758-4 are summarized in Table 31.

Table 31. Percent barium and strontium remaining in melt puck.

Specimen	Percent Remaining in Melt Puck	
	Barium	Strontium
L1P460-2	97.11%	76.73%
L1P756-4	98.59%	98.50%
L1P758-4	98.80%	98.45%

2.12.2.4 Noble Metals: Ruthenium, Rhodium, Palladium, and Technetium

The percent of ruthenium, rhodium, palladium, and technetium left in the melt pucks relative to the totals measured for L1P460-2 are 99.4, 99.9, 97.8, and 98.9%, respectively.

For L1P756-4, they are 99.6, 99.9, 99.3, and 99.9%, respectively. For L1P758-4, they are 99.8, 100.0, 99.2, and 99.8%, respectively. These are summarized in Table 32. The <1% fractions that were transported into the deposition tube are presented in the next section.

Table 32. Percent ruthenium, rhodium, palladium and technetium remaining in melt puck.

Specimen	Percent Remaining in Melt Puck			
	Ruthenium	Rhodium	Palladium	Technetium
L1P460-2	99.40%	99.90%	97.81%	98.87%
L1P756-4	99.56%	99.92%	99.28%	99.89%
L1P758-4	99.78%	99.99%	99.22%	99.84%

2.12.2.5 Lanthanide Group: Lanthanum, Zirconium, Neodymium, Europium, Promethium, and Samarium

The percent of lanthanum, zirconium, neodymium, europium, promethium, and samarium left in the melt pucks relative to the totals measured for L1P460-2, L1P756-4, and L1P758-4 are summarized in Table 33.

Table 33. Percent lanthanum, zirconium, neodymium, europium, promethium, and samarium remaining in melt puck.

Specimen	Percent Remaining in Melt Puck					
	lanthanum	Zirconium	Neodymium	Europium	Promethium	Samarium
L1P460-2	99.38%	98.73%	99.71%	99.91%	99.69%	99.86%
L1P756-4	99.92%	99.75%	99.94%	100.00%	99.96%	99.99%
L1P758-4	99.82%	99.83%	99.88%	99.95%	99.87%	99.93%

2.12.2.6 Cerium Group: Cerium and Plutonium (Plus Uranium)

The cerium, plutonium and uranium remaining in the melt puck relative to the totals measured chemically were between 97 and 100 percent. These are summarized in Table 34 for L1P460-2, L1P756-4 and L1P758-4 specimen. For specimen L1P460-2, the ORIGEN-MCNP values compared to the measured chemistry values for U and Pu were within 16 and 7 percent respectively.

Table 34. Percent cerium, plutonium and uranium remaining in melt puck.

Specimen	Percent Remaining in Melt Puck		
	Cerium	Plutonium	Uranium
L1P460-2	99.47%	97.17%	99.85%
L1P756-4	99.91%	99.22%	99.98%
L1P758-4	99.74%	97.68%	99.87%

2.12.3 Deposition Tube Chemistry Results

Chemical analysis and iodine recovery from the tube sections was performed using the 1% (0.5M) ammonium-hydroxide leach method from Reference 15 listed as Method II. Following analysis for iodine, 16M HNO_3 was added to obtain 2M of nitric acid in order to dissolve solids so that other fission products could be measured. A tube etch was performed following the tube leach using a fresh solution of 25 mL, 2M HNO_3 combined with 3mL, 12M HCL and 3 drops 24M HF to determine the quantities adsorbed. Note that any iodine that may have been adsorbed on the tube interior would be volatilized during this process and therefore not measured. The tube sections were batched according to the temperature region of the deposition tube, thus yielding temperature-resolved fission-product transport and deposition behavior data.

2.12.3.1 Halogens and Alkali Metals: Iodine, Cesium and Rubidium Transport

Temperature-resolved atom deposition of cesium (uncertainty 5–10/20%[i]) and iodine (uncertainty 5–10%) showing the ratio relative to each other are plotted in Figure 47, Figure 48 and Figure 49 for L1P460-2, L1P756-4, and L1P758-4, respectively. These plots demonstrate the excess of Cs relative to I and indicate that, while some of the Cs and I were

[i] The uncertainty range is based on quantities of ^{137}Cs measured after the initial rinse (5–10%) which were summed with totals following the tube etch (5–20%).

likely transported in the form of CsI, the Cs inventory in excess of CsI was transported as a different species, likely elemental Cs. These distribution ratios along the tube are based on the inventories measured in the tube only.

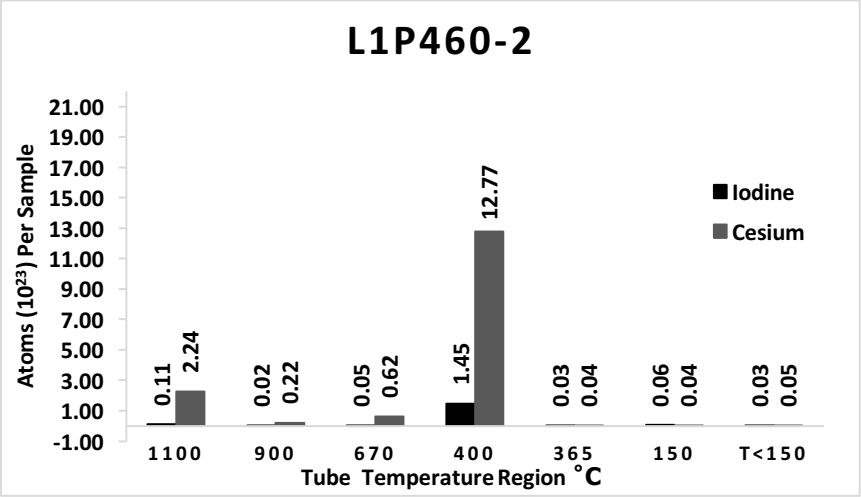

Figure 47. Temperature-resolved comparison of iodine and cesium deposition for L1P460-2.

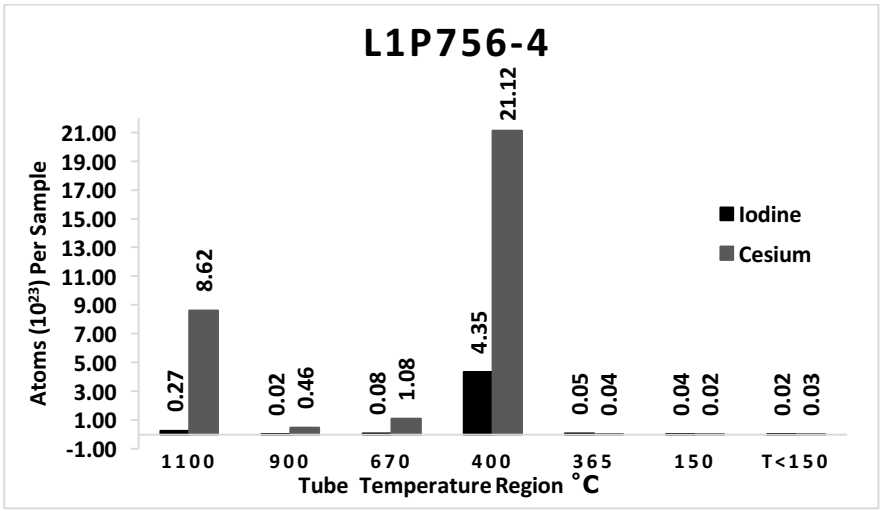

Figure 48. Temperature-resolved comparison of iodine and cesium deposition for L1P756-4.

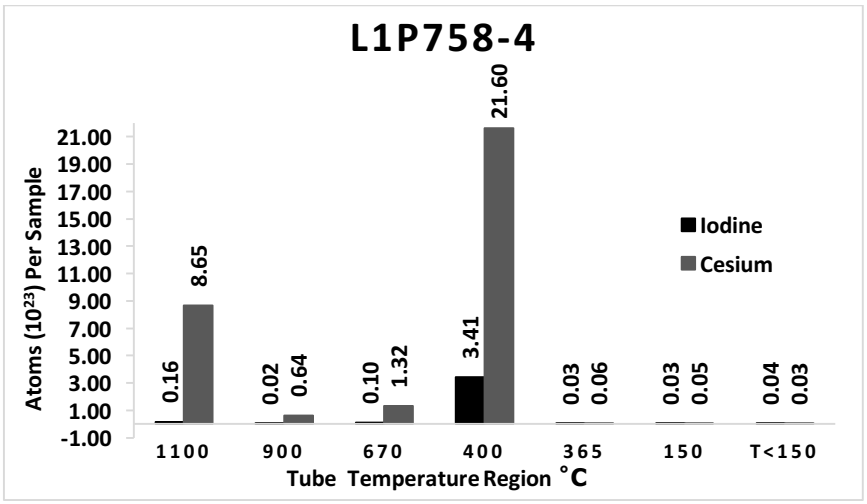

Figure 49. Temperature-resolved comparison of iodine and cesium deposition for L1P758-4.

Tube deposition behaviors of I and Cs are consistent for all the high-temperature samples, with 82–90% and 88–90% of the tube inventories deposited in the temperature region between 614 and 400°C for specimens L10460-2, L1P756-4 and L1P758-4 respectively. The plotted deposition fractions (relative percent) as a function of temperature are found in Figure 50, Figure 51 and Figure 52. A phase diagram showing a transition to the liquid phase at 627°C for CsI is shown in Figure 53. Because the tube sections were processed in batches (refer to Table 27), the temperature resolution in the tube chemistry data is coarse; this specific temperature location (490 *(400*[j]*)*–673) on the deposition tube would have been included in the 400°C sample batch of the tube. Deposition results are also consistent with the activity measured in the gamma scan for this region of the tube. The gross gamma-scan data (shown in Figure 45) indicate that the peak gamma-emitting fission-product deposition in the tube is ~600°C and is also consistent with the behavior that was observed for the DEVAP[50] experiment. While the DEVAP experiment introduced H_2O/H_2, the tube materials were similar.

[j] Italics are actual, measured furnace temperatures. Non-italics are estimates based on line fit equation

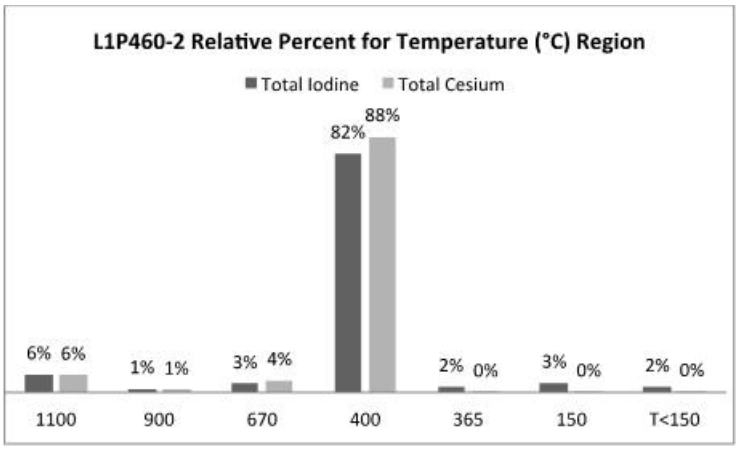

Figure 50. Relative percent of total iodine and total cesium deposited at different temperatures along tube length for sample L1P460-2.

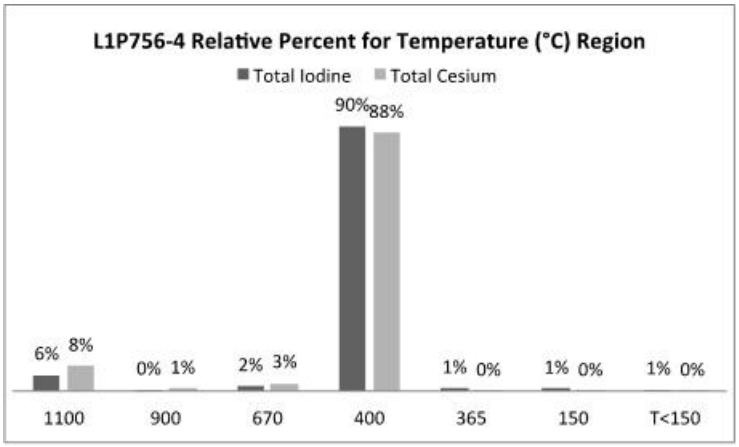

Figure 51.Relative percent of total iodine and total cesium deposited at different temperatures along tube length for sample L1P756-4.

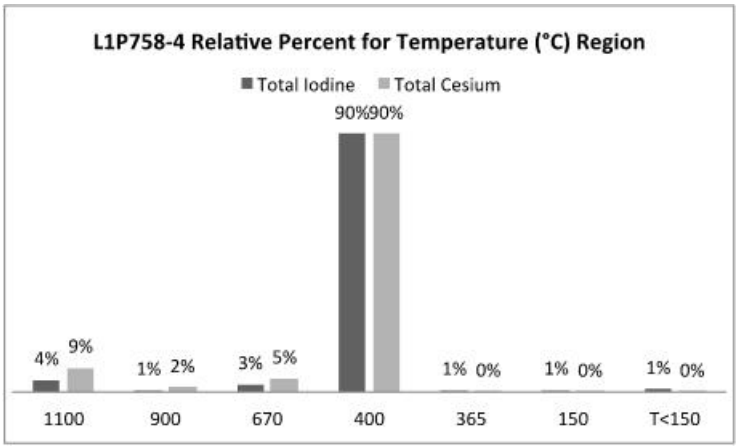

Figure 52. Relative percent of total iodine and total cesium deposited at different temperatures along tube length for sample L1P758-4.

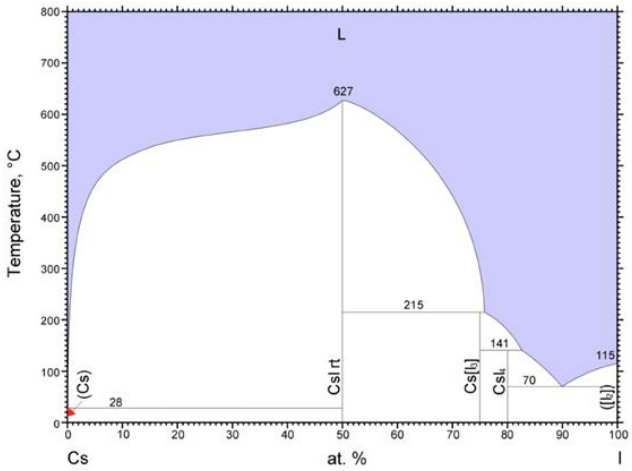

Figure 53. Phase diagram for CsI.[55]

The ratio of chemically and PGS measured tube-depositions for ^{137}Cs were used to estimate the inventories shown to be present in the crucible region of the test assembly. Using the gamma-scan data shown in Figure 44 for L1P460-2,[k] an estimate of 45% and of the Cs inventory was derived for deposition in the tube region and 55% retained in the crucible region, considering only cesium retained in the test assembly. It is not known whether any iodine was retained in the melt puck with the little remaining cesium as CsI or with the uranium as UI_3. At the test temperature of 1250°C, it is assumed that iodine total release percent would be near that of those reported for the U–Al system where 97.8% was released in argon at 1100°C. The chemistry/gamma scan ratio results for L1P460-2 are summarized in Table 35. Results in Table 14 for ^{137}Cs suggest that some cesium, and likely iodine, may have exited the test assembly and particulate filter in a gaseous form and been vented into the hot cell. It is assumed that this also occurred for L1P756-4 and L1P758-4.

[k]. Note that L1P756-4 did not receive a gamma scan, and crucible region for L1P758-4 had been removed prior to the scan activity for visual inspection of the test sample.

Table 35. Total ^{137}Cs inventories measured in tube and melt puck for L1P460-2 using analytical chemistry with scaling using ^{137}Cs gamma scan data to estimate ^{137}Cs remaining in the crucible region.

Sample	Total ^{137}Cs Measured via Chemistry in Puck (g)	Total ^{137}Cs Measured via Chemistry in Tube (g)	Total ^{137}Cs Estimated via the Chemistry/Gamma Scan Ratio Remaining in Crucible Region (g)	Percent ^{137}Cs Remaining in Puck Estimated via the Chemistry/Gamma Scan Ratio Data In Melt Puck
L1P460-2	0.30E-04	1.57E-04	1.91E-04	3.74%

For the U–Al fuel from [48], the reported cesium release in argon at 1100°C was 79.6%, and the value reported from [47] at 1105°C in helium is 69.5%. Release behaviors for cesium in an oxidizing environment from [48] and [47] are not in agreement, so predicting the release behavior for the U–Mo metallic fuel would be speculation if comparing to these other fuels systems. The oxide fuels showed higher retention of the Cs (in the form of Cs_2O) at similar temperatures; however, at the much-higher melt temperatures of the oxides, the Cs_2O disassociated, and the Cs was released.

The rule-of-thumb ratio of cesium to iodine inventory predicts 10 to 1. For L1P460-2, L1P756-4 and L1P758-4, the ratios were 9.3, 6.6 and 8.7 to 1 respectively. The rule of thumb for ^{127}I to ^{129}I inventory ratio is 20%. The ratios measured for L1P460, L1P758, and L1P756 are 32, 21, and 20 percent, respectively and plotted in Figure 54 through Figure 56. The plotted relative percentages of the iodine and cesium isotopic species deposited along the tube are shown in Figure 57 through Figure 59

Transport and deposition behavior for rubidium (uncertainty 5–20%) is shown in Figure 60. A large deposition in the 400°C temperature region is consistent with behavior of the iodine and cesium. An additional large deposition is noted at 1100°C, and two smaller ones at 900 and 670°C. Between 94 and 97% of the total chemically measured rubidium was transported up the tube. It may be that some Rb is not accounted for because not all

experiment components were chemically analyzed. Rubidium release behavior is not reported in the previous studies reviewed for this report.

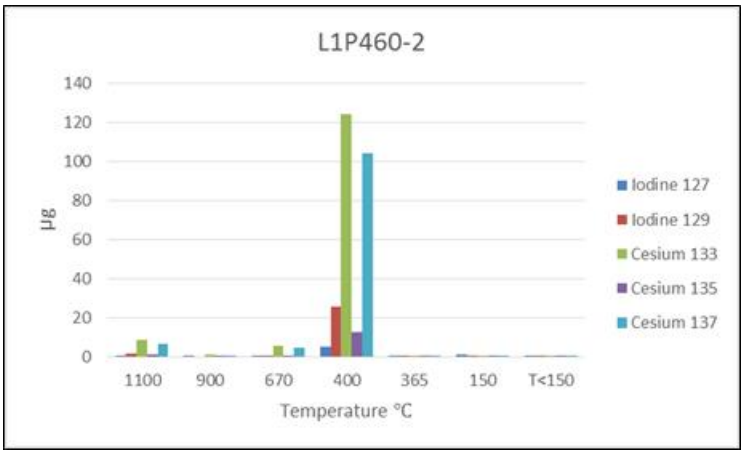

Figure 54. Iodine and cesium isotopic species measured in tube regions for sample L1P460-2.

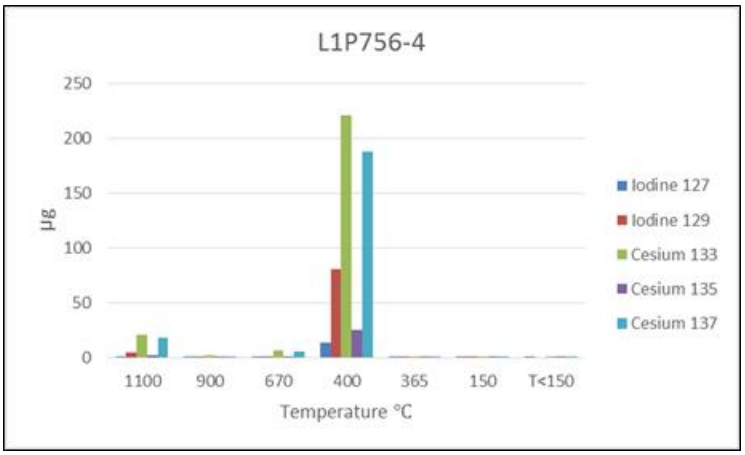

Figure 55. Iodine and cesium isotopic species measured in tube regions for sample L1P756-4.

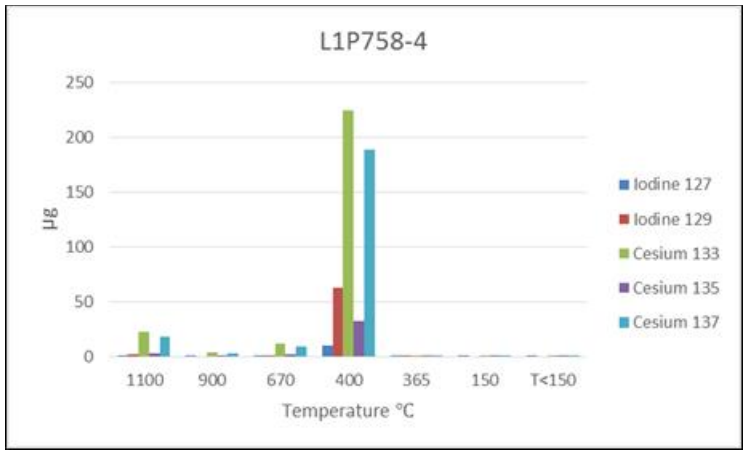

Figure 56. Iodine and cesium isotopic species measured in tube regions for sample L1P758-4.

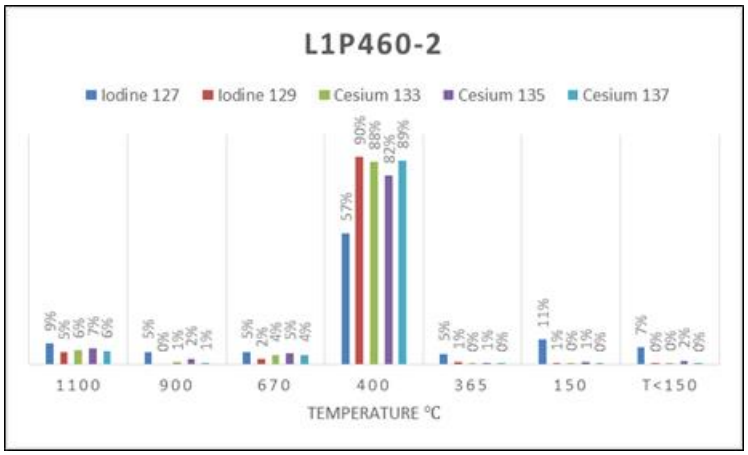

Figure 57. Relative percent of iodine and cesium isotopic species measured in tube regions for sample L1P460-2.

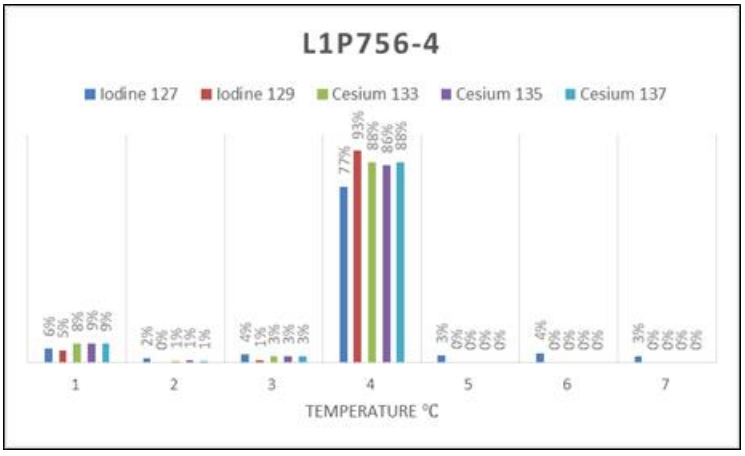

Figure 58. Relative percent of iodine and cesium isotopic species measured in tube regions for sample L1P756-4.

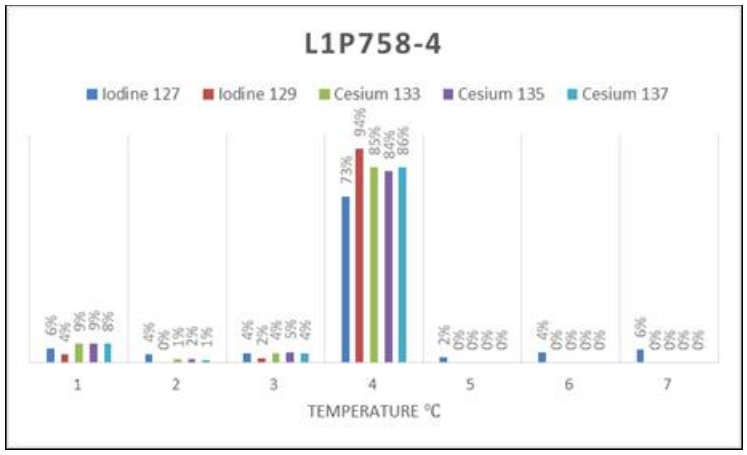

Figure 59. Relative percent of iodine and cesium isotopic species measured in tube regions for sample L1P758-4.

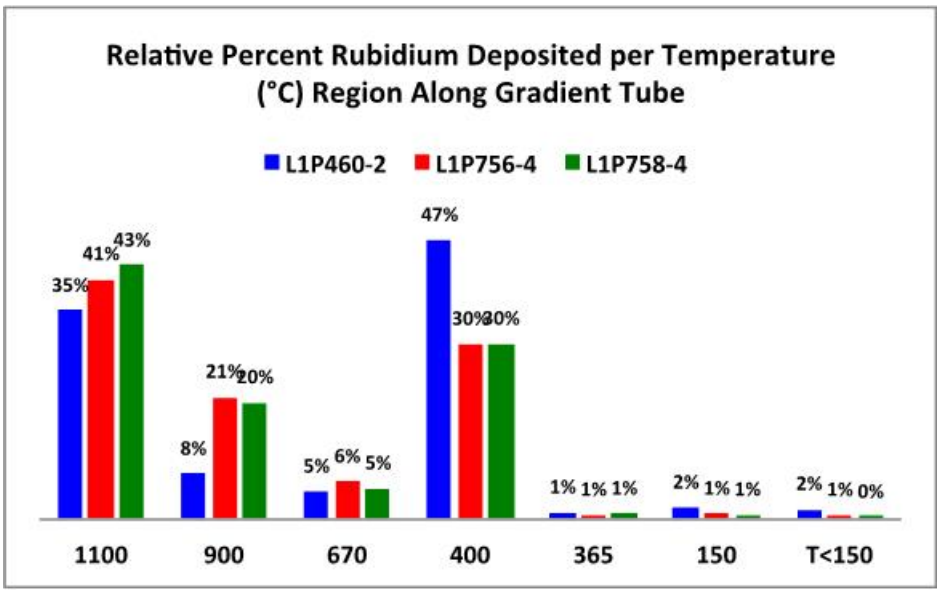

Figure 60. Relative percentages of total rubidium in tube, deposited in different temperature regions along tube length for samples L1P460-2, L1P756-4, and L1P758-4.

2.12.3.2 Tellurium Group: Tellurium Transport

Only a small amount of tellurium (uncertainty 5–20%), 1–9% of the total measured for the puck and tube combined, was transported up the deposition tube. It may be that some Te is not accounted for because not all experiment components were chemically analyzed. The primary deposition location is in the same 400°C region, illustrated in Figure 61, where most of the iodine and cesium were located. Tellurium release behavior, reported in

Reference 47 for UO_2, showed low releases in air, but high releases in helium. Data for U–Al alloy from Reference 47 shows higher release in air, but lower releases in helium. The U–Mo release behavior in argon is, therefore, more consistent with the metallic fuel.

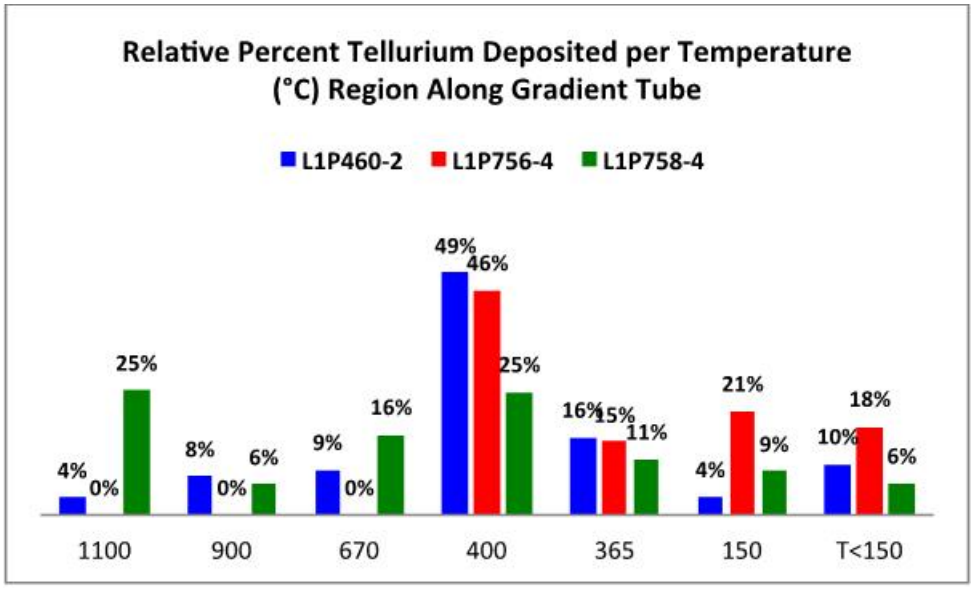

Figure 61. Relative percentages of total tellurium deposited in different temperature regions along the tube. Percentages are based on the total measured (only 1–9%) of tellurium in the tube region.

2.12.3.3 Barium and Strontium Group: Barium and Strontium Transport

Deposition behavior of a very small amount of the Ba and Sr (uncertainty 5–20% for both) along the thermal-gradient tube reveals no definite temperature-resolved patterns. The deposition ratios are illustrated in Figure 62, Figure 63, and Figure 64 for L1P460-2, L1P756-4, and L1P758-4, respectively. The ratio of the tube-deposition totals represent between 1 and 30% of the Ba and Sr inventory totals measured for the combined tubes and melt pucks. Data for barium and strontium are reported in Reference 47 on UO_2 fuel, with release quantities less than 1% until temperatures are beyond the 1250°C applied for this study.

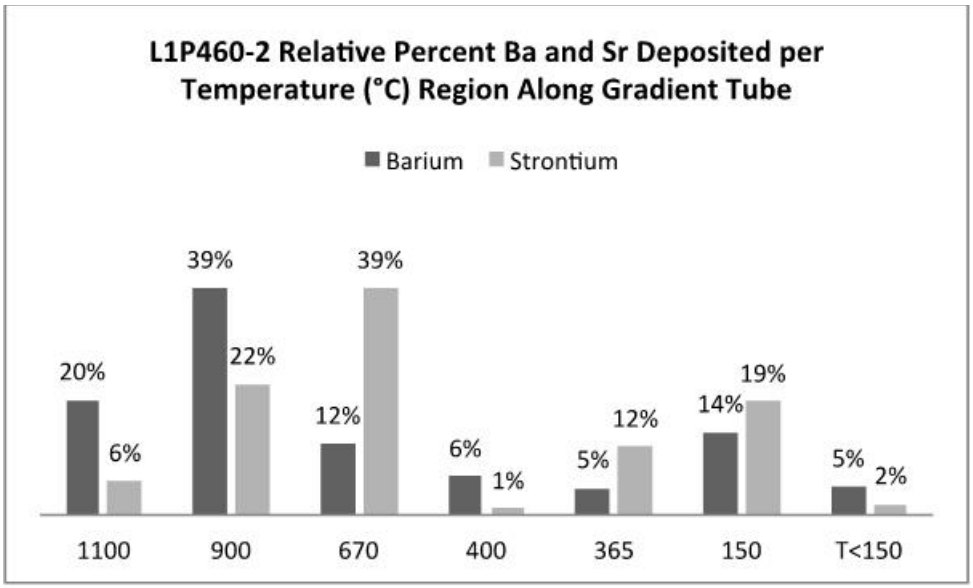

Figure 62. Sample L1P460-2. Relative percentages of total Ba and Sr deposited in different temperature regions along the tube length. Percentages are based on the total measured in the tube region.

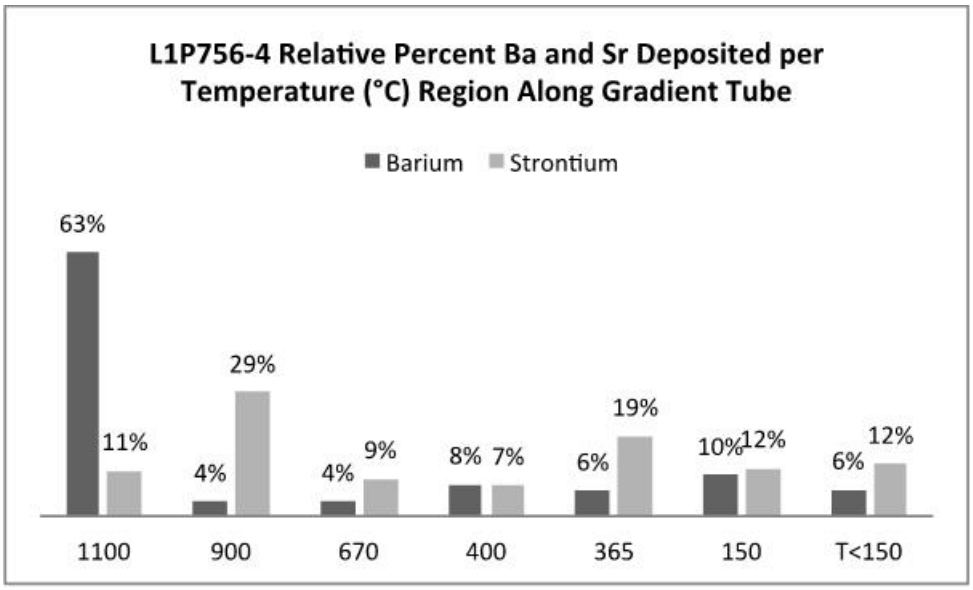

Figure 63. Sample L1P756-4. Relative percentages of total Ba and Sr deposited in the tube temperature regions. Percentage are based on the total measured in the tube region.

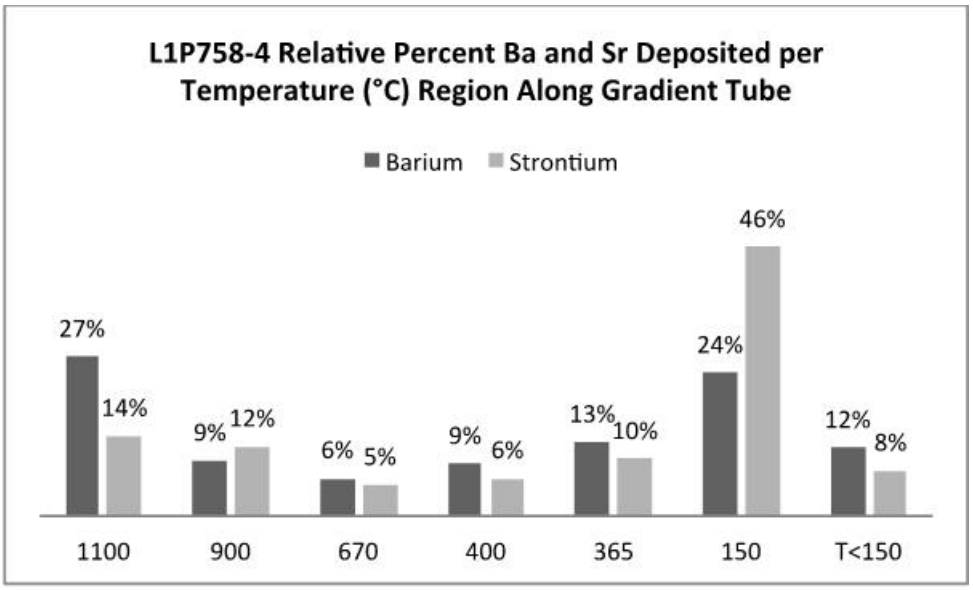

Figure 64. Sample L1P758-4. Relative percentages of total Ba and Sr deposited along the tube in different temperature regions. Percentages are based on the total measured in the tube region.

2.12.3.4 Noble Metals: Ruthenium, Rhodium, Palladium and Technetium Transport

The fission-product transport for ruthenium (uncertainty 5–20%), rhodium (uncertainty 10–20%), and palladium (uncertainty 5–20%) indicate inconsistent temperature-resolved deposition behavior between L1P460-2, L1P756-4, and L1P758-4. However, the measured quantities are so small that the ICP-MS uncertainties may be responsible for scatter in the data. Technetium (uncertainty 5–20%) exhibits a very strong trend for all three samples. Percentages for each species are compared in Figure 65 a, b, and c, for each sample. A comparison between each of the samples for the temperature-resolved deposition behavior for Ru, Rh, Pd and Tc is illustrated in Figure 66a, b, c, and d, respectively, for L1P460-2, L1P756-4, and L1P758-4. The line fit in each plot serves only to emphasize the differences and/or similarities in the data between the samples and does not imply a temperature-resolved gradient in the deposition behavior between the points. Percentages are based on the total measured in the tube region. Less than 1% of each of these

elements were transported up the tube. Ruthenium is the only one of these four species reported in the historical data referenced earlier, and only by Reference 47 for UO_2, with release in helium at a slightly higher temperature being very low (<1% at 1515°C). However, Reference 47 reports the release quantity in air as close to 100% for a temperature of 1200°C

.

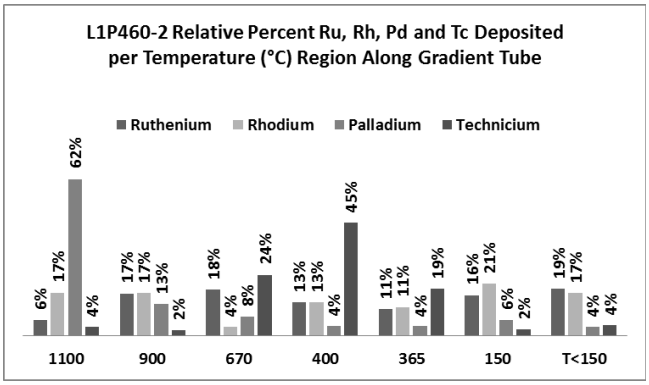

(a)

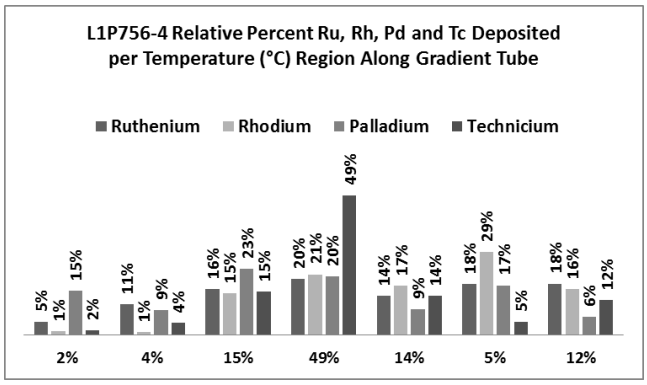

(b)

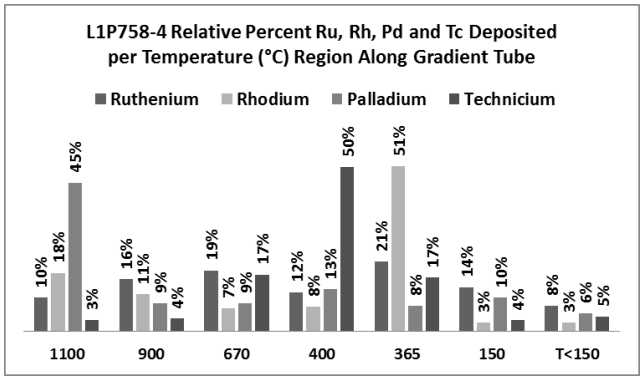

(c)

Figure 65. Relative percentages of total Ru, Rh, Pd, and Tc deposited in the tube temperature regions for samples L1P460-2, L1P756-4, and L1P758-4 shown in a, b, and c, respectively. Percentages are based on the total measured in the tube region.

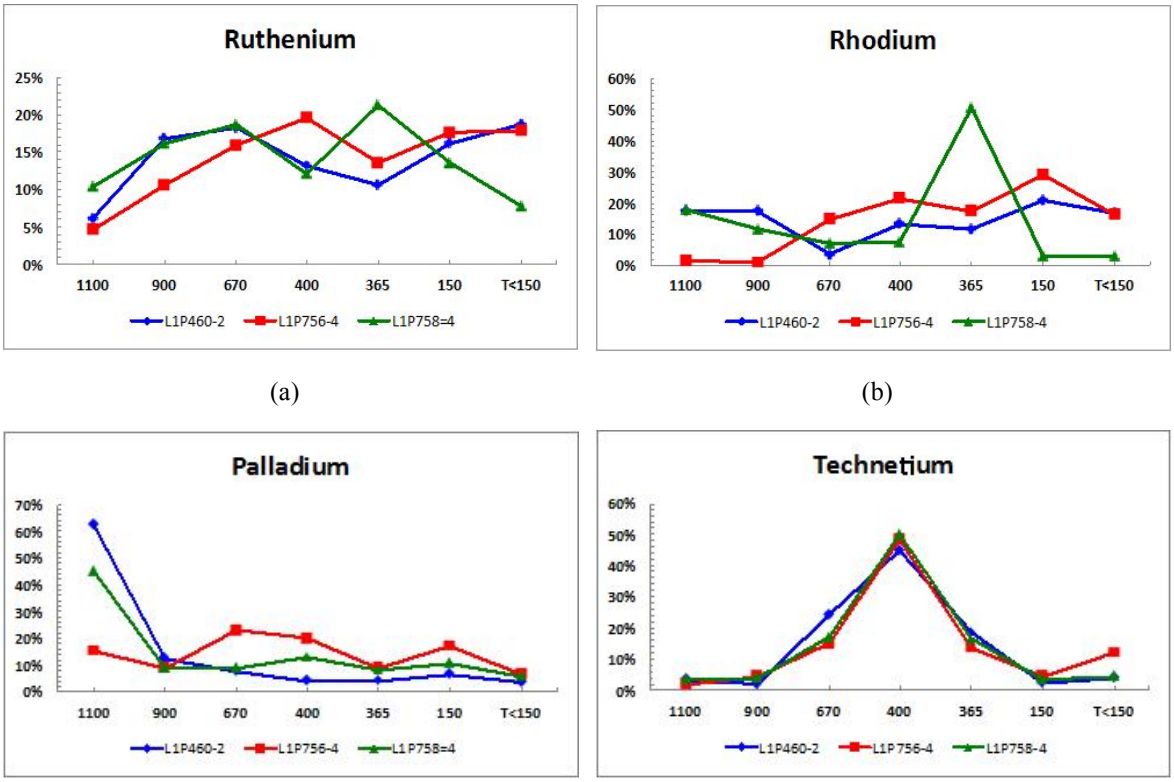

Figure 66. Temperature-resolved deposition behavior for Ru, Rh, Pd, and Tc deposited in the tube temperature regions are illustrated in a, b, c, and d, respectively for samples L1P460-2, L1P756-4, and L1P758-4. Percentages in percent are based on the total measured in the tube region.

2.12.3.5 Lanthanide Group: Lanthanum, Zirconium, Neodymium, Europium, Praseodymium, and Samarium Transport

A range of 0–1% of the total measured for the listed elements in the lanthanide group indicates virtually no transport behavior for these elements for the given test conditions.

2.12.3.6 Cerium Group: Cerium and Plutonium (Plus Uranium) Transport

Chemical analysis performed on the tube-rinse solution (following iodine recovery) and the tube etch yielded temperature-resolved deposition of cerium, uranium, and plutonium (uncertainty 5–20% for all). These are shown in Figure 67 a, b, and c, for the three samples for cerium, uranium, and plutonium, respectively. The percent distribution along the tube is

based on the total inventory measured in the tube only. However, when the transport of these heavy metals is considered in the context of the totals measured for the deposition tubes and the melt pucks together, the tube totals represent only 0.08, 0.2, and 3.5% or less for Ce, U, and Pu, respectively. Moreover, as seen in Figure 67, a, b and c, no apparent deposition pattern is apparent. This is consistent with that reported by Reference 47, with very low uranium transport, reported as <1% in air and 1.3% in helium.

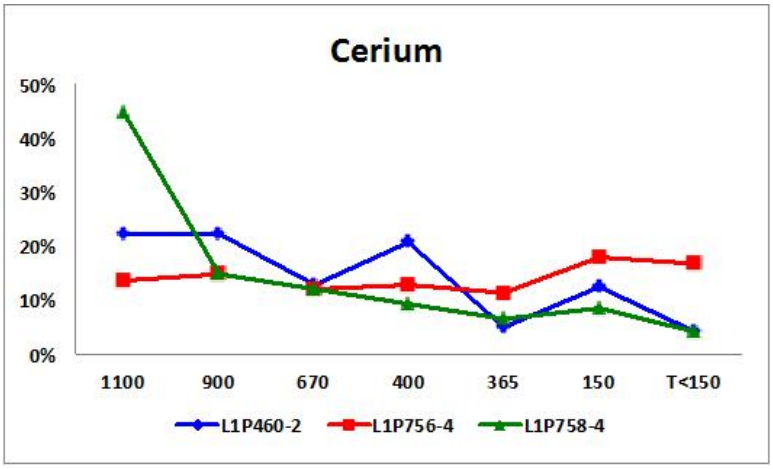

(a)

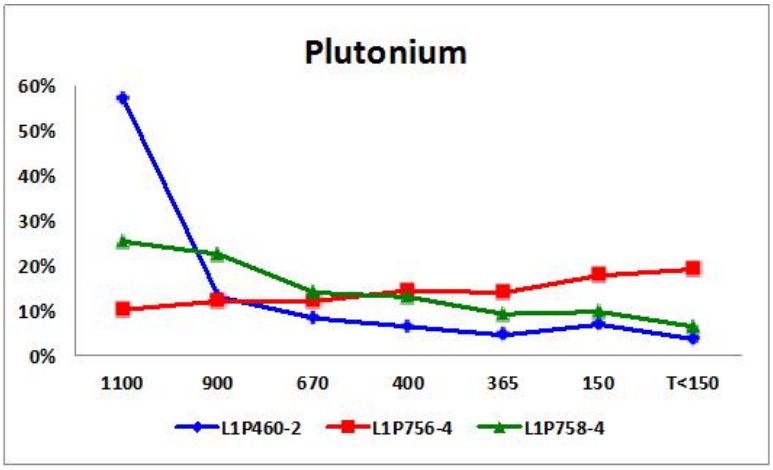

(b)

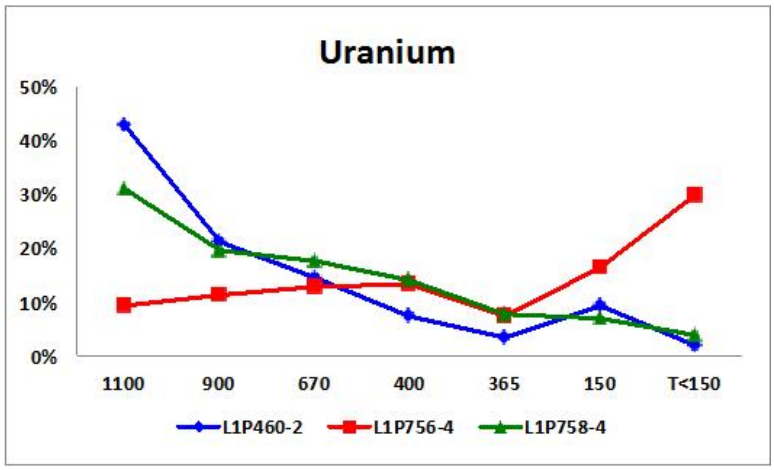

(c)

Figure 67. Temperature-resolved relative deposition percents in the tube for Ce, Pu, and U, shown as a, b, and c, for L1P460-2, L1P756-4, and L1P758-4, respectively.

2.13 Conclusions

Thirty-two monolithic fuel plates fabricated and irradiated to fission densities in the range of 3.6 x 10^{20} to 7.1 x 10^{21} fissions/cm^3 (average fission density) were blister tested during the basic and applied phases of the fuel-development program. The measured blister-threshold temperatures were as high as 550° and as low 359°C. The key findings from these preliminary blister-testing studies are as follows:

- Blister-threshold temperatures are a predictable function of fission density whereby periodic recrystallization of the fuel during irradiation increases mobility of fission gases.
- The blister-threshold temperature of monolithic fuel and the scatter in the data are consistent with the blister-threshold temperature of previously qualified fuel systems within the range of fission densities previously tested.
- Blisters form consistently in the higher-fission-density edge and/or corner regions of the plate.
- Two types of blister morphologies were observed. Type 1 blisters form at high temperature and low fission density and can propagate into the cladding. Type 2 blisters form at higher fission densities and propagate only over or into the fuel.
- Plates fabricated by the friction bonding method and hot isostatic press bonding method had similar blister-threshold temperatures and scatter.
- Based on limited data, there does not appear to be a strong influence of fission heating rate on blister-threshold temperature, however, the effect of fission heating rate appears to be co-variant with fission density.

Thermal cycling during blister threshold testing does not appear to have a large effect on the blister-threshold temperature. The fission-product-transport scoping study was successful in characterizing the transport and deposition behavior of iodine and cesium at 1250°C in a non-oxidizing environment and fission-product-release behaviors at the two test temperatures, 600 and 1250°C. Deposition of these fission products was primarily in the temperature range between 400 and 614°C. It is not known whether any iodine was retained in the melt puck with the little remaining cesium as CsI or with the uranium as UI_3. Iodine release from UAl_X tested in air at 1100°C in Reference 46 was 60%. At the temperature of 1250°C, it assumed that iodine total release percentage would be near that of those reported for the U–Al system where 97.8% was released in argon at 1100°C.

According to gamma-scan data only, approximately 45% of the ^{137}Cs was transported up the test assembly tube, and it is assumed all specimens exhibited the same transport behavior as L1P460-2. However, the ORIGEN-MCNP simulation suggests that some of the cesium exited the test assembly in a gaseous form. Because the inventories of iodine and cesium were located together in these temperature regions, it is assumed that some iodine was transported together with cesium in the chemical form of CsI. The excess Cs is assumed to have transported in the form of elemental Cs. This is supported by the literature cited in this report. Release behaviors for cesium in an oxidizing environment from References 47 and 48 are not in agreement, so predicting the release behavior for the U–Mo metallic fuel is not possible based on comparison to these other fuels systems. The oxide fuels showed higher retention of the Cs (assumed in the form of Cs_2O) at similar temperatures; however, at the much-higher melt temperatures of the oxides, the Cs_2O disassociated, and Cs was released. The presence of oxygen had the effect of reducing the release fraction of cesium

while increasing the release fraction of iodine. This may also be true of the U–Mo fuel and might have been demonstrated if the alumina crucible could have been analyzed. Further testing is needed to characterize these release and transport behaviors.

With the exception of rubidium for all the samples, and strontium for L1P460-2, well over 90% of the tellurium group, the barium and strontium group, the noble metals, the lanthanide group, and the cerium group elements were retained in the melt puck within the crucible.

There is potential to reduce the uncertainty in the data for future fission-product release and fuel-failure testing. It may be possible to achieve successful recovery of iodine from the melt puck by dissolving the puck in molten salts. The basis for this hypothesis is that some transport and retention of iodine into the sodium coolant is assumed in the studies of EBR-II fuels.[56] If the correct salt solution can be determined, it would provide an opportunity to determine whether any iodine remains in the fuel. Also, other chemical methods could be developed for iodine recovery from the melted fuel. Future fission-product retention/transport tests could include chemical analysis of the crucible region or use a crucible manufactured from material less likely to react with the fission products during the test. Failure testing of intact fuel-plate specimens would reduce the uncertainties associated with specimen sectioning and handling.

It is clear there are two common variables that influence release fractions in all fuel types. These are fission density and temperature. Higher fission-density/burnup levels result in the release of a larger fraction of the volatile fission products for a given temperature. This may be attributed to an increase in fission-product diffusion rates or changes in the microstructural features such as bubbles and cracks within the fuel. This trend is observable

in blister-threshold data for U–Mo monolithic fuel plates where blister-threshold temperatures (see Chapter 1) are a predictable function of the burnup and/or fission density of a given plate. Higher temperatures also result in larger release fractions of the volatile fission products, as seen in the historical data. It would be reasonable to assume that these fission-product-release behaviors would also apply to the U–10Mo fuel system.

Hobbins, et al.[57] conclude that cesium and iodine concentrations relative to hydrogen and steam determine the chemical form of both elements. The chemical form of iodine and cesium determines the transport behavior once they come out of the fuel. Increasing burnup causes restructuring in the solid state within the fuel during irradiation, potentially leading to the creation of high-rate diffusion paths, such as tunnel formation along grain boundaries. Such phenomena can affect the movement of noble gases and volatile fission products during irradiation and upon heat-up in accidents prior to fuel liquefaction or melting. Such observations have been made for high-burnup light-water-reactor fuel; however, the microstructural transitions are similar to those observed in the U–Mo fuel system. Focusing future fission-product-release tests on low-, medium-, and high-burnup fuel specimens would be prudent to better model the source terms presented for a range of operating conditions in different reactors.

This experiment did not provide fuel-plate or fuel-element time-resolved fission-product release rates or fission-product transport behavior in an oxidizing environment. Nor was the fission-product release testing representative of an actual severe accident because of the two-hour hold at the selected temperatures. Testing in an inert environment (argon in the case of this scoping study) results in data for iodine, cesium, tellurium, and ruthenium transport behaviors that are not representative of the true water/steam environment during

research and test reactors off-normal conditions. Performing additional melt tests in an oxidizing atmosphere (steam) and for shorter hold times would provide transport and deposition data that are more directly comparable to the actual environment for the driver core fuel plates during an accident event in a research or test reactor.

It is anticipated that the monolithic fuel system will exhibit melt-progression behavior that is different from the dispersion plate-fuel system. Little information exists on the core degradation mechanisms of U–10Mo fuel plates, and testing should be performed that would provide information on the behavior of this fuel system under severe accident conditions. In the previous analysis[58] for the ATR HEU UAlx core, it is assumed that the melt debris will relocate and freeze in 20–28 seconds for most maximum hypothetical accidents. This short time at temperature appears to be an important factor in calculating accident dose rates. If LEU U–10Mo fuel fission product release testing is performed with significantly longer hold times, as was done with this scoping study, it may be difficult or impossible to develop useful release rates for short-duration, high-temperature transients. Moreover, if slow ramp rates are used, it may be necessary to account for fission-product release that occurs during heating, in addition to those occurring when holding isothermally at the test temperature, thus increasing accident dose rates.

The review of earlier work also indicates that a wide range of temperatures should be tested. Temperatures as low as 350°C should be included to characterize the fission-product release associated with blistering. Temperatures up to 1500°C should be considered to capture the effect of potential superheat if the severe accident scenarios project the possibility of such temperatures.

2.14 Recommended Future Work

2.14.1 Melt Progression Behaviors

The scoping study does not provide melt-progression data to support the validation of the core-degradation portion of a severe-accident model. Such a model must be able to predict phenomena over several phases of accident progression to accurately predict the core-degradation behavior, which primarily involves characterizing the melting and relocation behavior of the core materials during a severe accident (e.g., relocation, refreezing, and material interactions). The following recommended tests could explore several separate effects that would be used to characterize degradation behavior and evaluate the sensitivity and accuracy of models in predicting the fundamental physics during core degradation:

1. Separately evaluate melt behavior of U10Mo foil and fuel plate by evaluating intact mini-plates and unclad U–10Mo fuel foils
2. Evaluate sensitivity of melt progression to burnup by evaluating both high-burnup and unirradiated specimens.
3. Simulate heat-up and melt of fuel for expected range of accident conditions such as 100°C/s (fast) ramp from 350°C until sample completely molten and 1°C/s (slow) ramp from 350°C until sample completely molten
4. Data acquisition should include:

    - Visual comparisons of melt progression
    - Measurement of relocated mass that can be used as a measure of melt progression for validation purposes
    - Monitoring of test specimen to determine if exothermic material interactions occur
    - Determination of the composition of melted fuel samples

- Monitoring of the environment conditions for use in model validation.

2.14.2 Fission Product Release

The review of earlier work indicates a wide range of test temperatures. Temperatures starting at 350°C should be included to characterize the fission-product release associated with blistering. Temperatures up to 1500°C would capture the effect of potential superheat provided the accident scenarios go to this temperature. The basis for this is the maximum test temperature of 1500°C used on the metallic uranium fuel systems and also the observation that the fission-product release testing for uranium-aluminum was performed at approximately 500°C above the melting point for that fuel system. Therefore, the following is recommended:

1. A test temperature range of 350–1500°C that captures blistering and superheat conditions
2. At-temperature hold times of approximately 2 minutes to be consistent with UAlx testing and expected time at temperature during severe accidents
3. Apply a heatup/cooldown rate of 20–30°C/s to avoid significant amounts of release during heatup and cooldown periods
4. Test irradiated fuel-plate specimens, both with and without aluminum cladding, to bound possible debris compositions in an actual severe accident
5. Test irradiated fuel-plate specimens of various burnup levels to bound differences in release rates and transport behaviors
6. Test irradiated fuel-plate specimens in oxidizing environments, preferably steam, because oxidizing environments have been shown to increase fission-product release rate.
7. Perform thermochemical modeling to predict/confirm chemical species formation.

8. Data acquisition should include:

    - Release fractions for iodine, and cesium
    - If possible, identify chemical form of iodine.
    - Measure test specimen, if possible, and furnace temperature

References

1. A. J. Kuperman, ed., *Nuclear Terrorism and Global Security: The Challenge of Phasing out Highly Enriched Uranium*, New York: Routledge Global Security Studies, 2013.
2. R. Escobar Galindo, et al., "A modified blister test to study the adhesion of thin coatings based on local helium ion implantation," *Thin Solid Films* 471 (2005), pp. 170-176.
3. Michael T. Heitzmann, et al., "Measurements of interface fracture strength between fiber-reinforced composite laminates and thin surface films using blister test," *Key Engineering Materials* 471–472 (2011), pp. 315-319.
4. http://jpkc.fudan.edu.cn/picture/article/348/1b/ee/6dce0ae740cf8673b53e4e96abb8/7aa78636-dda1-46b9-859b-95db3cb616f8.pdf.
5. J. H. O'dette, "Blister Formation in Rolled Aluminum," *Transactions of AIME* 209 (July 1957), pp. 924–929.
6. Daniel M. Wachs, et. al., *RERTR–10A Test: Overview and Breach Assessment*, INL/INT-10-17854, Idaho National Laboratory.
7. NUREG-1313, *Safety Evaluation Report related to the Evaluation of Low-Enriched Silicide-Aluminum Dispersion Fuel for Use in Non-Power Reactors*, U.S. Nuclear Regulatory Commission, July 1988.
8. L. G. Miller, et al., *Extended Life Aluminide Fuel Final Report*, EGG-2441 (June 1986).
9. G. L. Copeland, et al., "Irradiation Performance of Low-Enriched Uranium Fuel Elements," CONF-8410173-1, DE85 000172.
10. J. M. Beeston, et al., "Development and Irradiation Performance of Uranium Aluminide Fuels in Test Reactors," *Nucl. Tech.* 49 pp. 136-149 (1980).
11. G. L. Hofman, "Some Recent Observations On The Irradiation Behavior of Uranium Silicide Dispersion Fuel," CONF-8809221-6 DEC 90.
12. A. E. Richt, R. W. Knight, and G. M. Adamson, *Postirradiation Examination and Evaluation of the Performance of HFIR Fuel Elements*, ORNL-4714 Oak Ridge National Laboratory (1971).
13. J. L. Snelgrove, et al., *Evaluation of Existing Technology Base for Candidate Fuels for the HWR-NPR*, ANL/NPR-93/002 Argonne National Laboratory (1993).
14. R. R. Hobbins, et al., "Irradiation Testing to Verify Failure Predictions Produced by Post-Irradiation Testing," in R. M. Brugger, E. E. Burdick, W. C. Francis, R. L. Heath, and J. F. Kunze, *Nuclear Technology Division Annual Progress Report for Period Ending June 30, 1971*, Aerojet Nuclear Company report , pp. 132–134, ANCR-1016 (October 1971).
15. R. R. Hobbins, "INC-16-2 Irradiation Experiment," Idaho National Engineering Laboratory internal letter report (July 19, 1974).
16. M. J. Graber, et al., "Irradiation Testing of Sample Fuel Plates to Very High Burnups (INC-16-1)," in Brugger, R. M, et al., pp. 132–134.

17. M. J. Graber, "ATR Extended Burnup INC-16-1 Results," INEL internal letter report (1971).

18. J. L. Snelgrove, R. F. Domagala, T. C. Weincek, and G. L. Copeland, "Fuel Development Activities of the U.S. RERTR Program," Proc. Int. Mtg. on Reduced Enrichment for Research and Test Reactors, 24-27 October 1983, Tokai, Japan, Japan Atomic Energy Research Institute Report JAERI-M 84-073, pp. 34-42 (May 1984).

19. W. C. Francis, Aerojet Nuclear Company memorandum Fra-219-71 to H.R. Hilker, November 18, 1971.

20. M. F. Hrovat and H. W. Hassel, "Recent Status of Development and Irradiation Performance for Plate Type Fuel Elements with Reduced ^{235}U Enrichment at NUKEM," *Proc. Int. Mtg. on Reduced Enrichment for Research and Test Reactors, 24-27 October 1983, Tokai, Japan*, Japan Atomic Energy Research Institute Report JAERI-M 84-073, pp. 95-99 (May 1984).

21. R. F. Whitacre, *The UAl_X Dispersion System*, EGG-PRP-8783 Rev. 2 (March 1990).

22. M. J. Graber, et al., "Performance Evaluation of Core II and Core III Advanced Test Reactor Elements," Aerojet Nuclear Company Report ANCR-1027, Idaho National Engineering Laboratory (October 1971).

23. E. Perez, C. Kohut, D. Giorsetti, G. Copeland, and J. Snelgrove, "Irradiation Performance n CNEA UAlX and U3O8 Miniplates," Proc. Int. Mtg. on Reduced Enrichment for Research and Test Reactors, 24-27 October 1983, Tokai, Japan, Japan Atomic Energy Research Institute Report JAERI-M 84-073, pp. 67-76 (May 1984).

24. J. Gomez, R. Morando, E. E. Perez, D. R. Giorsetti, G. L. Copeland, G. L. Hofman, and J. L. Snelgrove, *Postirradiation Examination of High-U-Loaded Low-Enriched U3O8, UAl2, and U3Si Test Fuel Plates*, Proceedings of the 1984 International Meeting on Reduced Enrichment for Research and Test Reactors, Argonne National Laboratory report ANL/RERTR/TM-6 (CONF-8410173) (1985).

25. G. Thamm, E. Groos, and W. Krug, "LEU-Fuel Testing at KFA-Julich under the German AF Program—Plate Irradiation and PIE," *Proceedings of the 1987 International Meeting on Reduced Enrichment for Research and Test Reactors, Buenos Aires, Argentina, September 28–October 1*, 1987, Comision Nacional de Energia Atomica, Buenos Aires, pp. 182-194 (1990).

26. G. L. Copeland, G. L. Hofman, and J. L. Snelgrove, "Examination of U3Si2-Al Fuel Elements from the Oak Ridge Reactor," Proceedings of the 1986 International Meeting on Reduced Enrichment for Research and Test Reactors, Argonne National Laboratory report ANL/RERTR/TM-9 CONF-861185 (1988).

27. W. Krug, E. Groos, J. Seferiadis, and G. Thamm, "Final Results of Test-Irradiations with LEU-Plates at KFA Julich" Proceedings of the 1986 International Meeting on Reduced Enrichment for Research and Test Reactors, Argonne National Laboratory report ANL/RERTR/TM-9 CONF-861185 (1988).

28. A. Marajofsky, C. Kohut, and G. L. Hofman, “Irradiation Behavior of the CNEA’s Experimental Uranium Silicide Dispersion Fuel Plates” Proceedings of the 1986 International Meeting on Reduced Enrichment for Research and Test Reactors, Argonne National Laboratory report ANL/RERTR/TM-9 CONF-861185 (1988).

29. H. Sakai, et. al., “Post-Irradiation Examination of LEU Miniplates in the JMTR,” *Proceedings of the 1986 International Meeting on Reduced Enrichment for Research and Test Reactors*, Argonne National Laboratory, ANL/RERTR/TM-9 CONF-861185 (1988).

30. J. L. Snelgrove, “Overview of Reduced Enrichment Fuels- Development, Testing, and Specification,” Proceedings of the American Nuclear Society Winter Meeting (1987).

31. J. J. Snelgrove, G. L. Hofman, R. L. Frontroth, W. R. McDonell, H. B. Peacock, R. F. Whitacre, and G. L. Copeland, “Evaluation of Existing Technology Base for Candidate Fuels for the HWR-NPR,” Argonne National Laboratory Report ANL/NPR-93/002 (1993).

32. A. B. Robinson, et al., *Irradiation Performance of U-Mo Alloy Based ‘Monolithic’ Plate-Type Fuel—Design Selection*, INL/EXT-09-16807, Rev 1. July 2013.

33. INL/LTD-14-33575 “RERTR-12 Fabrication Summary Report” Idaho National Laboratory.

34. TEV-1745 “Bake-out Furnace Investigation,” Idaho National Laboratory Technical Evaluation.

35. TEV-1854”Bakeout Furnace Qualification for Testing of GTRI Fuel Plates,” Idaho National Laboratory Technical Evaluation.

36. TEV-1924 “RERTR–12 Blister Anneal Test Experiments.”

37. J. Netter, W. Wasserman., *Applied Linear Statistical Models*, Homewood, IL: Richard D Irwin, 1974.

38. J. Rest, et. al., *U–Mo Fuels Handbook*, ANL-09/31; 2009.

39. P. G. Medvedev, et. al., “Shutdown-Induced Tensile Stress in Monolithic Mini-plates As A Possible Cause of Plate Pillowing At Very High Burnup,” RRFM 2014 Transactions, RRFM2014-A0101.

40. Y. S. Kim, et. al., “Analysis of Fission Gas Bubbles and Microstructures of Irradiated U-Mo Fuel,” RERTR 2009-31st International Meeting On Reduced Enrichment For Research And Test Reactors.

41. J. L. Snelgrove, R. F. Domagala, G. L. Hofman, and T. C. Wiencek, The Use of U3Si2 Dispersion in Aluminum Plate-Type Fuel Elements for Research and Test Reactors, ANL/RERTR/TM-11, 1987.

42. G. L. Copeland, R. W. Hobbs, G. L. Hofman, and J. L. Snelgrove, Performance of Low-Enriched U3Si2-Aluminum Dispersion Fuel Elements in The Oak Ridge Research Reactor, ANL/RERTR/TM-10, 1988.

43. D. E. Burkes et al., “Measurement of Fission Gas Release from Irradiated U–Mo Monolithic Fuel Samples,” Journal of Nuclear Materials 461, pp. 61–71.

44. NUREG-1313, Safety Evaluation Report Related to the Evaluation of Low-Enriched Uranium Silicide-Aluminum Dispersion Fuel Use in Non-Power Reactors.

45. Toshikazu Shibata et al., "Release of Fission-Products from Irradiated Aluminide Fuel at High Temperature," International meeting on research and test reactor core conversions from HEU to LEU fuels, Argonne, IL, USA, 8 Nov 1982, CONF-821155-7, DE83 007956.

46. M. Saito et al., Further Data of Silicide Fuel for The LEU Conversion of JMTR, IAEA-SM-310.

47. G. W. Parker et al., Out-Of-Pile Studies of Fission-Product Release From Overheated Reactor Fuels At ORNL, 1955-1965," ORNL-3981.

48. J. L. Snelgrove et al., Evaluation of Existing Technology Base For Candidate Fuels For the HWR-NPR, UC-940, February 1993.

49. Jerry D. Christian, "Chemical Behavior of Iodine-131 during SRE Fuel Element Damage in July 1959," Prepared for in re Boeing Litigation, May 26, 2005.

50. G. Le Marois, and M Megnin, "Assessment of Fission-Product Deposits in the Reactor Coolant System: The DEVAP Program," Nuclear Safety 35, July-December 1994, pp. 213–221.

51. NUREG-1465, Accident Source Terms for Light-Water Nuclear Power Plants, February 1995. Note that discrepancies between the common understanding of elemental groupings and those seen in the table are justified in the NUREG.

52. HFEF-OI-7495, "DEOX Furnace."

53. INL/EXT-12-24101, RERTR-12 Insertion 1 Irradiation Summary Report.

54. TEV-1553, "Iodine Chemical Method Development."

55. http://www1.asminternational.org/asmenterprise/APD/ViewAPD.aspx?id=900828

56. S. M. Frank et al., "The Fate of Radiogenic Iodine during the Electrochemical Treatment of Spent EBR-II Fuel," Material Research Society, Symposium Proceedings, Volume 1265.

57. R. R. Hobbins, D. A. Petti, D. L. Hagrman, "Fission-Product Release from Fuel Under Severe Accident Conditions," Nuclear Technology 101 pp. 270–281.

58. PSAT 1131GT.QA.04, Rev. 0, "ATR Confinement Source Term", Attachment 1, dated June 9, 2008

Appendix A

Additional Monolithic Blister Anneal Data

A1.1 Per Blister Fission Density Data

The per blister threshold temperature of monolithic fuel is an alternative method for representing the blister threshold data. However, these data should be considered with the following considerations. The R-squared values, which provide an estimate of the goodness of fit, for the power fit that was applied to the per plate average fission densities yields a 0.6 and 0.4 for the local average and the local peak respectively. This is compared to the R-squared value of 0.74 for the per-plate average fission densities and the resultant blister threshold temperature. Trend development was accomplished using linear regression[37] methods following logarithmic transformation, resulting in a power law fit to the data. The trend models represent expected blister threshold temperatures relative to a given fission density.

The data and plots are provided in Table A-1 and in Figures A-1 and A-2, respectively, for a per blister resolution of the local-average and peak fission density. Figures A-1 and A-2 show per-blister threshold temperatures plotted as a function of the local average and the local peak densities, respectively. Individual confidence bounds are included for the models. The local average was calculated by averaging the fission densities per the nodes present within each blister region and the peak was taken as the highest fission density node within each blister region.

Table A-1. Blister-threshold temperature as a function of blister average and blister peak fission density.

Plate ID	Blister Average Fissions/cm^3	Blister Peak Fissions/cm^3	Blister-threshold Temperature °C
L5P1B5	3.64 x 10^{20}	5.59 x 10^{20}	>550[a]

Plate ID	Blister Average Fissions/cm^3	Blister Peak Fissions/cm^3	Blister-threshold Temperature °C
L5P2C8	1.11×10^{21}	1.98×10^{21}	>550[a]
L5P1B8	6.91×10^{20}	1.07×10^{21}	>550[a]
L1P772	5.29×10^{21}	6.62×10^{21}	424
L1P460	2.22×10^{21}	2.46×10^{21}	521
	2.58×10^{21}	3.05×10^{21}	521
	2.24×10^{21}	2.36×10^{21}	521
	2.34×10^{21}	2.32×10^{21}	521
	2.20×10^{21}	2.32×10^{21}	521
	2.21×10^{21}	2.21×10^{21}	521
	2.33×10^{21}	2.46×10^{21}	521
	2.65×10^{21}	2.89×10^{21}	521
L1P592	3.03×10^{21}	3.35×10^{21}	456
	2.76×10^{21}	2.91×10^{21}	456
L1P774	5.29×10^{21}	6.29×10^{21}	424
	4.54×10^{21}	5.24×10^{21}	424
	5.00×10^{21}	6.13×10^{21}	424
L1P595	4.56×10^{21}	5.40×10^{21}	424
	4.01×10^{21}	4.72×10^{21}	424
L1P758	5.58×10^{21}	7.56×10^{21}	391
L1P463	3.11×10^{21}	3.23×10^{21}	456
L1P756	6.63×10^{21}	8.33×10^{21}	391
L1P596	4.88×10^{21}	6.44×10^{21}	398
L1P464	4.33×10^{21}	4.90×10^{21}	398
L1P590	4.60×10^{21}	6.61×10^{21}	398
	4.86×10^{21}	6.94×10^{21}	398
L1P465	4.41×10^{21}	4.77×10^{21}	398
	4.97×10^{21}	5.21×10^{21}	398
L1P787	6.74×10^{21}	7.78×10^{21}	365
L1P7A1	5.51×10^{21}	6.34×10^{21}	365
	6.04×10^{21}	7.79×10^{21}	365
L5P3B2	3.13×10^{21}	3.44×10^{21}	475
	3.16×10^{21}	3.35×10^{21}	475
	3.29×10^{21}	3.29×10^{21}	475
L2P498	2.47×10^{21}	3.60×10^{21}	475
	3.11×10^{21}	3.21×10^{21}	475
	2.48×10^{21}	2.48×10^{21}	475
	2.54×10^{21}	2.54×10^{21}	475

Plate ID	Blister Average Fissions/cm^3	Blister Peak Fissions/cm^3	Blister-threshold Temperature °C
	2.82×10^{21}	2.82×10^{21}	475
	2.50×10^{21}	2.74×10^{21}	475
	3.03×10^{21}	3.03×10^{21}	475
L1P10T	6.55×10^{21}	1.21×10^{22}	400
	4.58×10^{21}	5.64×10^{21}	400
	4.11×10^{21}	4.51×10^{21}	400
	4.80×10^{21}	4.95×10^{21}	400
	7.50×10^{21}	8.72×10^{21}	400
L1P32Z	4.55×10^{21}	4.61×10^{21}	359
L1B33Z	4.85×10^{21}	4.94×10^{21}	391
L1B51Z	4.63×10^{21}	4.74×10^{21}	391
	4.91×10^{21}	5.01×10^{21}	391
L1P34Z	3.57×10^{21}	3.57×10^{21}	456
L1H36Z	4.56×10^{21}	4.61×10^{21}	391
	4.93×10^{21}	4.98×10^{21}	391
	4.96×10^{21}	4.98×10^{21}	391
L1H38Z	4.59×10^{21}	4.63×10^{21}	391
	4.42×10^{21}	4.42×10^{21}	391
	4.42×10^{21}	4.42×10^{21}	391
	4.42×10^{21}	4.42×10^{21}	391
	4.24×10^{21}	4.24×10^{21}	391
	4.30×10^{21}	4.30×10^{21}	391
	4.30×10^{21}	4.30×10^{21}	391
	4.20×10^{21}	4.20×10^{21}	391
	4.24×10^{21}	4.24×10^{21}	391
	4.24×10^{21}	4.24×10^{21}	391
	4.12×10^{21}	4.12×10^{21}	391
	4.12×10^{21}	4.12×10^{21}	391
	4.12×10^{21}	4.12×10^{21}	391
	4.07×10^{21}	4.07×10^{21}	391
	4.03×10^{21}	4.03×10^{21}	391
	3.98×10^{21}	3.98×10^{21}	391
	4.08×10^{21}	4.08×10^{21}	391
L1H35Z	4.68×10^{21}	4.68×10^{21}	391
	4.60×10^{21}	4.60×10^{21}	391
	4.55×10^{21}	4.55×10^{21}	391

a. Plates did not exhibit any blister indications during visual exam following the maximum blister anneal test temperature of 550°C.

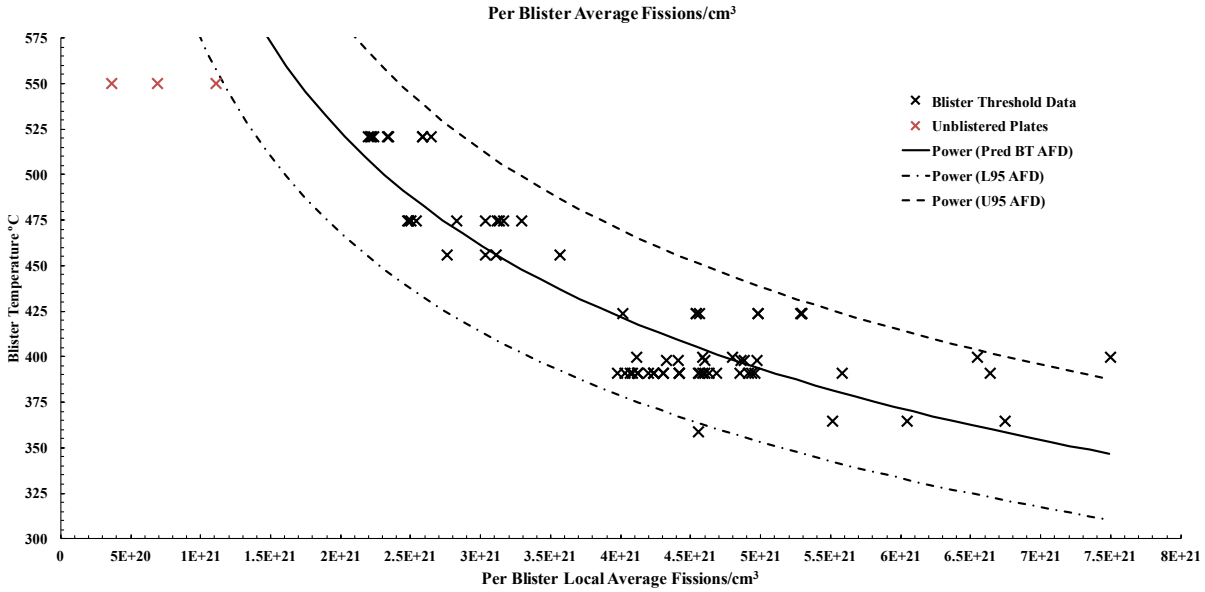

Figure A-1. Per blister average fissions/cm^3 with 95% confidence intervals plotted with plate blister-threshold temperature.

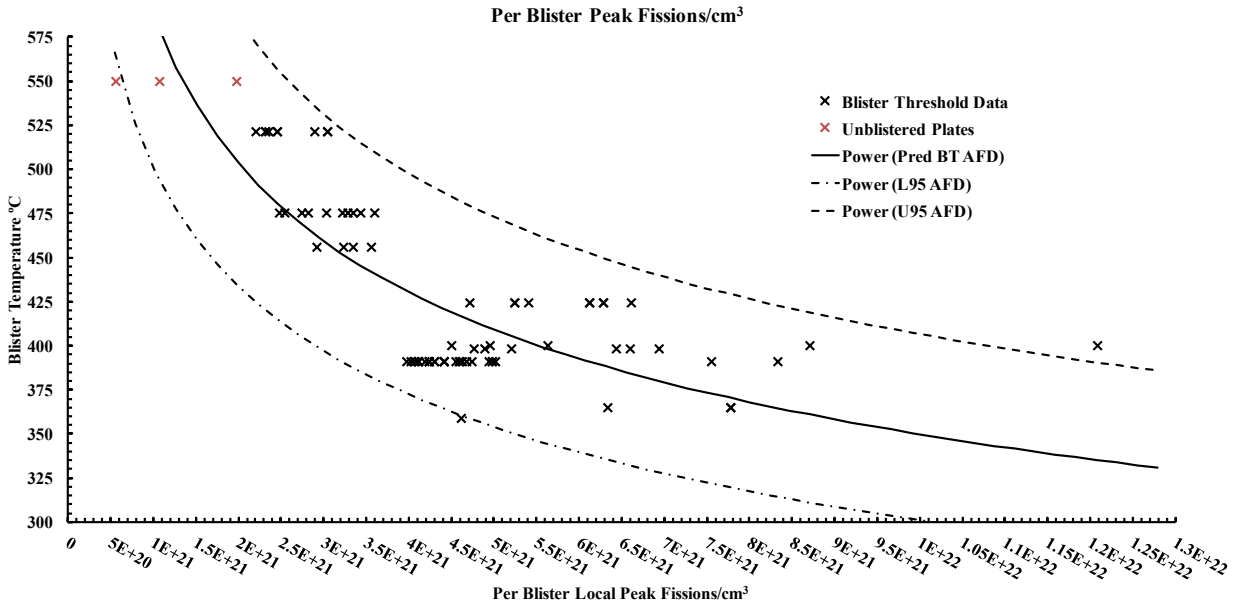

Figure A-2. Per blister local peak fissions/cm^3 with 95% confidence intervals plotted with plate blister threshold temperature.

A1.2 Additional Plate Thickness Blister Threshold Data

The confidence intervals of the thick fuel foil trends in Figure A-3 illustrate that uncertainties are significant due, in part, to the small blister-threshold-temperature data set for fuel plates with fuel-foil thicknesses of 0.013 (AFIP–4 plates), 0.020 (L2PXXX plates) and 0.025 (L5PXXX plates) inches (0.25, 0.33, 0.51 and 0.64 mm).

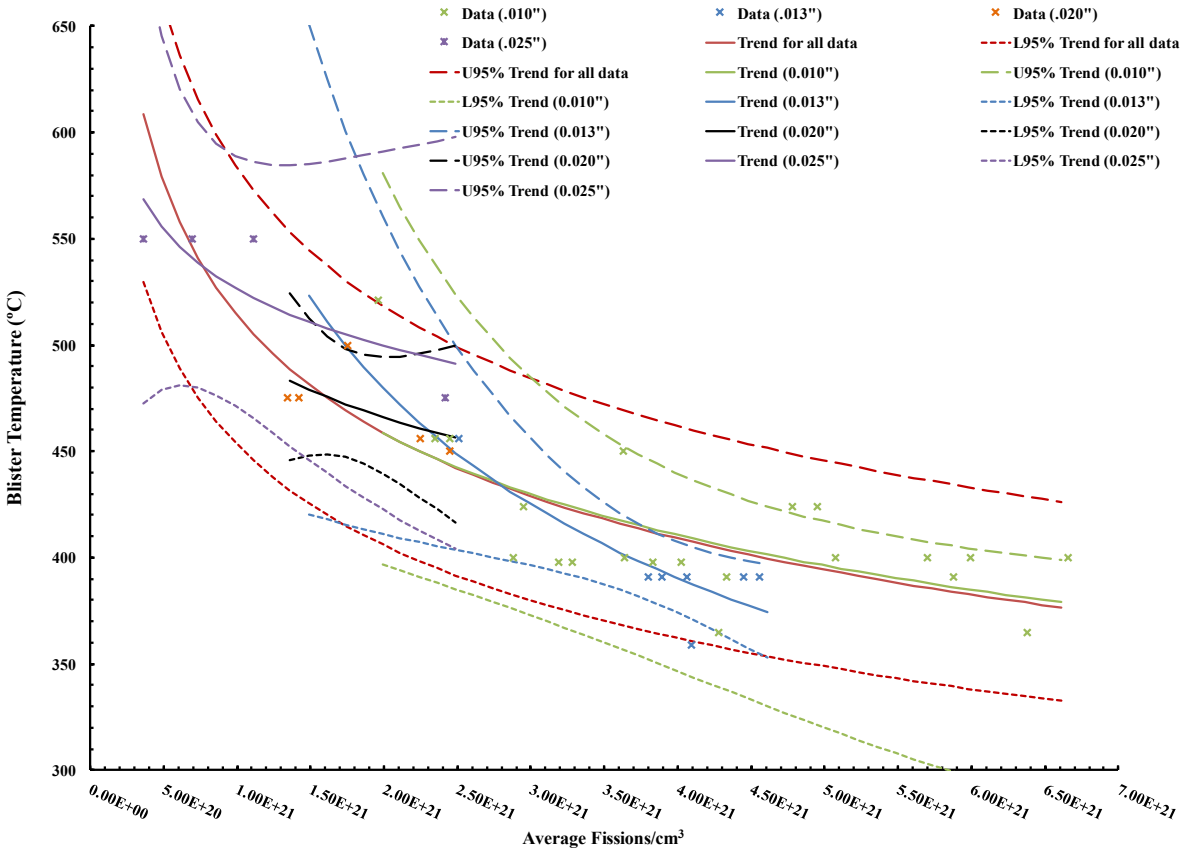

Figure A-3 Per plate thickness blister threshold temperatures with confidence intervals.

Appendix B

Summary of Irradiation Experiment Fabrication Variables[1] And Irradiation Conditions

Note: Fission density is extrapolated from original loading in the fuel per cm^3, and the number of U-235 and fertilized nuclide atom fissions during irradiation determined using Monte Carlo N-Particle Code (MCNP) and ORIGEN calculations. All fuel plates discussed in this document were fabricated using fuel foils that included a Zr barrier layer.

B1.1 Fabrication Variables

RERTR–9: U–10Mo foils were hot co-rolled with a zirconium interlayer to final thickness. Fuel-foil thickness was 0.010 in. Al–6061 clad was applied using the HIP process.

RERTR–10: U–10Mo foils were hot co-rolled with a zirconium interlayer to final thickness. Fuel-foil thicknesses were 0.010 and 0.020 in. Al–6061 clad applied using the HIP and friction bonding processes.

RERTR–12: Hot co-rolled and cold-rolled to final thickness with zirconium interlayer. Fuel foil thicknesses were 0.010, 0.020 and 0.025 in. Al–6061 clad applied using the HIP process.

AFIP–4: Hot rolled U–10Mo foils, cold-rolled to final thickness. Fuel-foil thickness was 0.013 in. Al–6061 clad applied using FB and HIP processes.

---

[1]. INL/EXT-12-26500 “Investigation Of The Cause Of Low Blister Threshold Temperature in The RERTR–12 and AFIP–4 Experiments”

B1.2 Irradiation Conditions

RERTR–9[m]

The RERTR–9A test assembly was irradiated in Cycles 139A and 140A. The RERTR–9B test assembly was irradiated in Cycles 140A, 140B, and 141A. The RERTR–9A/B test assembly is the combined 9A and 9B test assemblies, which were irradiated in Cycle 140A. These experiments were irradiated in the large-B position B-11. The power of this position in the core is represented by the south lobe power which is the average of the SW, C and SE lobe powers, S = (SW + C + SE)/3. Cycle 139A ran for 51.6 EFPDs at 24.0 MW, Cycle 140A ran for 46.5 EFPDs at 23.1 MW, Cycle 140B ran for 35.7 EFPDs at 22.6 MW, and Cycle 141A ran for 32.4 EFPDs at 22.8 MW. There was a Mid-Cycle SCRAM during Cycle 139A with duration of 3 days and Cycle 140B with duration of 8 days. This information is tabulated in Table B-1.

Table B-1. Irradiation history.

ATR CYCLE	RERTR–9A/B Test ID	RERTR–9 Capsules Irradiated	Dates Irradiated	Cycle EFPDs	Mid-Cycle Scram Decay Days	Post-Cycle Decay Days	South Lobe Source Power (MW)
139A	RERTR–9A	A,C	02/26/2007 – 04/21/2007	51.6	3	65	24.0
140A	RERTR–9A/B	A,B,C,D	10/16/2007 – 12/01/2007	46.5	--	15	22.6
140B	RERTR–9B	B,D	12/16/2007 – 01/26/2008	35.7	8	10	22.8
141A	RERTR–9B	B,D	02/05/2008 – 03/06/2008	32.4	--	55	23.1

RERTR–10[n]

The RERTR–10A test assembly was irradiated in cycle 142B in the large-B position B-9 and Cycle 143A in the large-B position B-11. The RERTR–10B test assembly was

[m]. INL/EXT-10-18421 “RERTR–9 Irradiation Summary Report”

[n]. INL/EXT-10-18456 “RERTR–10 Irradiation Summary Report”

irradiated in Cycle 143A in the large-B position B-11. The RERTR–10A/B test assembly is the combined 10A and 10B test assemblies. The power of position B-9 is represented by the north lobe power which is the average of the NW, C and NE lobe powers, N= (NW + C + NE)/3. The power of position B-11 is represented by the south lobe power which is the average of the SW, C and SE lobe powers, S = (SW + C + SE)/3. Cycle 142B ran for 52 EFPDs at 25.3 MW and cycle 143A ran for a total of 48.9 EFPDs at 24.4 MW. RERTR–10A failed (Plate L1P145) during cycle 143A and was removed after 26 EFPDs, RERTR–10B continued irradiation for an additional 22.9 days.

There were two Mid-Cycle SCRAMs during Cycle 142B with a duration of 3 days and 2 days, from dates 07/06/08 – 07/09/08 and 08/05/08 – 08/07/08 respectively. There were also two Mid-Cycle SRAMs during Cycle 143A with duration of 20 days and 5 days, from the dates 10/16/08 – 11/05/08 and 12/21/08 – 12/26/08 respectively. This information is tabulated in Table B-2.

Table B-2. Irradiation history for RERTR–10.

ATR CYCLE	RERTR–10A/B Test ID	RERTR–10 Capsules Irradiated	Dates Irradiated	Cycle EFPDs	Mid-Cycle Scram Decay Days	Post-Cycle Decay Days	North Lobe Source Power (MW)	South Lobe Source Power (MW)
142B	RERTR–10A	A,C	07/04/2008 – 08/30/2008	52	5	25	22.1	--
143A-1	RERTR–10A/B	A,B,C,D	09/24/2008 – 12/06/2008	26.0	25	--	--	25.4
143A-2	RERTR–10B	B,D		22.9		17	--	25.4

RERTR–12[o,p]

The RERTR–12 insertion 1 test assembly was irradiated in cycle 146A and cycle 146B in the large-B position B-11. The power of position B-11 is represented by the south lobe power which is the average of the SW, C and SE lobe powers, S = (SW + C + SE)/3. Cycle 146A ran for 50.5 EFPDs at average power of 112.1 MW (south lobe power of 25.4 MW) and cycle 146B ran for a total of 39.2 EFPDs at average power of 116.0 MW (south lobe power of 25.0 MW).

There was one mid-cycle SCRAM during Cycle 146A with a duration of 4 days from dates 02/14/2010 – 02/18/2010. There were no mid-cycle SCRAMs during Cycle 146B. This information is tabulated in Table B-3.

Table B-3. Irradiation history for RERTR–12 Insertion 1.

ATR CYCLE	RERTR–12 Capsules Irradiated*	Dates Irradiated	Cycle EFPDs	Mid-Cycle Scram Decay Days	Post-Cycle Decay Days	South Lobe Source Power (MW)	Total Core Power (MW)
146A	B,C,D	02/08/2010 – 04/03/2010	50.5	4	18	25.4	112.1
146B	A,B,D	04/21/2010 – 05/30/2010	39.2	0	20	25.0	116.0

The RERTR–12 insertion 2 test assembly was irradiated in cycle 150B, cycle 151A and cycle 151B. RERTR–12-3 and RERTR–12-4 were irradiated in the large-B position B-9 and RERTR–12-5 was irradiated in the large-B position B-11. The power of position B-9 is represented by the north lobe power which is the average of the NW, C and NE lobe powers, N = (NW + C + NE)/3. The power of position B-11 is represented by the south lobe power

o. INL/EXT-11-24101 “RERTR–12 Insertion 1 Irradiation Summary Report”

p. INL/EXT-11-27085 “RERTR–12 Insertion 2 Irradiation Summary Report”

which is the average of the SW, C and SE, S = (SW + C + SE)/3. Cycle 150B ran for 41.9 EFPDs at average power of 108.2 MW (north lobe power of 20.7 MW), cycle 151A ran for a total of 56.1 EFPDs at average power of 101.7 MW (north lobe power of 18.4 MW) and cycle 151B ran for a total of 51.3 EFPDs at an average power of 101.5 MW (south lobe power of 22.7 MW).

There were no mid-cycle SCRAMs during Cycle 150B. There was one mid-cycle SCRAM during cycle 151A with a duration of 3 days from 12/25/2011 – 12/28/2011. There were two mid-cycle SRAMs during cycle 151B from 3/22/2012 – 3/25/2012 and 3/27/2012 – 4/7/2012, total duration of 14 days. This information is tabulated in Table B-4.

Table B-4. Irradiation history for RERTR–12 Insertion 2.

ATR CYCLE	RERTR–12 Capsules Irradiated*	Dates Irradiated	Cycle EFPDs	Mid-Cycle Scram Decay Days	North Lobe Source Power (MW)	South Lobe Source Power (MW)	Total Core Power (MW)
150B	A,C,D	10/15/2011 – 11/26/2011	41.9	0	20.7		108.2
151A	A,B,C,D	12/14/2011 – 02/11/2012	56.1	3	18.4		101.7
151B	D	03/01/2012 – 05/05/2012	51.3	14		22.7	101.5

AFIP–4[q]

The AFIP–4 test assembly was irradiated during cycles 144B and 145A in the ATR Center Flux Trap (CFT). Cycle 144B ran for 51.7 effective full power days (EFPDs) with an average center lobe power of 22.4 MW (total core power of 104.5 MW). There was one mid-cycle SCRAM during cycle 144B with duration of 3 days. Cycle 145A ran for 54.7 EFPDs with an average center lobe power of 23.2 MW (total core power of 108.6 MW). There were

[q]. INL/EXT-11-23297 "AFIP–4 Irradiation Summary Report"

three mid-cycle SCRAMs during cycle 145A with duration of 2 days, 2 days and 3 days, respectively for a total of 7 days. This information is summarized in Table B-5.

Table B-5. Irradiation history for AFIP–4.

ATR CYCLE	AFIP Test ID	AFIP–4 Frames Irradiated	Dates Irradiated	Cycle EFPDs	Mid-Cycle Scram Decay Days	Post-Cycle Decay Days	Center Flux Trap Power (MW)	Total Core Power (MW)
144B	AFIP–4	A,B	5/11/2009 – 7/4/2009	51.7	3	63	22.4	104.5
145A	AFIP–4	A,B	9/5/2009 – 11/6/2009	54.7	7	18	23.2	108.6

Appendix C

Additional Data (Dispersion)

Table C-1 Compositions of ELAF fuel plates reported by [Miller 1986] and listed in Table 1.

			Plate Preirradiation								
Plate Number	Core Compact wt (g)	UAl_x wt (g)	Dry wt (g)	Wet wt (g)	B-10 wt (g)	U wt (g)	Actual Core Volume (cm^3)	U Density (g/cm^3)	Void Volume (%)	Plate Thickness (in.)	Core Length (in.)
	50 vol% UAl_3										
01	11.94	8.076	32.25	21.92	0.014	5.73	2.882	2.0	7.23	0.0510	10.31
03	11.96	8.075	32.17	21.86	0.014	5.73	2.899	—	7.51	0.0510	10.44
04	11.95	8.076	32.29	21.95	0.014	5.73	2.881	—	7.07	0.0512	10.37
05	11.94	8.076	31.99	21.73	0.014	5.73	2.908	1.970	8.04	0.0510	10.50
06	11.95	8.076	32.23	21.91	0.014	5.73	2.883	1.988	7.13	0.0512	10.56
07	11.95	8.075	32.18	21.85	0.014	5.73	2.912	1.968	8.04	0.0511	10.44
08	11.94	8.075	32.10	21.82	0.014	5.73	2.888	—	7.39	0.0511	10.50
09	11.96	8.075	32.31	21.95	0.014	5.73	2.898	—	7.47	0.0514	10.56
10	11.95	8.075	32.16	21.85	0.014	5.73	2.899	—	7.50	0.0512	10.69
								Average	7.49		
	50 vol% UAl_2										
13	13.70	10.057	33.41	23.18	0.020	7.93	2.998	2.645	10.98	0.0510	10.62
15	13.70	10.057	33.53	23.23	0.020	7.93	3.024	2.622	11.75	0.0512	10.56
16	13.69	10.057	33.41	23.16	0.020	7.93	3.014	2.631	11.49	0.0510	10.62
17	13.69	10.057	33.47	23.19	0.020	7.92	3.023	—	11.72	0.0511	10.62
18	13.70	10.057	33.56	23.30	0.020	7.92	2.973	—	10.23	0.0513	10.62
19	13.68	10.058	34.02	23.60	0.020	7.93	2.956	2.683	9.87	0.0519	10.69
20	13.69	10.057	33.96	23.52	0.020	7.92	3.002	2.638	11.02	0.0520	10.75
								Average	11.01		
	45 vol% UAl_2										
22	13.01	9.039	33.04	22.83	0.018	7.12	2.860	2.49	7.23	0.0510	10.37
23	13.02	9.038	32.95	22.77	0.018	—	2.867	—	7.32	0.0509	10.56
24	13.02	9.038	33.12	22.90	0.018	—	2.845	—	6.59	0.0513	10.56
25	13.02	9.038	32.96	22.74	0.018	—	2.904	—	8.48	0.0511	10.50
26	13.01	9.037	33.08	22.84	0.018	—	2.875	—	7.73	0.0512	10.56
27	13.03	9.037	32.84	22.68	0.018	7.13	2.891	2.466	8.08	0.0509	10.62
28	13.00	9.039	33.12	22.86	0.018	7.12	2.877	2.475	7.62	0.0510	10.62
								Average	7.58		

Table B-1. (continued)

			Plate Preirradiation								
Plate Number	Core Compact wt (g)	UAl_x wt (g)	Dry wt (g)	Wet wt (g)	B-10 wt (g)	U wt (g)	Actual Core Volume (cm^3)	U Density (g/cm^3)	Void Volume (%)	Plate Thickness (in.)	Core Lengtl (in.)
	40 vol% UAl_2										
29	12.51	8.018	32.82	22.50	0.016	6.33	2.867	2.208	5.81	0.0513	10.62
30	12.51	8.018	32.93	22.56	0.016	6.32	2.877	2.197	6.02	0.0519	10.62
31	12.51	8.019	32.81	22.46	0.016	6.32	2.901	—	6.80	0.0515	10.62
32	12.51	8.019	32.99	22.63	0.016	6.32	2.845	2.221	4.96	0.0515	10.69
33	12.50	8.018	32.49	22.28	0.016	6.32	2.875	2.198	6.08	0.0510	10.62

Table C-2. Fuel test plate compositions reported by [Beeston 1980]. The original test data and descriptions of fuel elements XA3G and XA8G as provided in [Graber 1971B] are reproduced here. Plates from A16D and XA20G were not blister tested. No data is available on elements UAl_x-8F, XA130K, or XA135K.

TABLE I

Operating Parameters of ATR Startup Program Fuel Elements
Which Were Destructively Examined

Fuel Element Number	Used in Core	Day of Operation	Mode of Operation	Type Fuel Element	Irradiation Position
A172C	II	35	250 MW Balanced	Std. U_3O_8	F11
XA3G	II	35	Balanced	7F UAl_x	F13
XA8G	II	35	Balanced	7F UAl_x	F14
A16D	III	27	250 MW 40-50-60 Unbalanced	Std. UAl_x	F11
XA20G	III	27	Unbalanced	7F UAl_x	F13
Fuel Material			U_3O_8	UAl_x	UAl_x
Core Matrix Material			X8001	X8001	X8001
Burnable Poison Material			B_4C	B_4C	B_4C
Boron Loading, mg Nat B/cc Core					
Plates 1, 2, 18, 19		5.2	5.2	14.2	
Plates 3, 4, 16, 17		5.2	5.2	7.5	
Plates 5 through 15		5.2	5.2	1.1	
Plate Cladding Material		6061-0 Al	6061-0 Al	6061-0 Al	
Side Plate Material		6061-T6 Al	6061-T6 Al	6061-T6 Al	
End Fitting Material		356 Al	356 Al	356 Al	

Table C-3. Fuel test plate composition for plate series 169 reported by [Beeston 1980] in Table 2. From [Hobbins 1974].

Table 2 F. Composition

Plate No.	wt. UAl_x (g)	UAl_x Mesh Size	wt. B_4C (mg)	wt. B^{10} (mg)	wt. U (g)	wt. U^{235} (g)	Enrichment %	Core Vol. (cm^3)	B^{10}/Vol. (mg/cm^3)	U^{235}/Vol. (g/cm^3)	Corresponding ATR 7F Loading
169-4	1.0530	-100	0.6	0.09	0.7468	0.6860	91.86	0.453	0.199	1.51	H
169-5	1.0274	-100	0.6	0.09	0.7286	0.6693	91.86	0.444	0.203	1.51	H
169-11	0.9468	-100	3.6	0.54	0.6715	0.6168	91.86	0.508	1.06	1.21	M
169-12	0.9514	-100	3.6	0.54	0.6747	0.6198	91.86	0.510	1.06	1.22	M
169-19	0.7648	-100	9.4	1.4	0.5424	0.4982	91.86	0.523	2.68	0.953	L
169-36	0.9492	-100+325	3.5	0.53	0.6554	0.6102	93.10	0.503	1.05	1.21	M
169-37	0.9807	-100+325	3.7	0.56	0.6772	0.6305	93.10	0.519	1.08	1.21	M
168-38	1.0090	-100+325	3.8	0.57	0.6967	0.6486	93.10	0.529	1.08	1.23	M
169-39	0.9632	-100+325	3.6	0.54	0.6651	0.6192	93.10	0.508	1.06	1.22	M
Nom. 7F High (5-15)	-	-100+325, <25%-325	-	-	-	-	-	-	0.199*[a]	1.56*[a]	H
Nom. 7F Med (3, 4, 16, 17)/Std.	-	-100+325, <25%-325	-	-	-	-	-	-	1.42*[a]	1.27*[a]	M
Nom. 7F Low (1, 2, 18, 19)	-	-100+325, <25%-325	-	-	-	-	-	-	2.70*[a]	1.02*[a]	L

*A fuel core thickness of 0.020in. (0.0508cm) has been assumed.

[a]W. C. Francis, "S-209 Tables", Aerojet Nuclear Co., Interoffice Correspondence, FRA-155-72, August 10, 1972.

Table C-4. Fuel test plate composition data for XA130K and XA135K reported by [Beeston 1980] in Table 2. From [Whitacre 1993].

Element and/or Sample	Uranium at/cm³ (x10²¹)	Fission Density (x10²¹)	Irradiation Temperature (°C)	Core Porosity (Vol. %)	Swelling $\frac{\Delta V}{V}$	^{10}B at/cm³ Meat (x 10²⁰)	^{10}B at/cm³ Matrix (x 10²⁰)	^{10}B / ^{235}U atom ratio	Ref.
Comp 3	2.48	0.75	150-200	10.5	1.4	0.63	0.90	0.025	19
Comp 4	3.32	1.00	150-200	14.0	0.3	0.63	1.03	0.019	19
Comp 9	2.48	0.75	150-200	10.5	1.0	0.63	0.90	0.025	19
584	3.40	0.68	150-200	4.6	0.6	0.71	1.10	0.021	20
587	3.40	1.52	150-200	4.6	5.1	0.71	1.10	0.021	20
621	3.65	1.18	150-200	4.1	2.5	0.71	1.14	0.019	20
622	3.65	0.80	150-200	6.2	1.0	0.71	1.14	0.019	20
623	3.65	1.13	150-200	4.5	2.5	0.71	1.14	0.019	20
625	3.65	0.48	150-200	4.5	1.5	0.71	1.14	0.019	20
169-11	3.38	2.16	100-200	8.4	4.7	0.64	1.02	0.021	21
169-12	3.39	2.27	100-200	8.4	5.9	0.64	1.02	0.020	21
169-19	2.65	1.84	100-200	6.6	4.7	1.61	2.28	0.066	21
169-36	3.34	2.35	100-200	7.9	6.4	0.63	1.01	0.020	21
169-37	3.34	2.38	100-200	7.8	6.0	0.65	1.03	0.021	21
169-38	3.39	2.34	100-200	7.0	7.4	0.65	1.02	0.021	21
169-39	3.35	2.23	150-200	7.5	5.7	0.64	1.02	0.020	21
XA8G	2.69	0.72	150-200	3 to 11	2.4[a]	1.69	2.10	0.068	15
XA8G	3.39	0.99	150-200	3 to 11	2.9	0.89	1.18	0.028	15
XA20G	3.39	0.21	150-200	3 to 11	1.8	0.89	1.18	0.028	15
XA8G	2.69	0.40	150-200	3 to 11	2.2	1.69	2.10	0.068	15
XA8G	4.10	0.68	150-200	3 to 11	3.0[a]	0.13	0.19	0.003	15
XA8G	3.39	0.54	150-200	3 to 11	1.7	0.89	1.18	0.028	15
XA8G	4.10	0.42	150-200	3 to 11	1.5	0.13	0.19	0.003	15
FUEL ELEMENTS									
XA130K & XA135K	4.25	2.00	150-200	5.94	6.3[a]	Probably low or zero based on the high uranium loading.			21
169-4	4.22	2.46	150-200 [b]	11.6	2.0	0.12	0.23	0.003	21
169-5	4.20	2.69	150-200 [b]	12.0	4.7	0.12	0.23	0.003	21
XA20G	3.39	0.69	150-200	3 to 11	3.7[a]	0.89	1.18	0.028	15

a Averages of growth data on fuel elements where fission density is within 0.15 x 10^{21} fissions/cm³.

b Temperature range is for fission densities between 1.2x10^{21} and value given.

Table 16 Growth and Swelling of Fuel Plate Cores and Samples

Table C-5. Fuel plate compositions from page 3 of [Graber 1971A] reported in in Table 3.

plates in each tier. Although there were nine compositions of fuel plates irradiated only the 7F high loaded and standard ATR (composition 157 and 158) will be discussed in this report. Composition 157 had a fuel core composed of 51.6 weight per cent -140 mesh UAl_x (70.5 per cent fully enriched uranium), 0.197 weight per cent B_4C (75.9 weight per cent B, 19.8 atom per cent ^{10}B) and the remainder MD-101 aluminum. The picture frame and clad were 6061 aluminum alclad with 5% 1100 aluminum. Composition 158 was similar to 157 except that 61.4 weight per cent of the UAl_x and 0.037 weight per cent of the B_4C were used. Table I lists composition 157 and 158 plates and the levels to which they were irradiated. Two of these samples, 157-38 and 158-65,were removed from the reactor after 9,434 MWd.

Table C-6. Fuel plate compositions reported in [Graber 1971C].

TABLE I

SWELLING AND BLISTER RESULTS FOR INC-16-1 SAMPLE FUEL PLATES

Composition	Plate No.	Calc. Fiss/cc	Blister Temp., °C	Core Swelling, % ΔV/V Measured	Core Swelling, % ΔV/V Expected[a]	% ΔV/V Fission Growth[b]	Fabrication Voids, %
ETR UAl_x	154-50	1.59×10^{21}	455	5.4	4.2	10.2	6.0
" "	154-47	1.36	260	4.2	3.1	8.7	5.6
ETR B_4C Foil, 3.8gB/el.	155-11	1.78	425	9.1	11.4	11.4	0.0
" "	155-23	1.60	425	8.6	10.2	10.2	0.0
ETR B_4C Foil, 4.6gB/el.	156-45	1.79	425	9.2	11.5	11.5	0.0
" "	156-64	1.63	425	8.7	10.4	10.4	0.0
ATR Standard Loading	157-30	1.98	480	5.1	7.5	12.7	5.2
"	157-31	1.77	510	5.9	5.5	11.3	5.8
"	157-38	1.48	510	4.4	4.4	9.5	5.1
ATR 7F High Loading	158-54	2.33	480	6.9	8.2	14.9	6.7
"	158-67	1.96	510	5.2	5.8	12.5	6.7
"	158-65	1.39	510	6.4	2.7	8.9	6.2
ATR 7F High 30 Mil Core	159-14	1.45	510	5.1	5.6	9.3	3.7
"	159-24	1.38	510	5.1	5.3	8.7	3.4
ATR 7F Low Loading	160-37	1.47	480	6.6	5.7	9.4	3.7
"	160-34	1.27	480	6.4	4.9	8.1	3.2
ATR 7F Low, Low Void	162-1	1.44	510	6.1	6.0	9.2	3.2
"	162-4	1.09	510	4.8	3.3	7.0	3.7
ATR Regular, Low Void	163-4	1.88	510	6.8	7.5	12.0	4.5
"	163-16	1.08	510	3.3	2.3	6.9	4.6

[a]Expected for 100% utilization of voids for fission product accommodation.

[b]Growth due to fissioning of ^{235}U on a core volume basis.